Combination of tissular multimodal spectro-imaging and optical clearing methods to improve detection depth in skin in vivo

Sergey Zaytsev

UNIVERSITÉ DE LORRAINE

Ecole Doctorale IAEM-Lorraine

Combination of tissular multimodal spectro-imaging and optical clearing methods to improve detection depth in skin *in vivo*

Thèse

Présentée et soutenue publiquement le 27 juin 2022

pour l'obtention du titre de

Docteur de l'Université de Lorraine

Mention «Automatique, Traitement du signal et des images, Génie informatique»

par

Sergey ZAYTSEV

Membres du jury:

Rapporteurs:	**Igor V. MEGLINSKI**	Professor, College of Engineering & Physical Sciences, Aston University, Birmingham, UK
	Dan ZHU	Professor, Britton Chance Center for Biomedical Photonics, Huazhong University of Science and Technology, Wuhan, China
Examinateurs:	**Walter BLONDEL**	Professeur des Universités, CRAN UMR 7039, Nancy, France Directeur de thèse
	Marine AMOUROUX	Ingénieure de Recherche, CRAN UMR 7039, Nancy, France Co-directrice de thèse
	Valery V. TUCHIN	Professor, Saratov State University, Saratov, Russia Directeur de thèse en cotutelle
	Elina A. GENINA	Professor, Saratov State University, Saratov, Russia Co-directrice de thèse en cotutelle
	Yuri V. KISTENEV	Professor, Laboratory for Biophotonics, Tomsk State University, Tomsk, Russia
Présidente de jury:	**Céline FROCHOT**	Directrice de Recherche CNRS, LRGP UMR 7274, Nancy, France
Invitée:	**Anne PLANAT-CHRÉTIEN**	Chercheuse – chef de projet, CEA-leti Minatec - DTBS/SEIVI/LS2P, Grenoble, France

Centre de Recherche en Automatique de Nancy – UMR 7039

CRAN

cnrs

“Great things are done by a series of small things brought together”

Vincent van Gogh.

Abstract

This thesis presents the results of research in the context of improved analysis of the skin optical properties using various optical techniques, such as multimodal tissular spectroscopy and optical coherence tomography (OCT) imaging. Since many years optical techniques of skin characterization are an effective alternative to traditional invasive diagnostic methods as they allow to get information about the structural and biochemical skin composition *in vivo* in real time, which led to their extensive implementation in the clinical practice of skin lesions analysis. In the last decades it was demonstrated that combined use of several optical techniques allows to increase the diagnostic accuracy by increasing the variety of data acquired in one measurement. Spatial resolution may also increase the diagnostic potential by providing depth discrimination (resolution) between assessed layers. Even though the main limitation for the use of the optical methods in skin diagnostics is the strong absorption and scattering of the latter, skin optical properties can be changed using the method of skin optical clearing (OC). The combination of optical clearing agents (OCA) with various chemical and physical enhancers of skin permeability may significantly improve the potential of multimodal optical approaches with spatial resolution.

The aim of the first experimental study within this thesis framework was (i) to investigate the effect of the OC process applied to *ex vivo* human skin samples on spatially resolved (SR) diffuse reflectance (DR) and autofluorescence (AF) spectra using two combinations of OCA and chemical permeation enhancers (CPE), and (ii) to quantify the clearing-like effect of drying and of spectroscopic probe pressure on skin. A spatially resolved multimodal spectroscopic device was used on a two-layered “hybrid” model made of *ex vivo* skin and fluorescent gel. Time kinetics of fluorescence and diffuse reflectance spectra demonstrated an increase in the gel fluorescence back reflected intensity after optical clearing. In addition, complementary experimental results showed increased light transmittance through the skin and confirmed that the improvement in the depth sensitivity of the multimodal spectroscopic approach was related not only to the dehydration and refractive indices matching due to optical clearing, but also to the mechanical compression of tissues caused by the application of the spectroscopic probe.

Since when translating these methods into clinical use there is a need to comply with established regulations, including the use of chemicals on healthy and pathologically changed skin of patients, the concentrations of the OCA used may need to be reduced in order to pass

the threshold of clinical utility and biocompatibility. Thus, the main goal of the consecutive experimental study was to experimentally evaluate, by using for the first time a Line-field Confocal OCT (LC-OCT) imaging technique, the efficacy of OC of human skin *in vivo* with biocompatible OCA combined with chemical and physical permeability enhancers. To satisfy the biocompatible concentration requirements, the mixtures of OCA and CPE were developed according to the FDA inactive ingredients database. To enhance the clearing effect, physical permeation methods were also used. By analyzing simultaneously the average intensity and contrast of the images obtained by LC-OCT technique, we determined the in-depth effectiveness of skin *in vivo* biocompatible OC. The results showed that the best increase in image intensity and contrast after 10 minutes of ultrasound-assisted clearing was achieved using a mixture of PEG/OA/PG. The results of the experimental data fitting with the hypothesized biphasic exponential association model are in a good agreement with experimental results. Thus, the effectiveness of OC with biocompatible concentrations of OCA was demonstrated.

Résumé

Le cancer de la peau est actuellement l'un des cancers humains les plus fréquents. Le carcinome basocellulaire (CBC) est le type de cancer de la peau le plus fréquent, avec une moyenne de 8 cancers de la peau sur 10 étant des CBC. Les sites d'apparition caractéristiques de ce type de cancer sont les zones du corps qui sont les plus activement exposées au soleil (la tête et le cou). La spécificité de la localisation du CBC conduit au fait qu'une méthode extrêmement précise de détermination des limites de la zone touchée est nécessaire, car (i) sans une précision de traitement suffisante, il existe un risque de récidive et (ii) une excision excessive (en cas de traitement chirurgical) affectant des zones de tissus sains se heurte à des problèmes esthétiques (si la technique PDT n'est pas utilisée). La méthode traditionnelle de diagnostic du cancer de la peau est l'examen histopathologique qui consiste à prélever un échantillon de tissu d'une zone cutanée suspecte pour un examen ultérieur en laboratoire. Les inconvénients évidents de cette méthode sont son caractère invasif et la durée de l'analyse des échantillons obtenus. Au cours des 20 dernières années, les méthodes d'imagerie optique[1]–[3] et de spectroscopie[4]–[6], qui sont basées sur l'interaction de la lumière avec les tissus biologiques, ont été largement étudiées pour caractériser les tissus épithéliaux en général et la peau en particulier[4], [5], [7], [8]. Leurs principales caractéristiques de non-invasivité, atraumaticité, sensibilité, et potentiel de transfert clinique en font des outils de diagnostic *in vivo* de premier intérêt, complémentaires à d'autres procédures cliniques de référence telles que l'histopathologie. Les méthodes de spectroscopies tissulaires *in vivo* en réflectance diffuse (RD)[9]–[11] et en autofluorescence (AF)[4], [5], [12]–[14] ou la combinaison des deux[15]–[17], et l'utilisation de plusieurs longueurs d'onde d'excitation pour une meilleure précision diagnostique [18], ont été largement étudiées pour leur applicabilité à fournir une information complémentaire sur les changements structurels et biochimiques accompagnant le développement de pathologies dans les tissus cutanés. Par exemple, une analyse bimodale combinant des caractéristiques spectrales RD et AF à excitation multiple [16], [18], [19] a permis d'obtenir une précision diagnostique accrue par rapport à une approche AF à excitation unique lors de la discrimination entre trois types d'hyperplasie cutanée de souris, ou entre des épithélium cylindrique versus précancers cervicaux de haut grade [20]. Cependant, la peau est un organe multicouches optiquement hétérogène, chacune des couches différant par son épaisseur et sa morphologie. Selon le type et le stade des changements pathologiques, différentes couches de la peau et leurs

composants structurels associés peuvent être affectés. Pour servir d'outil de diagnostic complémentaire efficace et précis, les techniques de spectroscopie optique doivent donc être capables de fournir une discrimination spatiale (résolution) entre les couches évaluées [21]–[25].

Cependant, en raison de la disparité des indices de réfraction (IR) entre les différents constituants de la peau et du milieu intercellulaire [26], et compte tenu de la structure hétérogène de la peau, les photons se propageant dans toute la peau sont fortement diffusés et absorbés. Cela limite par conséquent la pénétration de la lumière dans les tissus cutanés et les capacités de résolution en profondeur des techniques optiques [27]. Les moyens d'améliorer la profondeur d'exploration, le pouvoir de résolution et le rapport de contraste des méthodes optiques de caractérisation *in vivo* de la peau sont étudiés depuis plusieurs décennies. L'utilisation d'agents chimiques présentant un IR proche de celui des composants cellulaires de la peau conduit à une diminution des différences d'IR entre les composants tissulaires cellulaires et le fluide extracellulaire et, par conséquent, à une diminution de la diffusion cutanée. Avec une diminution de la diffusion cutanée, la profondeur de sondage et le contraste des méthodes optiques *in vivo* peuvent augmenter car davantage de photons balistiques peuvent se propager dans la peau. Cette technique a été appelée Clarification Optique tissulaire (OC)[28]–[30].

Une approche intégrée est nécessaire pour améliorer la précision diagnostique dans l'analyse clinique du cancer de la peau; dans notre cas il s'agit de combiner les avantages diagnostiques de plusieurs méthodes optiques dans une approche multimodale résolue spatialement et la technologie de clarification optique permettant d'améliorer la résolution en profondeur et le contraste de ces méthodes.

Cependant, la fonction barrière de la couche cornée (CC), qui limite l'utilisation de la plupart des agents de clarification optique (OCA) connus, doit également être prise en compte. De nombreuses études ont montré l'efficacité d'agents chimiques capables de perturber la structure naturelle de la kératine et des lipides de la CC, créant ainsi des voies de pénétration pour l'OCA à travers cette barrière. Ces agents chimiques, appelés Chemical Permeation Enhancers (CPE), sont représentés par plusieurs groupes de substances, parmi lesquelles les plus couramment retrouvées dans la littérature sont les alcools (éthanol, propylène glycol)[31], les solvants (diméthylsulfoxyde)[1], [2], des acides organiques (acides oléique et

linoléique)[1], [32], ainsi que des azones (azone et thiazone)[1], [3]. L'utilisation de CPE avec un OCA peut considérablement améliorer l'effet de clarification optique tissulaire.

En réponse aux problématiques scientifiques mentionnés ci-dessus, les objectifs de thèse suivants ont été définis et les travaux correspondants réalisés sont décrits dans ce manuscrit de thèse selon 4 étapes principales :

- Étude expérimentale de l'effet du processus OC appliqué à des échantillons de peau humaine *ex vivo* sur les spectres de RD et d'AF résolus spatialement en utilisant deux combinaisons d'OCA et de CPE;
- Quantification de l'effet de clarification provoqué par la déshydratation de l'échantillon et par la pression de la sonde spectroscopique appliquée sur la peau;
- Développement des compositions biocompatibles OCA/CPE qui pourraient être utilisées en toute sécurité sur les zones lésionnelles de la peau humaine *in vivo* en clinique;
- Quantification de l'efficacité OC *in vivo* d'OCA cliniquement compatibles à l'aide d'images de tomographie par cohérence optique confocale (LC-OCT).

Cette thèse représente le travail qui a été réalisé dans le cadre d'une cotutelle franco-russe (bourse doctorale franco-russe « Vernadski » de l'Ambassade de France en Russie) impliquant l'expertise complémentaire et la collaboration de deux équipes partenaires : le Centre de Recherche sur l'Automatique (CRAN) de l'Université de Lorraine (Nancy, France) et l'Institut de Recherche-Enseignement d'Optique et de Biophotonique (REI OBP) de l'Université d'Etat de Saratov (Saratov, Russie). Des protocoles expérimentaux impliquant la spectroscopie multimodalités résolue spatialement (RD et AF) de peau humaine *ex vivo* et *in vivo* et l'imagerie LC-OCT ont été menés au CRAN en collaboration avec l'hôpital régional de Metz-Thionville en France. Des protocoles expérimentaux complémentaires avec la peau de rats *ex vivo* sur la quantification de l'effet de clarification causé par la déshydratation de l'échantillon et par la pression de la sonde spectroscopique appliquée sur la peau ont été menés au laboratoire REI OBP en Russie.

Le manuscrit commence par une introduction. La première section «Motivation, aims and objectives» présente le contexte scientifiques, les problématiques et les principaux objectifs de cette étude. Le contexte spécifique de la thèse est fourni dans la section du même nom en Introduction. Les grandes lignes de la thèse sont présentées dans la section correspondante de l'Introduction ainsi que dans ce résumé.

Le chapitre 1 présente l'état de l'art, lié à cette thèse. Dans la section 1.1, la structure de la peau et ses propriétés optiques sont décrites, et les inconvénients évidents de l'utilisation des méthodes optiques existantes dans des conditions cliniques, associés aux propriétés hautement diffusantes de la peau, sont prises en compte. La section 2.1 est consacrée à l'application des méthodes optiques sur la peau. Diverses approches spectroscopiques sont décrites dans la section 1.2.1, tandis que les techniques d'imagerie sont présentées dans la section 1.2.2. Enfin, les techniques multimodales, qui sont des combinaisons de différentes techniques optiques, sont décrites dans la section 1.2.3. Dans la section 1.3, la méthode de clarification optique des tissus biologiques est présentée. Le principe de son action est donné dans la section 1.3.1, différents groupes d'OCA sont décrits dans la section 1.3.2 en termes de propriétés physiques et chimiques, d'avantages et d'inconvénients de leur utilisation et de toxicité potentielle. La section 1.3.3 fournit des informations sur diverses méthodes physiques et chimiques d'amélioration de la perméabilité des tissus biologiques. Ensuite, les exemples de la littérature scientifique sur l'utilisation de la clarification optique avec des techniques de diagnostic optique sont présentés dans la section 1.3.4.

Les chapitres 2 et 3 sont consacrés à la présentation des deux études expérimentales conduites au cours de la thèse et aux discussions des résultats expérimentaux obtenus au cours de la thèse. L'objectif principal de la première étude expérimentale présentée dans le chapitre 2 de ce manuscrit de thèse était (i) d'étudier l'effet du processus de clarification optique (OC) appliqué à des échantillons de peau humaine *ex vivo* sur des spectres DR et AF résolus spatialement (SR) en utilisant deux combinaisons d'OCA et de CPE, et (ii) pour quantifier l'effet de clarification de la déshydratation et de la pression de la sonde spectroscopique sur la peau. Pour l'étude du processus de l'OC, le modèle hybride *ex vivo* a été testé en combinaison avec la spectroscopie spatialement résolue. La configuration hybride des échantillons testés, constituée d'un morceau de peau (épiderme et derme) *ex vivo* posé sur un gel fluorescent, a permis d'analyser la contribution spectrale de différents fluorophores situés aux différentes profondeurs et leur cinétique lors de la clarification optique. Comme différentes distances de fibres de collection de spectroscopie multimodale sont sensibles à différentes profondeurs, cela a permis de discriminer différents processus de clarification à différentes profondeurs de peau. L'application topique de 2 combinaisons d'OCA et de CPE a démontré leur impact dans l'intensité accrue de la fluorescence et du signal DR acquis à partir de la couche de gel sous la peau. Dans le même temps, une réduction de la diffusion des

photons au sein ds couches de la peau sous l'action de l'OCA a provoqué une diminution de l'intensité des spectres AF détectés et une meilleure propagation en profondeur des photons dans la peau. Ainsi, l'OC s'est avéré être une technique efficace pour améliorer la détection d'un signal spectroscopique produit par les couches profondes de la peau. De plus, il a été expérimentalement confirmé que l'amélioration de la sensibilité en profondeur de la spectroscopie DR et AF en résolution spatiale n'est pas seulement liée à l'effet des OCA. Les résultats obtenus à l'état "déshydraté" nous ont permis de prouver que l'effet de la pression de la sonde optique contribue également au processus de clarification ainsi que l'appariement de l'indice de réfraction induit par l'OCA et la déshydratation. En cas d'absence de tout liquide appliqué sur l'échantillon de peau, une augmentation du signal spectroscopique était également liée à la perte d'eau par la peau *ex vivo* qui ne peut pas conserver ses propriétés et s'amincit avec le temps d'exposition.

L'objectif principal de la seconde étude expérimentale présentée au chapitre 3 était d'évaluer expérimentalement à l'aide de la technique de tomographie par cohérence optique confocale (LC-OCT) l'efficacité de la clarification optique de la peau humaine *in vivo* avec des OCA biocompatibles combinés à des activateurs de perméabilité chimiques et physiques. Pour rendre cette étude éventuellement transférable aux conditions cliniques réelles et pour satisfaire aux exigences de biocompatibilité des concentrations utilisées, nous avons développé les mélanges d'OCA et de CPE selon les objectifs de la thèse en utilisant la base de données des ingrédients inactifs de la Food and Drugs Administration (FDA). Du polyéthylène glycol-400 (PEG) ainsi que des solutions aqueuses de glucose et de saccharose ont été utilisés comme OCA. Le propylène glycol (PG), l'acide oléique (OA) et le diméthylsulfoxyde (DMSO) ont été utilisés comme CPE. Pour améliorer l'effet de clarification, des méthodes de perméation physique ont également été utilisées. En analysant l'intensité moyenne et le contraste des images obtenues par la méthode LC-OCT, nous avons déterminé l'efficacité en profondeur de l'OC biocompatible *in vivo* de la peau. Les résultats ont montré que la meilleure augmentation de l'intensité et du contraste de l'image après 10 minutes de clarification assisté par Ultrasons (US) a été obtenue en utilisant un mélange de PEG/OA/PG. Les résultats de l'ajustement des données expérimentales avec un modèle exponentiel biphasique sont en bon accord avec les résultats expérimentaux. Ainsi, l'efficacité de l'OC avec des concentrations biocompatibles d'OCA a été démontrée. D'autres perspectives de recherche dans cette direction pourraient impliquer l'optimisation de la composition du mélange biocompatible

OCA et CPE en élargissant la liste des produits chimiques à l'étude, ainsi que l'inclusion de cette technique dans de véritables études cliniques sur les lésions cutanées néoplasiques. Pour améliorer la capacité diagnostique de la méthode optique d'analyse cutanée, il est également judicieux d'utiliser une approche multimodale qui combine la technique d'imagerie OCT et diverses méthodes de spectroscopie optique.

Le dernier chapitre 4 conclut la thèse en résumant les principales contributions du travail de thèse et en offrant des perspectives futures.

Acknowledgements

I would like to express my gratitude to:

My supervisor in France, Prof. Walter Blondel, for giving me this invaluable opportunity to participate in the scientific interaction between the CRAN laboratory of the University of Lorraine in France and the Department of Optics and Biophotonics of the Saratov State University in Russia. For the opportunity to act as a link between the two research teams. For his comprehensive support during my stay in Nancy. For the hours spent correcting my articles, present thesis manuscript, discussing scientific work, results and directions for the development of our research. For great kindness to people, endless optimism and sense of humor even in difficult moments. For interesting conversations affecting all aspects, not only the scientific sphere. Finally, for a huge impact on my development as a scientist and researcher.

My co-supervisor in France, Dr. Marine Amouroux, for her great influence on my adaptation in a country that was initially unfamiliar to me. For the time spent helping me through various administrative procedures. For kindness and hospitality, which allowed me to feel like a part of the team. For moral and comprehensive support in difficult times. For involvement in joint scientific activities, discussion of scientific ideas, results and assistance in preparing reports at scientific conferences and scientific publications. For advice on scientific issues that influenced the development of my research skills.

My supervisor in Russia, Prof. Valery Tuchin, for giving me the opportunity to be part of an international research project. For patience, attentiveness and comprehensive advice, affecting all aspects of my scientific activity and expanding its potential. For the fact that I was able to get most of my knowledge and skills, based on his many years of research results, published in countless scientific articles and books. For his special views on scientific research, open to discussion and giving many interesting ideas. For opening this boundless world of physics to me.

My co-supervisor in Russia, Prof. Elina Genina, for her guidance, responsiveness and attentiveness since I was a bachelor student in her laboratory. For countless rich conversations and valuable advice. For the joint discussion of scientific results and the time spent on correcting my scientific publications and this manuscript. For inexhaustible optimism and a fresh look at things that allowed me to become a researcher and scientist, seeing such an example next to me.

Many thanks to the thesis monitoring committee members, Prof. Yuri Kistenev, Madame Céline Frochot and Madame Anne Planat-Chrétien, for their time spent on analyzing my scientific results, reading the thesis, your experience and invaluable contribution to this work. I would like to express special thanks to Dr. Ekaterina Borisova, who passed away untimely due to illness. Her invaluable contribution to my scientific research, based on her vast experience, certainly did not go unnoticed. I am very proud to have known her and had the honor of working with her.

I would also like to separately express my gratitude to Alexey Bashkatov, who, unfortunately, also passed away prematurely due to illness. His vast experience in the field of spectroscopy, biophotonics and physics in general has greatly influenced the development of my skills and my development as a scientist and researcher.

I would like to thank Prof. Igor Meglinski and Prof. Dan Zhu for taking the time out of their schedules and agreeing to read my thesis and participate in my defense as the undisputed experts in our field of research. For the opportunity to meet great scientists, whose work has always been an example of high quality and on which I relied in my scientific field.

I would like to thank the staff of the French Embassy in Russia and Campus France for providing me with funding and the opportunity to stay in France for research on a joint French-Russian PhD program within the framework of the “Vernadsky” PhD grant.

I would like to thank the staff of the international department of the Saratov State University, Dmitry Konakov, Maria Storozhenko and Daria Atkarskaya, for their invaluable help in organizing my studies within the framework of the joint PhD program. For advice and guidance on going through all the necessary administrative procedures and for their attention and kindness.

I would like to express my deep gratitude to the staff of the University of Lorraine, Madame Souad Boutaguermouchet, Madame Sabrina Divoux and Madame Chrstine Pierson, for their time spent on thorough assistance to me related to the issues of passing administrative procedures, solving local problems, organizing international cooperation between the two universities.

I also express my gratitude to the staff of the CRAN laboratory:

Director of the laboratory, Prof. Didier Wolf, for welcoming me to the lab and allowing me to complete this PhD thesis at CRAN.

And also, to all teachers, engineers and technicians of our laboratory. Thanks to you, I was able to become part of the team, share experience and knowledge, complete my project and have a great time. I wish you good luck with your future projects!

Many thanks to all my friends and colleagues that I met in France, who shared their experiences with me and with whom I had the pleasure of spending these 3 years: Victor Colas, Mickaël Gries, Eddy Robin, Yann Bailly, Axel Sorcinelli, Alex Hirtz, Lucie Lerouge, Maria Borozdova, Sidya Drame, Maxim Durand, Julien Pierson, Alicia Chateau, Justine Jubréaux, Manon Douyère, Sophie Tran, Maïssara El Gamah. I would like to thank all my friends and colleagues whom I forgot to mention for their friendship, various events attended, pastimes, advice and support, for making my life interesting, and for brunches, lunches and dinners together. I wish we meet again soon!

Special thanks to my dear friend Cyril Brzenczek, for being there at the most difficult moments, helping to get comfortable in a new place, helping to solve all sorts of problems, from sometimes even very insignificant in his opinion to complex, time-consuming problems. For a lot of joint time spent both within the walls of the laboratory and outside it. For a wonderful friendship, which I am very proud of.

Many thanks to my friends and family members in Russia, for giving me motivation and strength to do science, for always being there, despite the distance and adversity.

Thanks to Valentin Zaytsev, who is my closest family member, for his love, understanding and support.

Finally, I apologize to everyone I forgot to mention.

List of contents

List of figures

List of tables

List of symbols and abbreviations

AF	Autofluorescence
AFS	Autofluorescence Spectroscopy
AUC	Area Under the Curve
BCC	Basal Cell Carcinoma
Ce6	Chlorin e6
CPE	Chemical Permeation Enhancer
DFS	Drug-induced Fluorescence Spectroscopy
DMSO	Dimethyl sulfoxide
DR	Diffuse Reflectance
DRS	Diffuse Reflectance Spectroscopy
FAD	Flavin adenine dinucleotide
FWHM	Full Width at Half-Maximum
HA	Hyaluronic acid
IMC	Inverse Monte Carlo method
ISF	Interstitial Fluid
LC-OCT	Line-field Confocal Optical Coherence Tomography
NA	Numerical Aperture
NADH	Nicotinamide Adenine Dinucleotide Hydride
NIR	Near Infrared
NMSC	Non-Melanoma Skin Cancer
OC	Optical Clearing
OCA	Optical Clearing Agent
OCT	Optical Coherence Tomography
PBS	Phosphate-buffered saline
PEG	Polyethylene glycol
PG	Propylene glycol
RI	Refractive Index
SC	Stratum Corneum
SCC	Squamous Cell Carcinoma
SDS	Source-Detector Separation
SR	Spatially resolved
SR-DRmAF	Spatially Resolved Diffuse Reflectance and multiply excited Autofluorescence spectroscopy
UV	Ultraviolet
μ_a	Absorption coefficient
μ_s	Scattering coefficient

μ_s'	Reduced scattering coefficient
$\boldsymbol{\Phi}$	Radiation flux
$\boldsymbol{L}$	Path length
$\boldsymbol{g}$	Scattering anisotropy factor
$\boldsymbol{n}$	The refractive index
$\boldsymbol{c}$	Speed of light in vacuum
$\boldsymbol{v}$	Speed of light in biological tissue
$\boldsymbol{\delta}$	Depth of light penetration
$\boldsymbol{n_{scatter}}$	Refractive Index of the skin scatterers
$\boldsymbol{n_{ISF}}$	Refractive Index of interstitial fluid
$\boldsymbol{m}$	Relative Refractive Index of skin
$\boldsymbol{f_s}$	Volume fraction of skin scatterers
$\boldsymbol{V_s}$	Absolute volume of scatterers

Contributions

International journals

[IJ1] Prisca Rakotomanga, Charles Soussen, Grégoire Khairallah, Marine Amouroux, **Sergey Zaytsev**, Elina Genina, Hang Chen, Alain Delconte, Christian Daul, Valery Tuchin, Walter Blondel, **(2019)** Source separation approach for the analysis of spatially resolved multiply excited autofluorescence spectra during optical clearing of ex vivo skin, *Biomedical optics express*, 2019, 10 (7), pp.3410-3424. ⟨10.1364/BOE.10.003410⟩

[IJ2] **Sergey M. Zaytsev**, Marine Amouroux, Grégoire Khairallah, Alexey N. Bashkatov, Valery V. Tuchin, Walter Blondel, Elina A. Genina, **(2022)** Impact of optical clearing on ex vivo human skin optical properties characterized by spatially resolved multimodal spectroscopy, *Journal of Biophotonics*, 2022, 15 (1), e202100202. https://doi.org/10.1002/jbio.202100202

Under submission:

[IJ3] **Sergey Zaytsev**, Marine Amouroux, Valery V. Tuchin, Elina A. Genina, Walter Blondel **(2022)** Investigation of the effect of enhanced *in vivo* skin optical clearing with biocompatible agents on the effectiveness of monitoring by the LC-OCT method, *JBO* (submitted).

International conferences

[IC1] Prisca Rakotomanga, Charles Soussen, Grégoire Khairallah, Marine Amouroux, **Sergey Zaytsev**, Elina Genina, Valery Tuchin, Frédéric Marchal, Alain Delconte, Hang Chen, Wei Feng, Dan Zhu, Walter Blondel. **(2018)** Estimation of skin optical properties modified by an optical clearing agent and measured using bimodal tissue spectroscopy*, Saratov Fall Meeting, SFM'18 - 6th International Symposium "Optics and Biophotonics"*, Sep 2018, Saratov, Russia

[IC2] Walter Blondel, Prisca Rakotomanga, **Sergey Zaytsev**, Grégoire Khairallah, Charles Soussen, Elina Genina, Wei Feng, Dan Zhu, Valery Tuchin, Marine Amouroux. **(2019)** Modifications of skin optical properties throughout optical clearing process based on spatially resolved autofluorescence and diffuse reflectance tissue spectroscopy, *12th International Photonics and Optoelectronics Meetings, POEM 2019 – 7th Sino-French Optoelectronics Forum*, Nov 2019, Wuhan, China

[IC3] Prisca Rakotomanga, **Sergey Zaytsev**, Marine Amouroux, Charles Soussen, Grégoire Khairallah, Elina Genina, Valery Tuchin, Walter Blondel. **(2019)** Analysis of skin intrinsic fluorophore contributions during optical clearing: source separation technique applied to spatially resolved multiply excited autofluorescence spectra, *Saratov Fall Meeting, SFM'19 - 7th International Symposium "Optics and Biophotonics" - 23rd International School for Junior Scientists and Students on Optics, Laser Physics & Biophotonics*, Sep 2019, Saratov, Russia

[IC4] **Sergey Zaytsev**, Elina Genina, Alexey Bashkatov, Marine Amouroux, Walter Blondel, Valery Tuchin. **(2020)** Effect of probe pressure and drying on ex vivo skin UV-VIS-NIR spectroscopic signals, *SPIE/COS Photonics Asia (Digital Forum)*, Oct 2020, Beijing, China. pp.11553-50, ⟨10.1117/12.2575195⟩

[IC5] Sophie Tran, **Sergey Zaytsev**, Viktoriya Charykova, Munira Yusupova, Alexey Bashkatov, Elina Genina, Valery Tuchin, Walter Blondel, Marine Amouroux. **(2020)** Analysis of image features for the characterization of skin optical clearing kinetics performed on in vivo human skin using spectral-domain and linefield-confocal optical coherence tomography (OCT), *SPIE/COS Photonics Asia (Digital Forum)*, Oct 2020, Beijing, China. pp.11553-98, ⟨10.1117/12.2575173⟩

[IC6] **Sergey Zaytsev**, Walter Blondel, Marine Amouroux, Grégoire Khairallah, Alexey Bashkatov, Valery Tuchin, Elina Genina. **(2019)** Optical spectroscopy as an effective tool for skin cancer features analysis: applicability investigation, *Saratov Fall Meeting, SFM'19 - 7th International Symposium "Optics and Biophotonics" - 23rd International School for Junior Scientists and Students on Optics, Laser Physics & Biophotonics*, 2019, Saratov, Russia. pp.1145706, ⟨10.1117/12.2564201⟩

[IC7] Vadim Genin, Prisca Rakotomanga, **Sergey Zaytsev**, Elina Genina, Ekaterina Lazareva, Grégoire Khairallah, Marine Amouroux, Charles Soussen, Hang Chen, Wei Feng, Dan Zhu, Alexey Bashkatov, Walter Blondel, Valery Tuchin. **(2018)** Research and development of effective optical technologies for diagnostics in dermatology, *Saratov Fall Meeting, SFM'18 - Optical and Nano-Technologies for Biology and Medicine*, Sep 2018, Saratov, Russia. ⟨10.1117/12.2528700⟩

[IC8] Walter Blondel, Marine Amouroux, **Sergey Zaytsev**, Elina Genina, Victor Colas, Christian Daul, Alexander Pravdin, Valery Tuchin. **(2020)** Skin autofluorescence modifications during optical clearing, *Saratov Fall Meeting, SFM'20 - 8th International Symposium "Optics and Biophotonics" – 24th International School for Junior Scientists and Students on Optics, Laser Physics & Biophotonics*, Sep 2020, Saratov, Russia

[IC9] Walter Blondel, **Sergey Zaytsev**, Victor Colas, Grégoire Khairallah, Prisca Rakotomanga, Charles Soussen, Elina Genina, Christian Daul, Valery Tuchin, Marine Amouroux. **(2020)** Study of the impact of optical clearing on skin absorption, scattering and autofluorescence properties, *19th International Conference on Laser Optics, ICLO 2020 (6th International Symposium on Lasers in Medicine and Biophotonics)*, Nov 2020, St Petersburg, Russia

[IC10] **Sergey Zaytsev**, Walter Blondel, Marine Amouroux, Gregoire Khairallah, Valery Tuchin, Elina Genina. **(2020)** Optical spectroscopy as an effective tool for skin cancer features analysis: applicability investigation, *SPIE Photonics Europe 2020 (presentation at online forum)*, 06-10 april 2020.

[IC11] Elina A. Genina, Alexey N. Bashkatov, **Sergey M. Zaytsev**, Marine Amouroux, Walter Blondel, Valery V. Tuchin, **(2020)** Physical impacts on epidermal permeability in vivo for optical clearing agents, *SPIE Photonics Europe 2020 (presentation at online forum)*, 06-10 april 2020.

[IC12] **Sergey M. Zaytsev**, Alexey N. Bashkatov, Walter Blondel, Marine Amouroux, Valery V. Tuchin, Elina A. Genina, **(2020)** Impact of ex vivo skin dehydration on collimated transmittance spectra kinetics, *Proceedings Volume 11845, Saratov Fall Meeting 2020: Optical and Nanotechnologies for Biology and Medicine*; 118450M (2021) https://doi.org/10.1117/12.2589589

[IC13] **Sergey M. Zaytsev**, V. V. Tuchin, E. A. Genina, Walter Blondel, Marine Amouroux, **(2022)** Development of multimodal approaches for improvement of in vivo optical clearing effect in human skin, *LALS 2021*, Nancy, France.

Book chapters

[BC1] Walter Blondel, Marine Amouroux, **Sergey Zaytsev**, Elina Genina, Victor Colas, Christian Daul, Alexander Pravdin and Valery Tuchin, Human skin autofluorescence and optical clearing, Chapter 5 in *Handbook of Tissue Optical Clearing: New Prospects in Optical Imaging* (Edited By Valery Tuchin, Dan Zhu, Elina A. Genina), ISBN 9780367895099, **2022**.

Introduction

Motivation, aims and objectives

Skin cancer is currently one of the most common human cancers. Basal cell carcinoma (BCC) is the most frequent type of skin cancers, with an average of 8 out of 10 skin cancers being BCC. Typical appearance sites for this type of cancer are the areas of the body that are most actively exposed to the sun (the head and neck area). The specificity of BCC localization leads to the fact that an extremely accurate method of determining the boundaries of the affected area is required, since (i) without sufficient treatment accuracy there is a risk of recurrence and (ii) excessive excision (in case of surgical treatment) affecting areas of healthy tissue is fraught with aesthetic problems (if the PDT technique is not used). The traditional method for diagnosing skin cancer has been histopathological examination, which involves taking a tissue sample from a suspicious skin area for subsequent laboratory examination. The obvious disadvantages of this method are its invasiveness and the duration of the analysis of the obtained samples. Over the past 20 years, optical imaging[1]–[3] and spectroscopy[4]–[6] methods, which are based on the interaction of light with biological tissues, have been widely studied to characterize epithelial tissues in general and skin tissues in particular[4], [5], [7], [8]. Their key features of non-invasiveness, atraumaticity, sensitivity, cost-efficiency and clinical transfer potential, make them *in vivo* diagnostic tools of primary interest, complementary to other clinical gold standard procedures such as histopathology. *In vivo* skin diffuse reflectance (DR)[9]–[11] and autofluorescence (AF)[4], [5], [12]–[14] spectroscopies or the combination of both[15]–[17], and the use of multiple excitation wavelengths for a better diagnostic accuracy[18], have been widely investigated for their applicability to provide a complementary information about the structural and biochemical changes accompanying the development of pathologies in skin tissues. For example, bimodal analysis combining multiply excited AF and DR spectral characteristics[16], [18], [19] resulted in increased diagnostic accuracy compared to a single excitation-AF approach when discriminating between three types of mice skin hyperplasia, or between normal columnar epithelium versus high-grade cervical precancers[20]. However, skin is an optically heterogeneous multilayer organ, each of the layers differing in thickness and morphology. Depending on the type and stage of pathological changes, different layers of the skin and their related structural components may be affected. To serve as efficient and accurate complementary diagnostic tool, optical

spectroscopy techniques thus have to be capable of providing spatial discrimination (depth resolution) between assessed layers[21]–[25].

However, because of the Refractive Index (RI) mismatch between the various skin constituents and intercellular fluid[26], and given skin heterogeneous structure, the photons propagating throughout the skin are strongly scattered and absorbed. This consequently limits light depth penetration in skin tissues and resolution capabilities of optical techniques[27]. The ways to improve the probing depth, the resolving power and the contrast ratio of optical methods of skin *in vivo* characterization have been studied for several decades. The use of chemical agents featuring a RI close to that of skin cellular components leads to a decrease in the RI mismatch between the cellular tissue components and the extracellular fluid and, consequently, to a decrease of skin scattering. With a decrease in skin scattering, the probing depth and contrast of *in vivo* optical methods may increase since more ballistic photons can propagate within the skin. This technique has been called tissue Optical Clearing (OC)[28]–[30].

Therefore, we believe that an integrated approach is required to improve the diagnostic accuracy in the clinical analysis of skin cancer, which implies the combined use of *in vivo* multimodal optical spectro-imaging methods and of skin optical clearing technique. The multimodal approach will allow combining the photodiagnostic complementary advantages of different tissue characterization optical methods with the spatial discrimination between probed skin constituents, while the optical clearing technology will help to improve the depth resolution and contrast of these methods.

However, the barrier function of the stratum corneum (SC), which limits the use of most of the known optical clearing agents (OCA), must also be considered. Many studies have shown the effectiveness of chemical agents that can disrupt the natural structure of keratin and SC lipids, thereby creating penetration pathways for the OCA through this barrier. Such chemical agents, called Chemical Permeation Enhancers (CPE), are represented by several groups of substances, among which the most commonly found in the literature are alcohol (ethanol, propylene glycol)[31], solvents (dimethyl sulfoxide)[1], [2], organic acids (oleic and linoleic acids)[1], [32], as well as azones (azone and thiazone)[1], [3]. The use of CPE together with OCA can significantly enhance the OCAs effect.

Taking into account the problems mentioned above, the following objectives were addressed in this thesis work:

- Experimental investigation of the impact of OC process applied to *ex vivo* human skin samples on DR and AF spectra using a spatially resolved (SR) multimodal spectroscopy device “SpectroLive” dedicated to skin optical biopsy and two combinations of OCA and CPE;
- Quantification of the clearing-like effect caused by the sample drying and by the spectroscopic probe pressure applied on skin;
- Development of the biocompatible OCA/CPE compositions that might be safely used at the lesional human skin areas *in vivo* in clinics;
- Quantification of *in vivo* OC efficacy of clinically-compatible clearing agents using images acquired by line-field confocal-optical coherence tomography (LC-OCT).

Specific context of the thesis

This thesis represents the work which was done within a French-Russian co-supervision frame (French-Russian PhD grant «Vernadski» from the French Embassy in Russia) involving the complementary expertise and collaboration of two partner teams: Research Center on Automatic Control (CRAN) of University of Lorraine (Nancy, France) and Research-Educational Institute of Optics and Biophotonics (REI OBP) of Saratov State University (Saratov, Russia). Experimental protocols involving human skin *ex vivo* and *in vivo* SR DR and AF spectroscopy and LC-OCT imaging were conducted at CRAN in collaboration with the Metz-Thionville regional hospital in France. Complementary experimental protocols with the rat skin *ex vivo* on the clearing-like effect quantification caused by the sample drying and by the spectroscopic probe pressure applied on skin were conducted at REI OBP laboratory in Russia.

Thesis outline

The manuscript starts with an introduction. The first section «Motivation, aims and objectives» provides the motivation, actuality, and main objectives of this study. The specific context of the thesis is provided in the section of the same name in Introduction. The outline of the thesis is presented in current section.

Chapter 1 presents the state of the art, related to this thesis. In Section 1.1, the structure of skin and its optical properties are described, and the obvious disadvantages of using existing optical methods in clinical conditions, associated with the highly scattering properties of skin,

are considered. Section 2.1 is devoted to the application of optical methods on skin. Various spectroscopic approaches are described in Section 1.2.1, while the imaging techniques are presented in Section 1.2.2. Finally, the multimodal techniques, which are combinations of different optical techniques, are described in Section 1.2.3. In section 1.3, the method of optical clearing of biological tissue is presented. The principle of its action is given in Section 1.3.1, different groups of OCA are described in Section 1.3.2 in terms of physical and chemical properties, advantages and disadvantages of their use, and potential toxicity. Section 1.3.3 provides an information about various physical and chemical methods of enhancing the permeability of biological tissues. Then, the scientific literature examples of the use of optical clearing with optical diagnostic techniques are presented in Section 1.3.4.

Chapters 2 and 3 are dedicated to present the experimental results obtained during the PhD work. An impact of optical clearing on *ex vivo* human skin optical properties characterized by spatially resolved multimodal spectroscopy was the main aim of the experimental study presented in Chapter 2. Chapter 3 presents the results of the consecutive experimental protocol, which main goal was to estimate *in vivo* OC efficacy of clinically compatible clearing agents by the means of LC-OCT imaging technique.

The last Chapter 4 concludes the thesis by summarizing the key findings of the PhD work and providing future perspectives.

1. State of the art

1.1. Skin structure and optical properties

Skin is the largest human organ, with an area of about 2 m^2. The skin accounts for about 15% of the total body weight of a person[33]. Being an interface between the human body and the environment, the skin performs a natural function of a physiological barrier, protecting the body from ultraviolet (UV) rays, external physical influences and retaining water inside the body[34]. The skin consists of three main layers: epidermis, dermis and adipose tissue (hypodermis). Due to its inhomogeneous structure, the interaction of light with the skin is complex and therefore the skin is considered to be a highly scattering medium.

In general, when the light penetrates into biological tissues through the air-tissue interface, part of the radiation incident on the interface is reflected, and the rest penetrates into the tissue. When the radiation that has passed inside propagates through the biological tissue, it is attenuated due to the mechanisms of **absorption** and **scattering**. The optical property of a biological tissue that characterizes its absorption is the absorption coefficient $\boldsymbol{\mu_a(\lambda)}$, which determines the fraction of the radiation flux $\Phi(\lambda)$ absorbed over a unit path length L *in an absorbing medium :* $\mu_a(\lambda) = -d\Phi(\lambda)/dL$[26], [35]. The scattering coefficient of a biological tissue $\boldsymbol{\mu_s(\lambda)}$ is an optical property that determines the attenuation of a collimated radiation beam during propagation through a non-absorbing medium: $T(\lambda) = exp(-\mu_s(\lambda)L)$[26], [35], [36]. The typical unit of measure for these two coefficients is cm^{-1}. Knowing both coefficients, it is possible to calculate the total attenuation coefficient of the medium as[37]

$$\mu_t(\lambda)=\mu_a(\lambda)+\mu_s(\lambda). \quad (1)$$

Upon a single elastic scattering act, a photon deviates from its original direction, which is affected by the wavelength λ of the scattered photon and the size of the scatterer in the biological tissue. In this case, the average angle Θ, by which the direction of the photon's motion deviates during each scattering event, determines the value $\boldsymbol{g}$, which is called the scattering anisotropy factor[26], [35], [38]. This value varies from -1 to 1 with g=-1 corresponding to total backscattering, g=0 to isotropic scattering (Rayleigh scattering) and g=1 to forward scattering[26], [38], [39].

The coefficient that determines the directness of scattered photons is called the reduced scattering coefficient, since it takes into account such optical properties as the scattering

coefficient $\mu_s(\lambda)$ and the scattering anisotropy factor g, and is determined by the formula[26], [38], [39]

$$\mu_s' = \mu_s(1 - g). \quad (2)$$

Another relevant optical property of biological tissues is their refractive index (RI), which makes it possible to determine the speed of radiation propagation in the medium and also to determine the change in its direction when passing through the interface between the media. The refractive index is determined by the formula

$$n=c/v, \quad (3)$$

where c is the speed of light in vacuum and v is the speed of light in biological tissue[35]–[37].

1.1.1. Epidermis

The epidermis is the outermost skin layer, performing a protective function. It belongs to the multilayer epithelial tissue group. The thickness of the human epidermis layer in most cases varies in the range of 75-150 µm, although in the facial area this thickness is only 20 µm, and in the plantar areas (palms, feet) it reaches up to 5000 µm[26], [40], [41]. Conventionally, the epidermis can be divided into 4 or 5 (**Figure 1**) layers (depending on the area considered), which, in turn, can be divided into living and non-living epidermis.

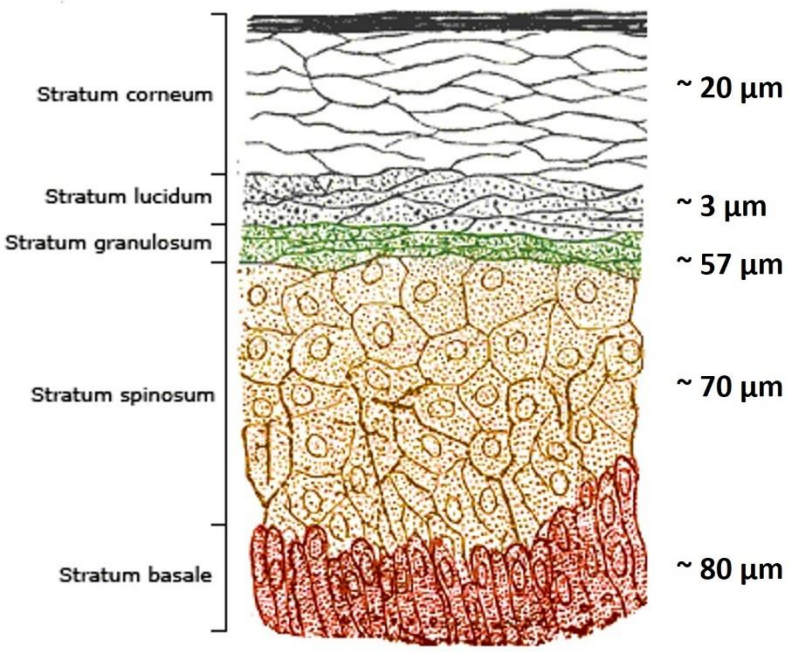

Figure 1. Schematic representation of the epidermis structure, indicating the corresponding layers[42].

The outermost layer of the epidermis is the **stratum corneum** (SC), whose average thickness is 20 µm or 20 cell layers[40], [41]. It is an example of a non-living epidermis layer, as it consists mainly of dead, non-nuclear keratinocytes that have transformed into flat

lamellae. The intercellular domain of the SC occupied by a lipid bilayer consisting mainly of fatty acids, cholesterol, and sphingolipids. This structure of keratinocyte lamellae and lipid bilayer, called in the literature “brick and mortar”, makes the SC a dense medium that makes it difficult for external molecules to diffuse in both directions[26], [40], [43] and thus represents a protective screen against chemical as well as mechanical damage. The physico-chemical SC barrier properties depend on its water content. The SC water supply from the inside of the body occurs due to the sweat glands and diffusion through the underlying tissues saturated with water. The outer cellular layers of the SC are in balance with the environment in terms of their water content, while the deep layers of the SC are in balance with the neighboring living layers of the epidermis, which are well hydrated. Due to this, a water concentration gradient is present in the SC, causing transepidermal water loss[26].

The next layer, the **stratum lucidum**, is found under the SC only in the areas of the palm and sole, and together with the remaining 4 layers forms the so-called "thick skin". It usually consists of 3-5 layers of dead keratinocytes, which are filled with eleidin, an intermediate form of keratin[26].

Under the stratum corneum (or under the stratum lucidum, in the case of the palms and soles) is the **stratum granulosum**. This is the surface layer of the so-called living epidermis, the average thickness of which is ~57 μm[41]. It consists of keratinocytes containing keratohyalin granules. On the border with the SC, these cells secrete lamellar bodies rich in proteins and lipids into the intercellular space, while losing their nuclei and organelles. Subsequently, this leads to the corresponding formation of dead keratin scales and lipid bilayer in the SC.

Below, between the stratum granulosum and stratum basale, there is a **stratum spinosum** – layer of the epidermis, where the active keratinization of multifaceted keratinocytes begins to occur. This layer also contains Langerhan cells, which are involved in the immune system functioning. The thickness of this layer is approximately 70 μm[41].

On the border with the dermis, being separated from it by the basement membrane, there is the lowest germinating layer of the epidermis - **stratum basale**, consisting of a single layer of columnar basal cells. Its average thickness is 80 μm[41]. In this layer, cell division occurs by some of the basal cells, from which the entire process of formation of keratinocytes and subsequent keratinization of the epidermis begins. This process continues constantly and determines the renewal of the human epidermis.

The two lower layers of the epidermis also contain melanocytes - cells that produce the pigment melanin. Contained in melanosomes, it is transported through the sprouts of melanocytes to the epidermal keratinocytes, where it protects them from the UV damaging effects. The content of melanin in the skin determines its pigmentation, divided for practical purposes by the Fitzpatrick scale into six phototypes from the first i.e. the lightest (Celtic) corresponding to people adapted to environment of low UV radiations (sunlight), to the sixth (African) i.e. the darkest corresponding to people with most resistance to the effects of UV radiation and almost no chance of sunburn[26].

Melanin is one of the main components of the skin that determines its absorption properties. It absorbs radiation passing through the epidermal layer in almost the entire visible spectral range, with increasing absorption when shifted to the short-wavelength region of the visible spectrum[26], [36]. The absorption coefficients $\mu_a(\lambda)$ measured by the integrating sphere and the Inverse Monte Carlo (IMC) method for a 100 µm layer of the epidermis at wavelengths of 337 nm, 577 nm and 633 nm are, respectively, 32 cm^{-1}, 10.7 cm^{-1} and 4.3 cm^{-1}[35], [44].

The scattering coefficients $\mu_s(\lambda)$ of the epidermis greatly exceed absorption. At wavelengths of 337 nm, 577 nm, and 633 nm they are 165 cm^{-1}, 120 cm^{-1} and 107 cm^{-1}, respectively[35]. The main contributor to the scattering of the epidermis is optical inhomogeneity caused by the difference in RI between the main structural components of the epidermis (commonly referred to as scatterers) and the surrounding fluid, such as the cellular cytoplasm or interstitial fluid (ISF), mainly composed of water with a small amount of dissolved salts[45], [46]. In addition to this, the non-living epidermis represented by the SC and the remaining layers of the epidermis differ in their total RI in the visible and near infrared wavelengths (1.5-1.55 for the SC versus 1.34-1.39 for the living epidermis)[36], [47], [48], which is caused by several factors, the major ones being the difference in each layer's structure as well as the uneven distribution of water concentration among the epidermal layers[26], [49].

1.1.2. Dermis

The dermis is the fibrous connective tissue layer of the skin located under the epidermis (**Figure 2**). It performs mainly trophic and supporting functions, which determines its structure. The main components of the dermis are structural proteins in the form of fibers (which is why it is referred to as fibrous tissues) - elastin and, mainly, collagen. The interfiber

space is filled with the main substance, consisting of water and salts dissolved in it. The volume fraction of water in the dermis is ~70%[26], [36], [50], [51].

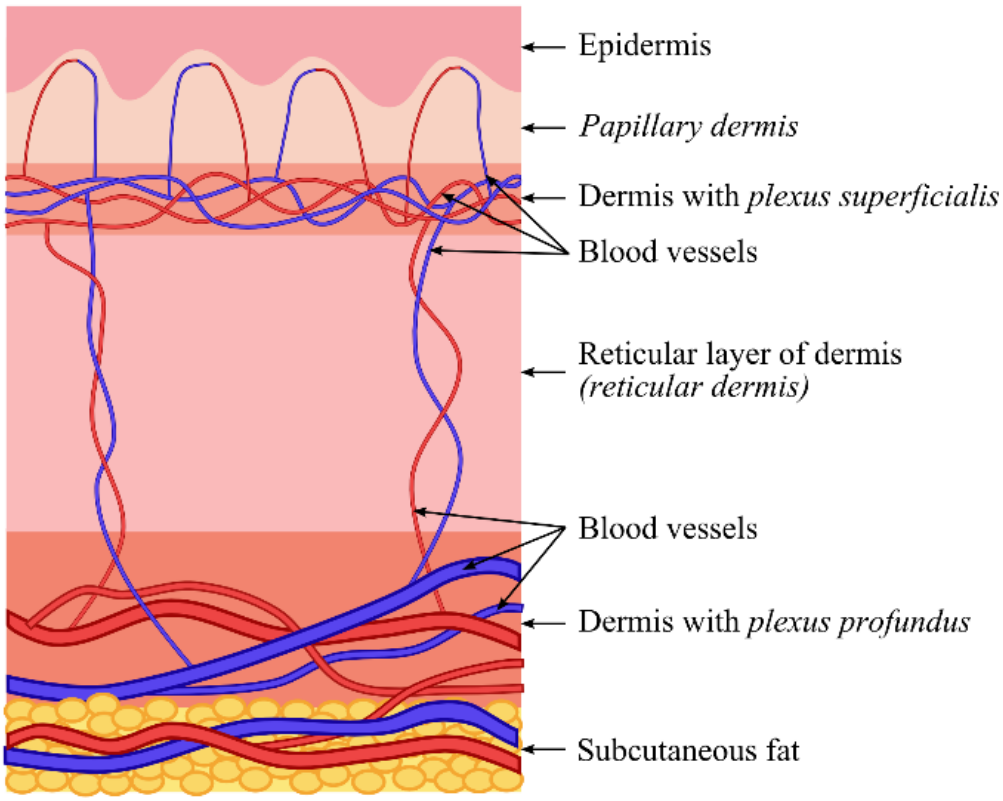

Figure 2. Schematic representation of skin layers[41].

The dermis is divided into two layers. The first layer is the **papillary dermis**. It is connected to the epidermis by a basement membrane and is so named because of the protrusions called papillae, which contribute to the trophism of the epidermis due to the large area of contact with it. In this layer, there are terminal blood capillaries and lymphatic plexuses, extending, respectively, from the arterioles that form the subpapillary (superficial) arterial network in the lower part of this layer and from the superficial lymphatic plexus, which lies below the superficial arterial network. The structure of collagen fibers in this layer is mainly thin (about 60 nm in diameter[26]) and loose. The average thickness of this layer is about 100 µm[36].

The **reticular dermis** is the lower region of the dermis that smoothly passes into the adipose tissue. It is usually much thicker than the overlying papillary dermis (1–2 mm thick)[36], [52]. It is characterized as a dense irregular connective tissue containing ordered bundles of collagen fibers, which is reflected in its name. Elastin fibers are located mainly in this layer as a network[53]. The reticular dermis performs elastic properties, giving the skin elasticity. In most parts of the human body, sweat and sebaceous skin glands, as well as hair

follicles, originate in this layer[36]. On the border with adipose tissue, there is a deep cutaneous arterial network connected to the superficial arterial network by "branches" penetrating the reticular dermis[26], [41], [52].

The blood contained in the dermis determines the absorption properties of this layer, as well as the melanin in the epidermis. The main blood elements that absorb visible radiation are hemoglobin, bilirubin and β-carotene[36]. The absorption coefficients $\mu_a(\lambda)$ (obtained by the IMC method) for a 200 μm dermis layer at λ=337 nm, 577 nm and 633 nm, are respectively 23 cm^{-1}, 3 cm^{-1} and 2.7 cm^{-1}[35], [44]. At the same time, with a shift to the infrared region of the spectrum, absorption of water begins to be observed, which is contained in large quantities in this skin layer.

Collagen fibers are the main skin components which determine its scattering properties. Dermal scattering coefficients $\mu_s(\lambda)$ were measured by the IMC method for wavelengths of 337 nm, 577 nm and 633 nm as 227 cm^{-1}, 205 cm^{-1} and 187 cm^{-1}, respectively[35]. Such large values can be explained by the fact that scattering occurs on collagen fibers and their bundles due to the large difference in RI between collagen and the liquid surrounding the fibers, which consists mainly of water. The dependence of the scattering nature on the degree of order and size of collagen fibers is also observed. For example, the papillary dermis is characterized by strong backscattering due to the small size of the collagen fibers contained in it compared to the wavelengths of the visible range ($d<\lambda$). In the reticular dermis, due to the relatively large size of the collagen bundles, strong forward scattering takes place[36], [54]. The dermis RI in the near infrared (NIR) and visible wavelengths is approximately 1.4[48].

1.1.3. Adipose tissue

The **adipose tissue**, or **hypodermis**, is the lowest layer of human skin, attached by fibrous ligaments to the deep fascia[55]. It is composed of loose connective tissue as well as fibroblast cells, macrophages, and (predominantly) adipocytes (**Figure 3**). This layer contains blood vessels, as well as the glandular parts of some sweat glands and the roots of hair follicles[26].

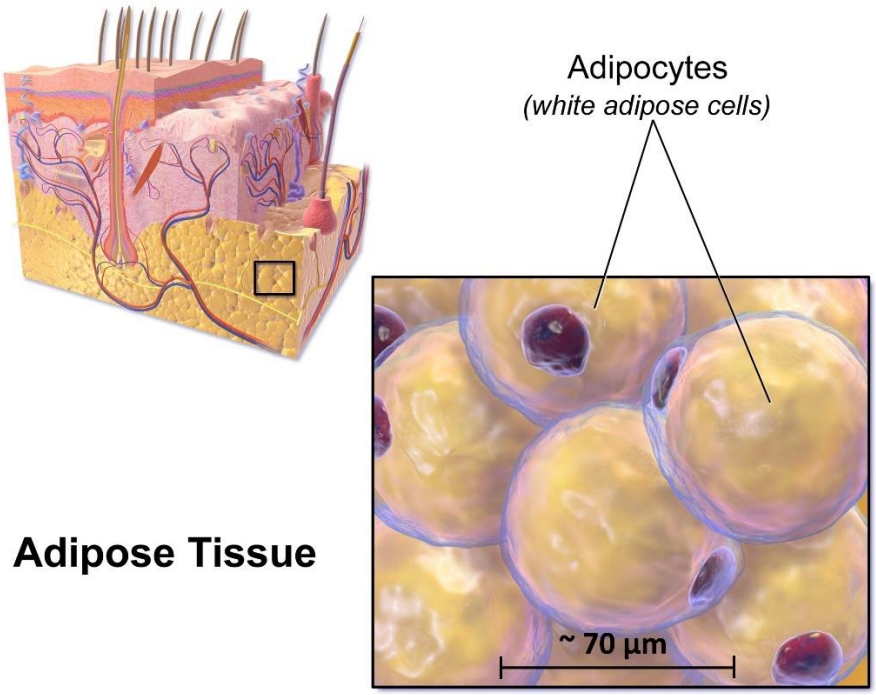

Figure 3. Micro anatomy of subcutaneous fat[56].

Subcutaneous fat, represented in the hypodermis by adipocytes, is its most spreaded layer[57]. It consists of adipocytes grouped into lobules, which are surrounded by connective tissue that performs a supporting role[41]. Fat in the form of triglycerides occupies almost the entire volume of adipocytes, and their cell nuclei are relatively small in size and located on the edge of the cell[41]. These cells are relatively large in size (20-120 µm) and serve to store energy and perform a thermoregulatory function. The space between cells is occupied by interstitial fluid, capillaries and nerves[41]. Recently, it was demonstrated that innate arrangements of the individual adipocytes may act as a cascade of quasi-ordered microscale lenses confining propagation of light within the adipose tissue similar as in lens lightguides[58].

The absorption of the hypodermis is determined by the water and lipids in it, as well as the elements of the blood contained in the vessels (hemoglobin, bilirubin, β-carotene)[26], [36]. At a wavelength of 633 nm, the hypodermis absorption coefficient was measured by the integrating sphere and IMC method as 1.4±0.3 cm^{-1}[59] at g=0.8. Scattering in the hypodermis occurs mainly on lipid droplets uniformly distributed in adipocytes. The reduced scattering coefficient of the hypodermis in the same work was calculated as 2.54±0.3 cm^{-1} at g=0.8. The RI of adipose tissue in the NIR and visible wavelength ranges is approximately 1.44–1.45[60], [61].

1.1.4. Limitations of the use of optical methods

The general optical properties of the skin, which is a heterogeneous medium, are a combination of the local optical properties of its individual components, which form layers of different structure[26]. Optical properties, in turn, directly depend on the wavelength λ of radiation. Therefore, the potential of using non-invasive or minimally invasive optical methods for skin examination is related to the need to consider the specific absorption bands of certain skin absorbers, such as, for example, melanin, hemoglobin, water and lipids[26], [36], [62], [63]. Also, from the sections above the scattering coefficient of the skin layers $\mu_s(\lambda)$ is significantly higher at the respective wavelengths than the absorption coefficient $\mu_a(\lambda)$. Moreover, there is an inverse dependence of the scattering coefficient on the wavelength λ in the visible and NIR spectral ranges, which reflects the contribution of the Rayleigh scattering components (the emission wavelength is much larger than the diameter of the scatterers) and Mie scattering (the emission wavelength is equal to or less than the diameter of the scatterers)[35]. An interesting optical property that relates the absorption and scattering coefficients, as well as the scattering anisotropy factor, is the depth of light penetration into the biological tissue ($\boldsymbol{\delta}$). It reflects how deeply light at a certain λ can penetrate a medium before its intensity due to losses associated with absorption and scattering is 37% of the initial intensity[26], [35]. In the diffuse approximation, this quantity is the inverse of the effective extinction coefficient μ_{eff} expressed as[64], [65]

$$\delta = \frac{1}{\mu_{eff}} = \frac{1}{\sqrt{3\mu_a(\mu_a - \mu_s')}}. \quad (3)$$

To avoid the reduced depth of light penetration due to the absorption bands of certain components of biological tissue, optical methods require the use of certain wavelengths of the visible and near infrared ranges. Nowadays, a lot of data has been obtained on the optical properties of blood and various biological tissues, and due to the presence of local maxima in δ associated with absorption and scattering spectra, five so-called "diagnostic windows" have been proposed for diagnostic and therapeutic purposes, representing wavelength ranges[66]: 350-400 nm, 625-975 nm, 1100-1350 nm, 1600-1870 nm and 2100-2300 nm.

However, even within these diagnostic ranges, the skin still has strong scattering properties. This results in relatively low depth resolution and contrast, and the full potential of optical methods is limited to imaging or spectra acquisition only from the upper layers of

biological tissues. This is the main limitation of the use of optical methods in the diagnosis and therapy[26].

1.2. Optical methods for skin diagnostics

For many years, the main method of diagnosing skin diseases in the clinical setting was a visual inspection conducted by a dermatologist, which required special training and experience, but at the same time did not deprive this method of a certain subjectivity[67]. To obtain information about the biochemical composition of the skin, for example, to differentiate between skin cancer and non-malignant lesions, it was necessary to use such gold standards as histological examination and biopsy. Obvious drawbacks with this approach are invasiveness, the inability to obtain results in a short period of time *in situ*, and unreliability, since samples taken for research could be spoiled during preparation.

The development of technologies in the optical field, such as the advent of lasers to the market, as well as the development of computer technologies, led to the emergence of a large number of optical methods, many of which quickly found their way into medical diagnostics[17], [26]. Their common advantages are relative compactness (allowing the use of optical methods in clinics), speed of obtaining results, as well as non-invasiveness, coupled with the use of safe electromagnetic radiation ranges. In this subchapter, the main optical methods of imaging and spectroscopy that have found application in modern skin diagnostics will be reviewed, their advantages and disadvantages will be considered, and examples of the combined use of several optical methods that enhance the advantages and compensate for the disadvantages of the latter are given.

1.2.1. Spectroscopic techniques

The measurement of skin optical parameters, such as, for example, scattering and absorption, in the UV, visible and NIR ranges laid the foundation for the optical spectroscopic methods. These methods are mainly based on the use of fiber optic probes, which is convenient for measurements on any part of the body. As described in the previous section, the skin is a heterogeneous organ in its structure and contains many scatterers and absorbers, such as hemoglobin, melanin, water, lipids, collagen, elastin and keratin[26]. The measurement of a single spectrum makes it possible to estimate the molecular concentration

of these skin structural elements. By comparing the spectra obtained on the skin area that causing doubts for a specialist with the spectra measured on healthy skin (the so-called reference spectra), it becomes possible to determine the type of neoplasm, depending on the change in the concentration of a particular component[18], [68]–[70].

Fluorescence spectroscopy

Fluorescence spectroscopy has been actively used for skin analysis since the end of the last century[71]–[78]. It is based on the phenomenon of fluorescence - the emission of photons by molecules in an excited state (fluorophores). When a fluorophore absorbs an incident photon (typically UV or visible light), the energy of the absorbed photon causes the molecule to go from the ground state to one of the excited singlet electronic states, S1 or S2[26]. From this state, a transition back to the ground state is possible due to radiative (fluorescence (k_f) or phosphorescence) or nonradiative processes (nonradiative relaxation or internal conversion (k_{IC})) (**Figure 4**). Upon transition to the ground state due to fluorescence, the molecule emits a photon whose energy is lower than the energy of the absorbed photon and is related to (i) the difference in the energy of the two electronic states of the molecule and (ii) the thermal dissipation loss of the absorbed energy by the molecule. Therefore, the wavelength λ_{em} of the emitted photon is greater than that of the absorbed one (λ_{exc}). The intensity of the fluorescent radiation is proportional to the intensity of the radiation incident on the skin. Both low-coherent light (xenon lamps) and high-coherent laser radiation are used as light sources for fluorescence spectroscopy[26], [79], [80]. Spectroscopic probes are usually made in a fiber configuration, which makes it easy to measure any area of the skin.

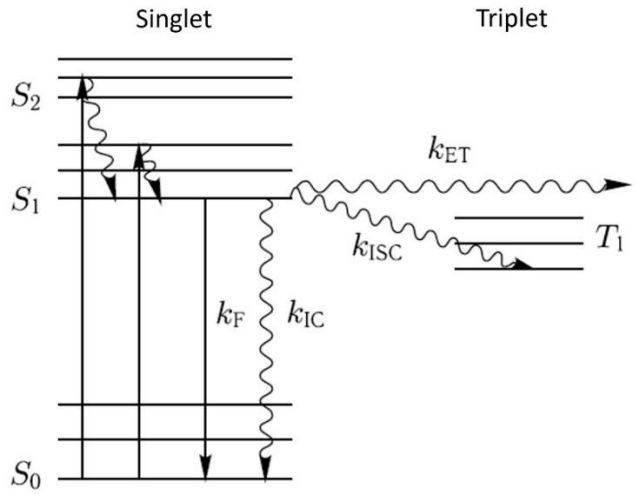

Figure 4. Jablonski diagram of molecular energy levels and transition rates. Straight lines are radiative transitions, wavy lines are nonradiative transitions[26].

The skin contains several naturally occurring fluorophores found in various layers. In general, the excitation wavelength of 315 nm is the cutoff wavelength separating epidermal and dermal fluorophores[78]. The main skin fluorophores (**Figure 5**), which are considered to be internal biomarkers of pathological processes, are metabolic products (tryptophan, NADH, FAD, porphyrins) of the skin and its structural components (keratin, collagen, elastin)[70]. Various pathological processes in the body lead not only to changes in the structure of the skin, but also to biochemical changes accompanied by variations in the fluorescent signal of a particular biomarker. The effectiveness of fluorescence spectroscopy, which specializes in the analysis of internal skin biomarkers (the so-called autofluorescence spectroscopy - AFS) has been shown in many works[16], [18], [69], [70], [81]–[85]. For example, some studies have shown that when comparing the AF spectra of healthy skin and skin with BCC, pronounced peaks at 620 and 680 nm, corresponding to protoporphyrin IX, are observed in the BCC spectra (**Figure 6**)[83], [86]. An *in vivo* analysis of AF spectra conducted in different studies on BCC[83], [86]–[90], squamous cell carcinoma (SCC)[88], [89] and melanoma[91] showed that when using excitation wavelengths in the range of 337-442 nm, consistent results are observed, showing a decrease in the fluorescence signal of pathologically altered areas in comparison with healthy skin. The strongest differences were found in the wavelength range of 370–395 nm between the autofluorescence intensity spectra of BCC and healthy skin.

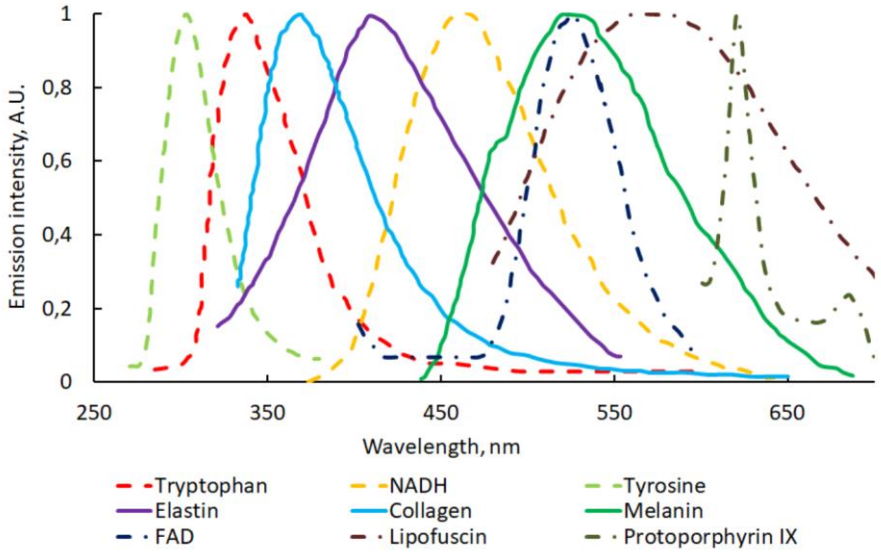

Figure 5. Monte Carlo simulated emission spectra of skin fluorophores[92].

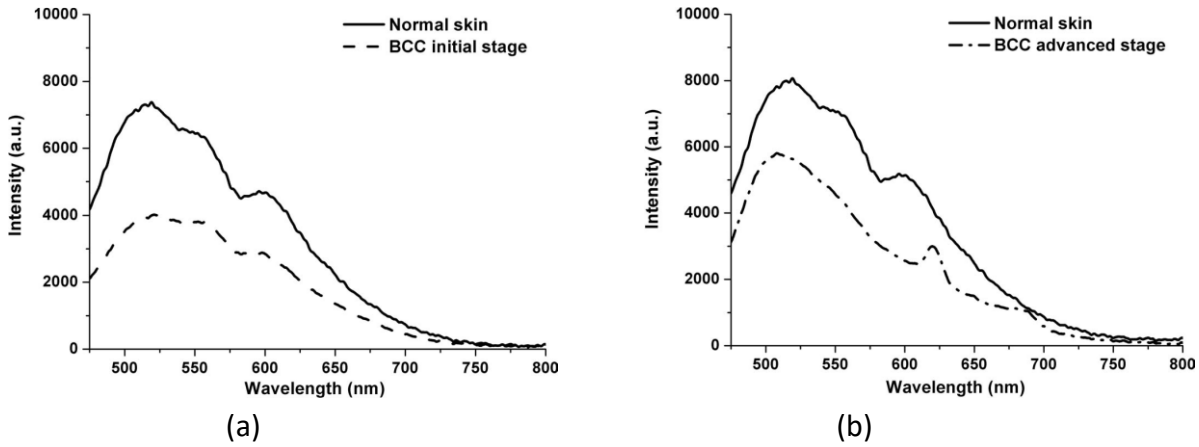

(a) (b)

Figure 6. Comparison of the fluorescence spectra of normal skin with (a) initial stage of BCC and (b) two-year BCC, excited at 405 nm[83].

The main disadvantages of AF spectroscopy are the low intensity of emission by endogenous fluorophores, the high sensitivity of the fluorescence signal to internal factors (pH and temperature), the high physiological diversity between different skin areas of the same patient and between patients, and the difficulty in distinguishing the spectral contributions of individual fluorophores to the AF signal due to strong spectral overlap of their excitation and emission spectra[26]. Due to the strong scattering of light by the skin, the penetration depth of λ_{exc} mainly used in AF spectroscopy does not exceed 1 mm[79].

The intensity of skin fluorescence can be increased by the use of exogenous fluorophores, which can be deposited in diseased cells (mainly cancer cells) and serve as markers for the presence of certain diseases, showing their characteristic, high-intensity peaks in the fluorescence spectra. This fluorescence technique is called the drug-induced fluorescence spectroscopy (DFS). Clinical studies have shown that DFS has a definite advantage over AFS due to the high intensity of exogenous fluorophores. However, the choice of an appropriate fluorophore, the time it takes for the fluorophore to accumulate in the affected areas of the skin, and the potential side effects of using an exogenous substance, coupled with the need for documented approval for its use are the main limitations of the DFS technique.

The use of DFS versus histology for early detection of non-melanoma skin cancer (NMSC) has been controversial. On the one hand, some studies reported high sensitivity and specificity of the method[93], [94], on the other hand, some scientific groups reported the lack of DFS potential in the early diagnosis of precancerous skin changes[95], [96].

Despite the obvious disadvantages, obtaining information about the biochemical structure of the skin in real time, offered by the method of fluorescence spectroscopy, makes this method attractive for the clinical diagnosis of skin lesions.

Diffuse Reflectance spectroscopy

The first works that experimentally demonstrated the efficiency of diffuse reflectance spectroscopy (DRS) appeared back in 1939[97]. Since then, the experimental setup has undergone significant changes, mainly to increase its portability through the use of a small spectrometer connected to a computer and a light source. The fiber optic probe, which is mainly used in modern versions for delivering incident radiation to the skin and recording reflected light, allows measurements in any geometry from various skin areas *in vivo*[33]. The principle of DRS is that the recorded spectra contain not only the component of direct (specular) reflection from the skin surface. Only 4% of the incident radiation is reflected directly by the skin surface. Most of the incident visible radiation passes into the skin to a depth of 1 mm, where it experiences many scattering events on natural scatterers before it goes out, where it is recorded by a fiber probe. The multiple scattering means that the photon travels a long way inside the skin, and is likely to be absorbed by skin chromophores[33], [79]. Thus, the obtained DR spectra contain characteristic areas (bands) formed due to the presence of various chromophores in the skin. The main skin chromophores are shown in **Table 1**.

Table 1. The main skin chromophores in the visible and NIR ranges. Data taken from[79].

Chromophore	Absorption bands (nm)	Skin parameter
Oxyhemoglobin	412, 542, 577	Capillary and arteriolar blood
Deoxyhemoglobin	430, 555, 753	Venous blood
Melanin	No peaks, monotonous decrease towards longer wavelengths	Skin pigment
Water	760, NIR bands	Interstitial fluid, edema

The use of DRS for skin diagnostics is based on the analysis of changes in DR spectra that occur as a result of structural changes at the cellular and subcellular levels induced by pathological processes. The use of diffusion approximation, various numerical methods, and the use of absorption spectra of pure components[98]–[102] allow to get an information on the concentration of internal absorbers (**Figure 7**), which, together with structural information, makes DRS a suitable method for analyzing the skin for early detection of pathological processes.

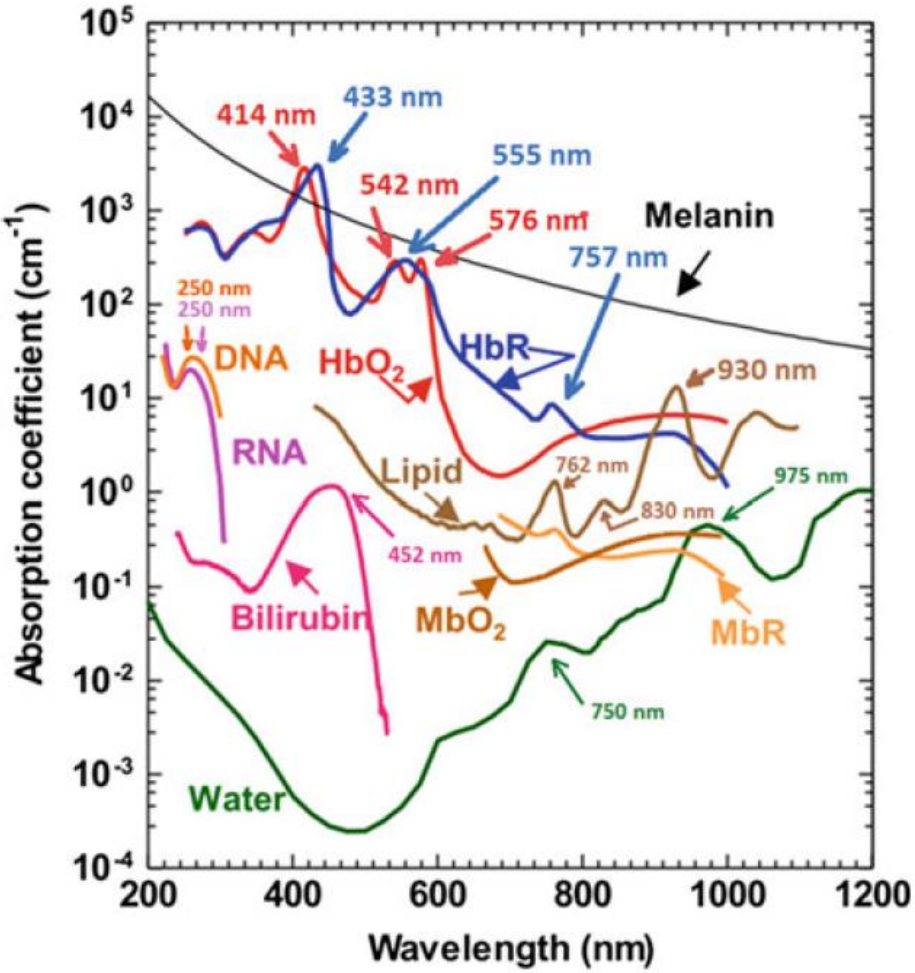

Figure 7. Absorption spectra $\mu_a(\lambda)$ from various components of skin and other biological tissues[35].

In the works carried out at the end of the last century, it was shown that it is possible to determine the spectral features of various facultative pigmentations, which is difficult to implement during visual examination and previously required histological analysis[103]–[107]. It turned out that epidermal pigmentation caused by ultraviolet and solar radiation differs from natural pigmentation when analyzing DR spectra. For example, the spectra of skin induced by UVB radiation differ from the spectra of constitutive (natural) pigmentation at short wavelengths (<335 nm), and the pigment caused by UVA radiation shows significant differences from constitutive pigmentation in the visible part of the spectrum.

In recent years, DRS has been actively used to differentiate between healthy and cancerous skin, and also skin subjected to precancerous changes. The obtained values of specificity and sensitivity varied, on average, for different groups of researchers, between 72-92% and 64-92%, respectively. These values directly depend on various spectral characteristics, such as the integral value of the absorption and reduced scattering coefficients (**Figure 8**)[108], [109], the overall slope of the spectral curve[110], or the integral value of the

diffuse reflection value in specific spectral regions[111]–[113], calculated for healthy and lesional areas of the skin.

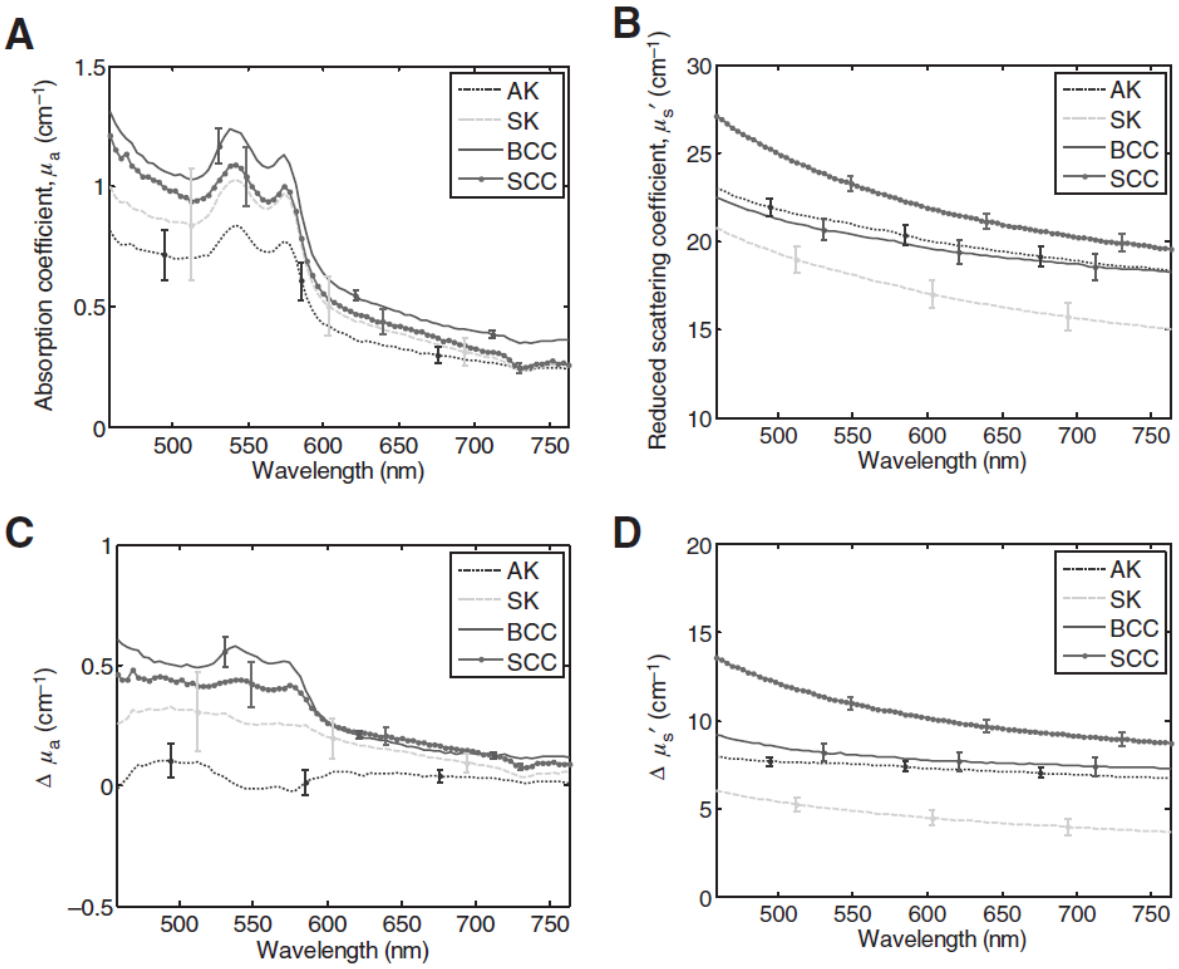

Figure 8. Average absorption coefficient spectra (a), average reduced scattering coefficient spectra (b), average differential absorption coefficient spectra (c), and average differential reduced scattering coefficient spectra (d) for SCC, BCC, actinic keratosis (AK), and seborrheic keratosis (SK). The error bars represent standard errors[109].

Thus, among the advantages of DRS, one can single out the speed, accuracy, and non-invasiveness in diagnosing the structural and biochemical composition of the skin. Accordingly, this technique significantly exceeds the analytical capabilities of the human eye, having high sensitivity and specificity in the differential analysis of pathological processes, and, therefore, eliminates invasive histological methods of analysis. The main disadvantage of DRS is the small (up to 1 mm) depth of penetration of incident radiation, caused by strong scattering of the skin upper layers.

Raman spectroscopy

This method of spectroscopy is based on the effect of Raman scattering, discovered in 1921. With this type of scattering, unlike Rayleigh, an inelastic interaction of a photon with a

certain molecule occurs, because of which the photon energy changes up or down, depending on the difference between the initial and final vibrational energy levels of the scattering molecule. These scattering events, therefore, appear in the recorded spectra as a series of peaks that are specific for different molecules. This makes it possible to analyze the molecular composition of the sample under study using its Raman spectrum[26]. Since approximately one photon is recorded in Raman scattering approach for every billion emitted photons, Raman spectroscopy was applied for skin diagnostic purposes only in the second half of the 20th century, with the invention of lasers - highly coherent monochromatic light sources that make it possible to focus a high-intensity photon flux onto a small area[114]–[121]. The use of this technique in combination with fiber optic probes has allowed for easily accessible measurements of any area of the skin *in vivo* and *ex vivo*[122], [123].

The modern use of Raman spectroscopy in skin diagnostics is mainly aimed at identifying the processes that accompany skin cancer. Many methods are used to analyze Raman spectra[122]–[128], including complex approaches such as analysis involving neural networks[129]. In most of the studies carried out, it was concluded that it is preferable to combine different methods of analyzing the obtained spectra.

An *in vivo* study of BCC by Raman spectroscopy showed high sensitivity in the differentiation of this skin lesion (above 90%) with somewhat lower specificity - 54-95%[123], [130], [131]. At the same time, the study on skin samples[124], [125], [128], [129] showed even higher values of sensitivity and specificity (about 100% and >85%, respectively). These results allow to conclude that Raman spectroscopy can be used as a good addition to the existing methods in traditional surgery in determining the boundaries of pathological tissue to be excised, and as a better alternative to histological examination in terms of simplicity and speed of implementation.

Also, in the last decade, studies have been performed on the differentiation between melanoma and benign pigmented formations (**Figure 9**)[122]–[124], [126], [127], [129], [131], since melanoma is the most dangerous type of skin cancer and the effectiveness of therapy depends on the accuracy and speed of diagnosis. *In vivo* studies have shown 100% sensitivity and 70-78% specificity, which allows for further comparative studies with the traditional dermoscopic method for determining pigmented malignant tumors for subsequent implementation in standard medical practice[122], [131]. *Ex vivo* studies have shown even more encouraging results when trying to distinguish melanoma from other pigmented lesions,

normal skin areas, BCC, or metastatic tumors[124], [126], [127], [129]. The markers used to allow differentiation were lipids, polysaccharides, amide I, collagen III, elastin, melanin, phenylalanine, and DNA[124]–[129]. Moreover, as in the case of BCC, a comprehensive analysis showed even more reliable results[124], [129].

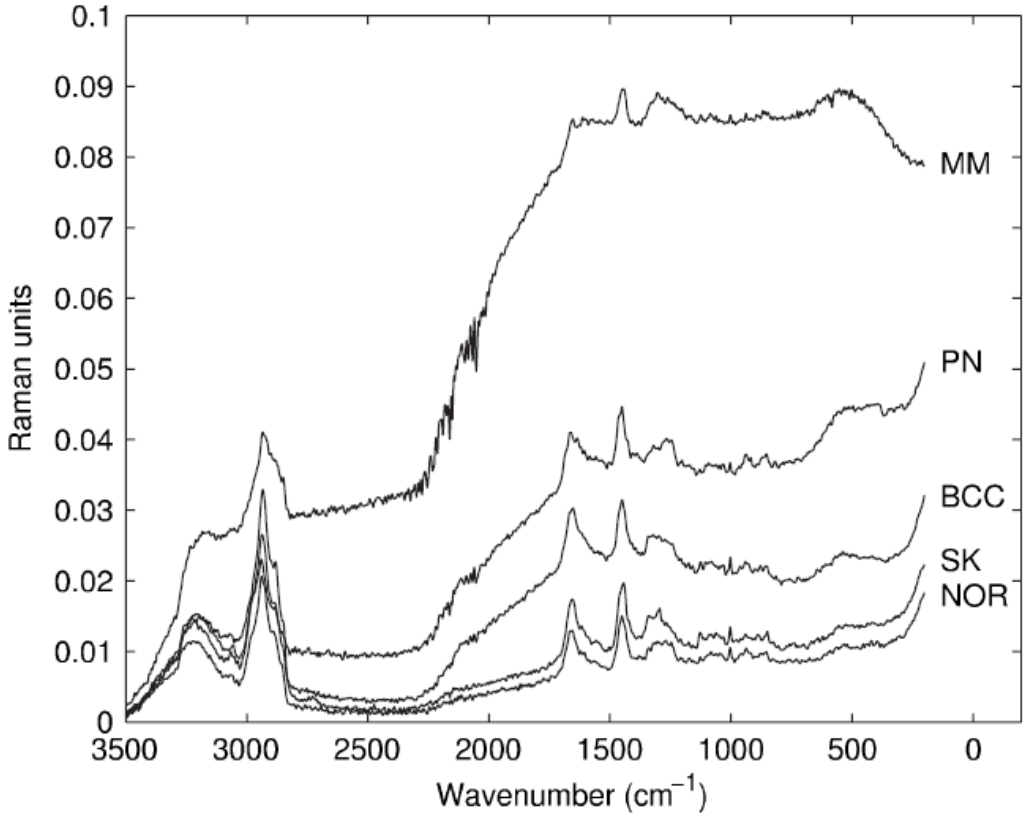

Figure 9. NIR-FT Raman spectra of normal skin (NOR), pigmented nevi (PN), melanoma (MM), basal cell carcinoma (BCC), and seborrheic keratosis (SK)[129].

Thus, the obvious advantages of Raman spectroscopy are its applicability not only *ex vivo*, but also *in vivo*, which avoids invasive interventions, as in histological studies, as well as its high speed, specificity, and sensitivity. Among the drawbacks, one can single out a small penetration depth caused by strong skin scattering, as well as the difficulty or even impossibility of differentiating the received signal in depth[26], [79]. However, the latter problem was solved by combining Raman spectroscopy and confocal microscopy (so-called Raman microscopy), which made it possible to obtain independent Raman spectra with depth resolution for thin skin volumes[118].

1.2.2. Imaging techniques

Unlike spectroscopic methods, imaging methods are not aimed at obtaining information about the biochemical composition of the studied biological tissue. They make it possible to obtain real-time images of the structures under study, which is an undoubted advantage in the clinical differentiation of pathological skin formations. The disadvantages of traditional methods such as visual examination by a dermatologist or histological examination are either the limitation of the analysis to the surface layer of the skin, or the invasiveness of the process of taking a sample for subsequent imaging. The non-invasiveness of the imaging of skin structure in depth is an obvious advantage of optical imaging methods, which led to their research in this direction.

Confocal microscopy

Confocal microscopy or confocal laser scanning microscopy (CLSM) has been widely used since the end of the last century in skin diagnostics[132]–[134] to visualize its structure at the subcellular and cellular levels, having greater resolution and contrast than conventional microscopes. In a confocal microscope, the optical system focuses the laser radiation used as a light source to a point on the biological tissue under study. Scattered or fluorescent radiation[135], [136] from the sample is then detected by the detector, with a pinhole located between the sample and the detector cutting off all signal coming from outside the focal plane. The resulting image is a slice containing only the image of the thin focal plane. Thus, the main advantage of confocal microscopy is obtaining optical sections of the cellular structure of the examined skin with high resolution (1 μm)[79]. By axial and lateral scanning of the focal point, multiple images of the skin can be obtained, which can then be combined into a 3D skin image. The main limitation in the use of confocal microscopy for skin analysis is the high scattering of the upper layers of the skin, which limits the probing depth to 200 μm.

Since the beginning of the 20th century, confocal microscopy has been widely used both in scientific research and in clinical diagnostics of the skin (diagnosis of pathological formations, inflammatory and infectious processes, monitoring the effectiveness of selected treatments, determining the boundaries of skin tumors, etc.)[137]–[149].

Confocal microscopy has been shown to be useful in diagnosing non-melanoma skin cancer. The work[150] showed the possibility of monitoring the local immune response to the therapy of basal cell skin cancer using fluorescent confocal microscopy. The effectiveness of

pre-surgical analysis of the affected area of the skin and determination of the tumor excision boundaries were demonstrated in the work[151]. Sensitivity and specificity values in the range of 80-98.6% have been obtained in the diagnosis of precancerous skin conditions[142].

However, the main attention of scientists is paid to differentiation of benign pigmented skin lesions and melanoma using confocal microscopy[140], [152]–[158]. Typical image analysis included the study of such specific features that accompany the development of pigmented malignant skin lesions, such as epidermal disorder, the presence of pagetoid cells, disruption of the normal dermis-epidermis junction, the appearance of bright cell nuclei, cellular atypia[155], [156], [158], etc. By collective analysis or using only one expert, the development of various diagnostic criteria showed that confocal microscopy can be used as an effective method for diagnosing this kind of skin lesions, showing sensitivity and specificity values above 80%.

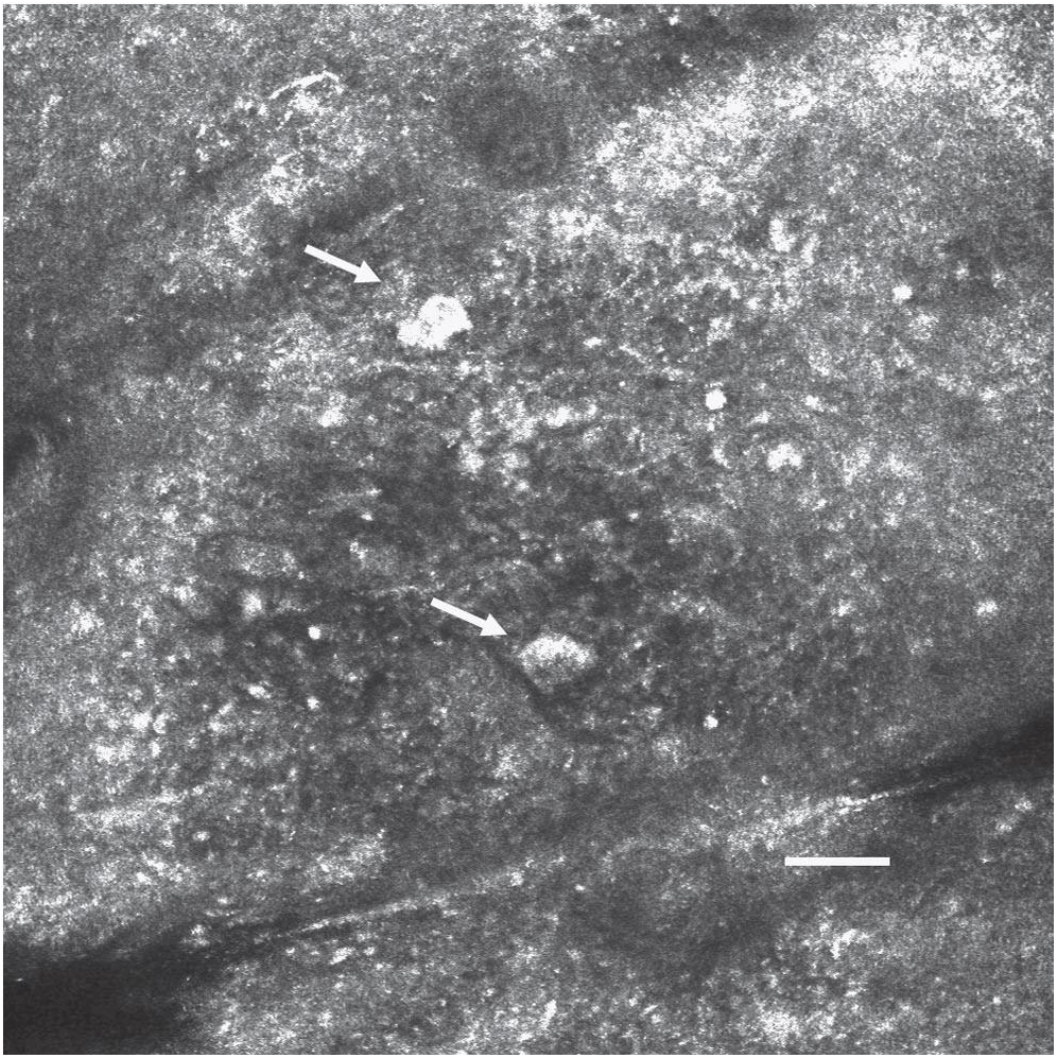

Figure 10. *In vivo* image of large pagetoid cells (white arrows) in the upper epidermal layer of lentigo melanoma (LMM) (0.2 mm Breslow thickness) obtained by confocal microscopy. Bar=50 μm[158].

Multiphoton microscopy

Multiphoton microscopy is a fluorescent imaging technique that provides images of the skin cellular and subcellular structures[26], [30]. Unlike conventional fluorescence microscopy, this method is based on a non-linear process in which two or more photons during a single quantum event are absorbed by a molecule, transferring it to an excited energy state. As a result, the energy of the emitted fluorescent photon is two or more times, depending on the method, the energy of the exciting photons. Therefore, the wavelength of the fluorescent photon is proportionally smaller than the wavelength of the excitation photons. Since the probability of two-photon excitation is very low, femtosecond pulsed lasers serve as sources of exciting radiation for the method of multiphoton microscopy, which make it possible to confine a high-intensity photon beam in time and space by focusing it to a point on the sample under study. Thus, as in confocal microscopy, it is possible to obtain an image of a thin skin layer corresponding to the position of the focus of the optical system. However, there is no pinhole in the optical system implemented in multiphoton microscopy. Here, sectioning is carried out due to the special distribution of the point spread function, which leads to focusing of the laser beam in a very thin tissue volume (~1 femtoliter). By scanning the laser beam, it becomes possible to obtain 3D *in vivo* fluorescent images of the skin cellular structure in real time[26]. Most skin fluorophores have excitation bands in the 400-500 nm range. In multiphoton microscopy, excitation occurs at wavelengths in the near infrared range (~700-1000 nm). Since skin scattering in this spectral region is much lower than in the visible range, the probing depth exceeds that of confocal microscopy by a factor of 5 and is up to 1 mm with a lateral and axial resolution of 0.64 μm and 3.35 μm, respectively[159]. Moreover, this fluorescence imaging method is well suited for imaging cellular structures since excitation wavelengths have less destructive effect on living cells than visible wavelengths[37].

As a result of research, it has been shown that multiphoton microscopy in the diagnosis of various types of skin cancer has the same capabilities as traditional histopathological invasive examination, with advantages in terms of image acquisition speed and non-invasiveness[160]–[162]. In addition to imaging, the distribution of exogenous and endogenous fluorophores can be analyzed using image processing algorithms to qualitatively assess and interpret signs of skin cancer. In a study on single cells[163] in the skin, this algorithm showed sensitivity and specificity values of 82% and 78%, respectively. The effectiveness of monitoring the growth of melanoma cells was shown in the work[164], where

the growth of the primary tumor and the associated vasculature was visualized in vivo using two-photon microscopy (**Figure 11**).

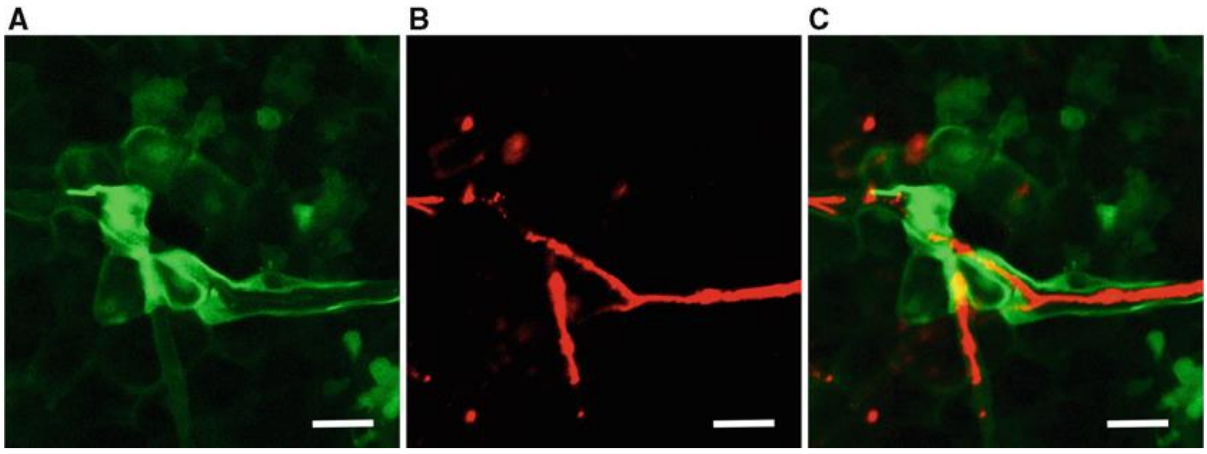

Figure 11. Two-color *in vivo* image of melanoma tumors in the mouse ear by two-photon microscopy. (a) Approximately 70 µm thick optical section of the dermis showing GFP-expressing melanoma tumor cells. (b) Blood vessels labeled with Dylight594 Tomato Lectin. (c) Overlay image of GFP and Tomato Lectin. In these figures, it is possible to observe a distinct angiotropism of individual melanoma cells spreading along the vessels. Scale bar length 50 µm[164].

Second harmonic generation microscopy

Second harmonic generation (SHG) microscopy is a non-linear microscopy method based on the eponymous optical effect[26], [165]. It consists in the interaction of two photons of the same frequency with a nonlinear material, as a result of which they are combined and a new photon is generated, whose energy is equal to twice the energy of the original photons, and the wavelength, respectively, is half their wavelength. Since the observation of this effect requires laser radiation to pass through materials with a non-centrosymmetric structure, some biological materials, such as collagen, capable of assembling into rather large, ordered non-centrosymmetric structures, have become an object of interest in the application of SHG microscopy to the analysis of biological tissues. Typically, photons generated by the second harmonic effect are characterized by their forward propagation pattern. However, some biological structures with a size of the order of one tenth of the wavelength of the second harmonic signal could generate a signal both in forward and backward direction. Often used in this microscopy, ultrashort titanium-sapphire lasers that generate radiation in the red and near infrared wavelength ranges make it possible to perform 3D imaging of the skin cellular structure at a depth of several hundred micrometers with high axial and lateral resolution, without using a pinhole, as in confocal microscopy[36]. Since contrast in SHG microscopy is achieved without excitation of molecules by incident light, as in fluorescence microscopy, but due to the difference in the ability of molecules to modulate second-harmonic light, the

studied molecules are not affected by the phototoxic effect and photobleaching[166], [167]. This is the main advantage of SHG microscopy for *in vivo* imaging of skin cell structures. There is also microscopy based on a special harmonic generation case - third harmonic generation. This method is very sensitive to differences in refractive indices and is therefore used to visualize cell interfaces and intercellular spaces[168].

Pathological changes in the skin connective tissue, fibrosis, and skin cancer lead to changes in the fiber structure of collagen. Since SHG microscopy is very sensitive to collagen structures, it has found wide application in the diagnosis of skin lesions[169], [170]. In particular, when determining the boundaries of skin melanoma *ex vivo*, the high accuracy of the SHG microscopy method was shown due to the presence of a second harmonic signal in intact collagen fibers and the complete absence of this signal in areas affected by melanoma. Moreover, the results obtained by SHG microscopy showed a high level of correlation with the standard method of histological examination ($p<0.002$)[171]. This accuracy of border determination allows transferring this technique to clinical practice, allowing real-time non-invasive determination of the boundaries of the affected areas of the skin *in vivo*, thereby simplifying the surgical treatment procedure.

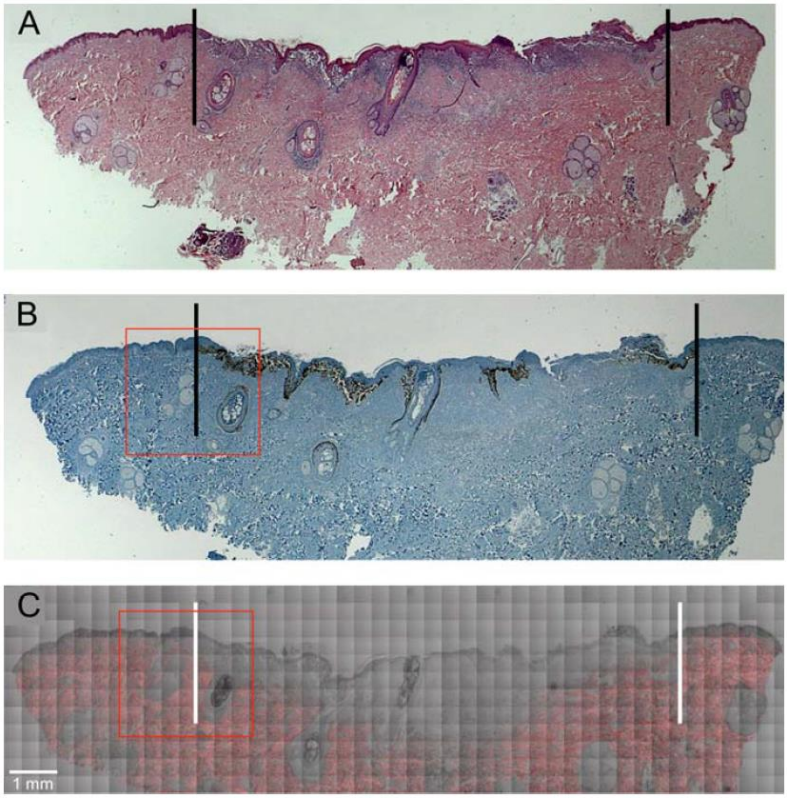

Figure 12. Comparison of melanoma margins obtained from H&E (A) and Melan-A (B) stained sister sections and comparison with SHG microscopy image (C), showing high correlation ($p<0.0012$) . The vertical lines (black lines in A and B; white lines in C) represent the lateral margins of the melanoma as determined by two independent histopathologists (A and B) and an independent researcher (C). Scale bar = 1 mm[171].

Optical coherence tomography

One of the widely used skin imaging methods since the early 1990s is Optical Coherence Tomography (OCT)[172]. This is an interferometric method in which the image of the tissue structure is obtained by registering low-coherent light backscattered or reflected by tissue[26], [173]. The original version of OCT was Time-domain OCT (TD-OCT), the main feature of which was the fast translation of the reference mirror of the internal interferometer, allowing for the axial time-dependent scanning of skin[26]. From this method, Full-field OCT (FF-OCT) was developed, characterized by the ability to acquire "in face" skin images without the need to scan along the specimen[174]. Another method is Frequency- (or Fourier) domain OCT (FD-OCT). Its feature is the absence of scanning of the reference mirror; instead, scanning is carried out by the wavelengths of the source[175]. Finally, a recently invented technique is Line-field Confocal OCT (LC-OCT). It combines the advantages of TD-OCT and confocal microscopy and provides 3D images of tissue at high-resolution allowing to distinguish the cellular structure of the skin[176].

Comparatively (relative to other optical methods of skin diagnostics) high penetration depth (0.5-2 mm, depending on the OCT technique) is the main advantage of this method, which made it one of the most commonly used methods for non-invasive real-time analysis of skin morphological properties[26].

Many works have been devoted to the diagnosis of skin actinic keratosis[177]–[180]. Dysplasia and disruption of the epidermal structural integrity were clearly visible on the obtained OCT images in the form of white stains. Sensitivity and specificity values above ~80% were obtained in a study on the differentiation of skin areas into healthy and affected by actinic keratosis[178], [179]. The work[179] showed that although the visual differentiation of the affected area into actinic keratosis and skin cancer is impossible using the OCT technique, the application of machine learning algorithms to the obtained images made it possible to carry out this differentiation with an accuracy of more than 73%.

Most of the applications of OCT in skin cancer analysis in the last decade have been devoted to basal cell carcinoma[179]–[183]. When analyzing areas of BCC localization, the skin layers, perfectly displayed in OCT imaging of healthy samples, were noticeably distorted by the appearance of black round artifacts, and it also became possible to observe changes in the skin epidermal geometry[179], [180]. Despite the difficulties in determining the stage of BCC development by OCT, this method of skin optical diagnostics showed high accuracy in

determining the deep-lying boundaries of the tumor, compared in efficiency with invasive histopathological methods for determining the lesion boundaries (**Figure 13**)[181]–[183]. The main drawback of the OCT method can be considered the lack of biochemical information about the imaged skin areas. However, high penetration depth combined with high resolution, speed and non-invasiveness makes OCT an effective method for determining the boundaries of lesional skin areas for further surgical treatment.

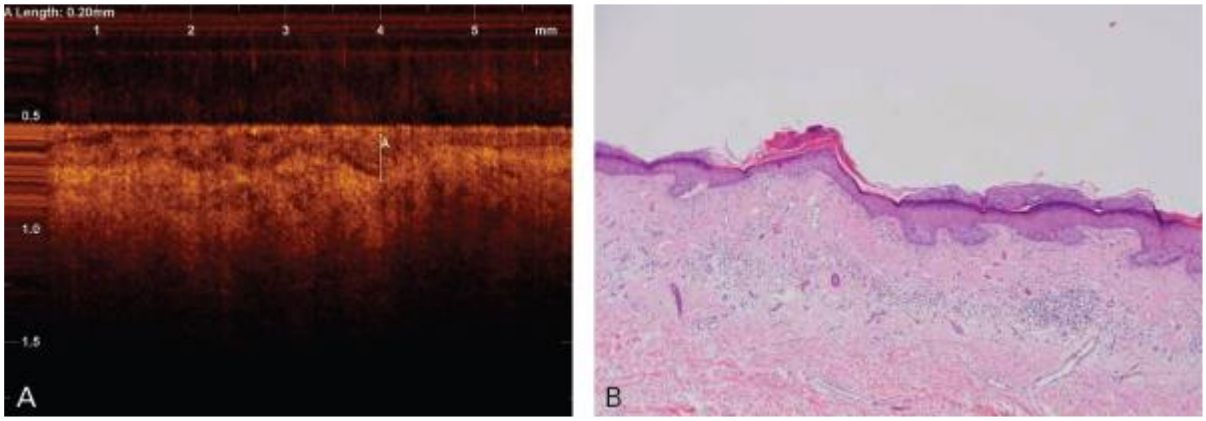

Figure 13. (A) OCT image of a superficial BCC showing tumor buds attached to the epidermis. Noticeable reduced reflectivity (darkening) at the periphery of the tumor and increased reflectivity (bright areas) of the surrounding stroma. (B) Histopathologic specimen of the same lesion showing tumor buds attached to the epidermis (H&E; ×40 magnification)[182].

Hyperspectral Imaging

In most optical methods, the signal is recorded from one point in the sample or is averaged over a certain volume of biological tissue. However, with the introduction of the hyperspectral imaging method, it became possible to receive a signal simultaneously from large areas of biological tissue, which contains spectra obtained in an extended wide range of electromagnetic radiation (not only visible) for each of the pixels of the analyzed image. The so-called hyperspectral data cube obtained with this imaging method makes it possible to detect and localize spectral anomalies in absorption, reflectance, or fluorescence, which are characteristic "imprints" of pathological processes[17], [184], [185]. Thus, this method allows for high-resolution contrast imaging of lesional skin areas. Since the resulting data arrays are too complex to interpret, typical methods for extracting useful data and classifying in biomedical hyperspectral imaging currently include technologies such as support vector machine[186]–[189], multilayer perceptron[190], spectral information divergence[191], spectral unmixing[192], etc.

In works on the study of skin diseases by hyperspectral imaging, much attention is paid to the differentiation of skin cancer. The work[193] showed the effectiveness of the

determination of various pathological conditions of histological skin sections by cross-correlation analysis of hyperspectral images. In vivo studies of Kaposi's sarcoma[194] have demonstrated the ability to assess tumor angiogenesis and pathological metabolism by analyzing NIR hyperspectral skin images.

A recent study[195] demonstrated the ability to differentiate between healthy skin and non-melanoma skin cancer by analyzing hyperspectral images in the visible range. Moreover, the wavelength range of 430-520 nm has been shown to be effective in differentiating types of neoplastic processes.

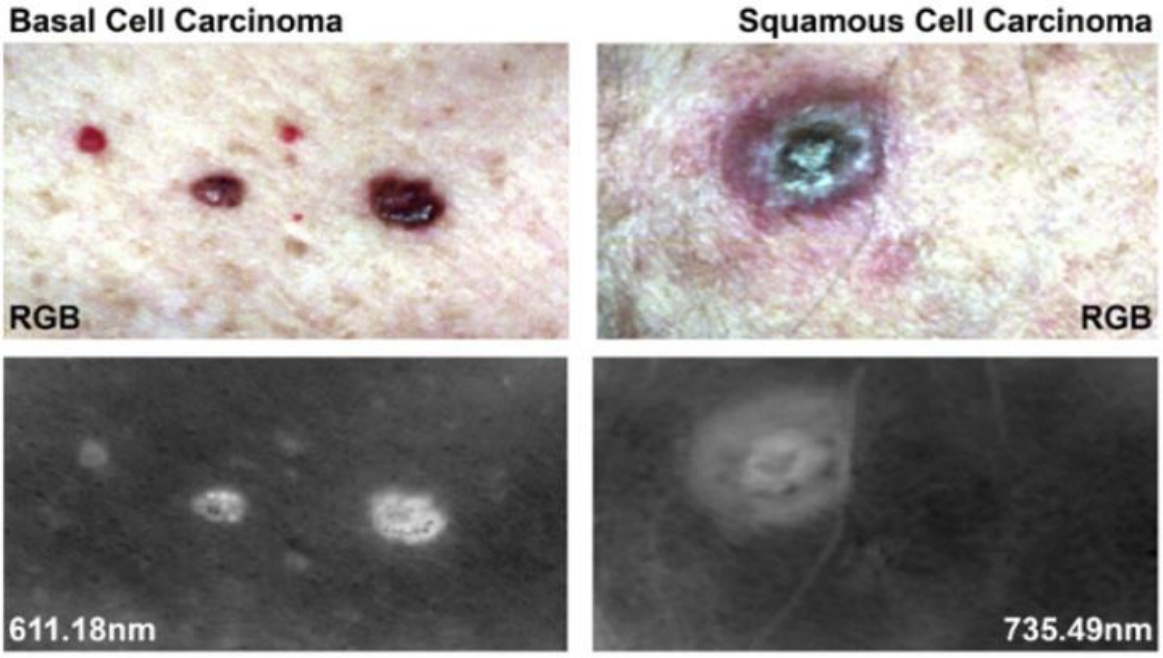

Figure 14. Visualization of different skin lesions at single bands (611.18 nm and 735.49 nm) of hyperspectral images, as well as their corresponding RGB images[195].

In the past few years, hyperspectral imaging has been actively used in solving such a complex dermatological problem as the diagnosis of pigmented malignant tumors[196]–[198]. In particular, when differentiating between benign pigmented lesions and melanoma, sensitivity and specificity values of 87.5 and 100%, respectively, have been demonstrated[197], making this method an effective alternative to traditional histological examinations.

1.2.3. Multimodal techniques

In the last decade, along with the separate use of optical methods for the diagnosis of skin diseases, various combinations of optical methods have been proposed and tested[17]. Due to the huge variety of types of malignant skin tumors, as well as dysplastic benign changes , the entire range of spectral characteristics, which contain the so-called markers of metabolic

processes, is not available for analysis by a single optical method. For example, skin fluorescence spectroscopy is well established in the diagnosis of non-melanoma skin cancer and associated precancerous lesions, but it is poorly applicable in the diagnosis of pigmented benign lesions and differentiation into healthy skin and melanoma due to the weak fluorescence signal produced by pigmented areas of the skin. Thus, the combination of several optical methods allows expanded diagnostic potential of optical methods.

One of the most frequently used multimodal methods in the scientific literature in recent years is the combination of fluorescence spectroscopy and diffuse reflectance spectroscopy for the diagnosis of pathological skin changes. For example, it has been demonstrated in the works[16], [19] that bimodal analysis by fluorescence spectroscopy at several excitation wavelengths and diffuse reflectance spectroscopy leads to an increase in diagnostic accuracy compared to a single fluorescence spectroscopy method when discriminating three types of skin hyperplasia. Thompson *et al*.[87] reported 87% of correctly diagnosed cases of BCC using this multimodal method. According to the results of the study by Rajaram *et al*.[84], the sensitivity and specificity for the diagnosis of BCC by this method is up to 94 and 89%, respectively, while the sensitivity for the detection of actinic keratosis and squamous cell carcinoma is 100%, although the specificity for these specific neoplasms is reduced (50%) . Differentiation into healthy skin and such types of skin formations as hemangioma, fibroma and angiokeratoma, as well as their differentiation among themselves, was performed using laser fluorescence spectroscopy and diffuse reflectance spectroscopy with sensitivity and specificity values above 90%[199]. Borisova *et al*. presented in their work[81] the results of differentiation into dysplastic nevi and skin melanoma. The resulting sensitivity and specificity values were 92% and 78%, respectively.

The study[15] presented the results of the simultaneous analysis of malignant skin lesions using fluorescence spectroscopy, diffuse reflectance spectroscopy, and Raman spectroscopy (**Figure 15**). The results of the classification were compared with the results of standard histopathological examinations. When differentiating melanomas from benign pigmented lesions, sensitivity and specificity values of 100% were obtained. The same values when differentiating the examined skin areas into carcinoma and actinic keratosis were 95 and 71%, respectively. Differentiation of healthy skin from a group of diseases (actinic keratosis, basal cell carcinoma, squamous cell carcinoma) showed a sensitivity of 90% and a specificity of 85%.

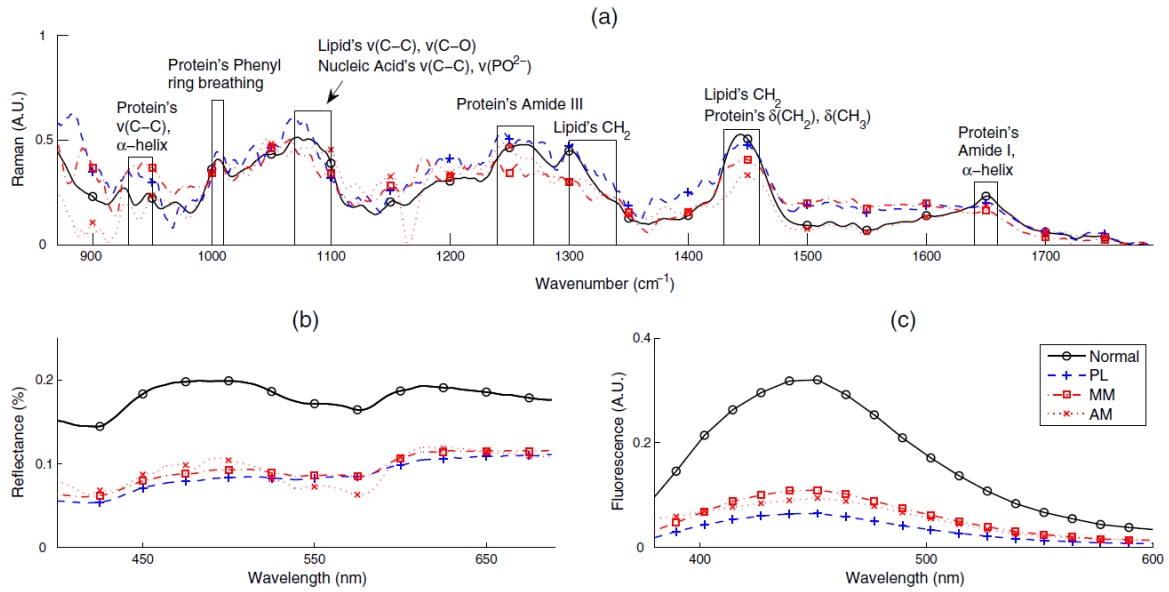

Figure 15. Mean spectra of melanoma (MM), nonmelanoma pigmented lesions (PL), and normal skin. One of the melanoma lesions is an amelanotic melanoma (AM): (a) Raman spectroscopy, (b) DR spectroscopy, and (c) fluorescence spectroscopy[15].

The limited diagnostic potential of reflectance confocal microscopy, expressed in providing non-specific morphological information about the analyzed skin, can be overcome by its combination with two-photon microscopy. The work[200] showed the effectiveness of such a multimodal technique in visualizing the detailed structure of healthy and cancerous skin, including the cellular structure and extracellular matrix.

OCT, along with all its advantages described above, also has the main disadvantage expressed in the ability to only visualize the structure of the tissue without providing the specialist with information about the biochemical composition of the skin being examined. Carstea and co-authors demonstrated the potential of combined use of OCT and fluorescence spectroscopy, which made it possible to obtain, in addition to structural information, also complementary biochemical information about the analyzed skin[201].

The combination of two-photon microscopy and second-harmonic generation microscopy has shown promising results in detecting morphological and spectroscopic differences between healthy skin, BCC, and melanoma[202]. This combination of imaging modalities, supplemented by coherent anti-Stokes Raman spectroscopy (CARS) technology, was used to define the boundaries of lesional skin in the work[203]. BCC and SCC showed an increased signal from two-photon microscopy, while the second harmonic signal was insufficient for differentiation. Unlike BCC, SCC made it possible to register a strong CARS signal. In addition, the multimodality of this method made it possible to obtain prognostic information about lipid metabolism and the interaction of the tumor and stroma.

Thus, the combined information obtained by using multimodal optical methods makes it possible to non-invasively analyze the structural and biochemical modifications of the skin with high resolution, which makes it possible to use these methods for the clinical diagnosis of skin lesions and to determine the boundaries of tumors for surgical treatment *in vivo* in real time. However, the strong scattering of light by the skin remains a major problem which limits the probing depth of the aforementioned optical methods.

1.3. Optical Clearing of skin

As described in section 1.2. of this chapter, the main factor limiting the potential of optical methods in skin diagnostics is the strong skin scattering, which significantly reduces their contrast and probing depth. The main reason for the strong scattering of skin, as discussed earlier, is the RI mismatch between structural elements (scatterers), such as cell membranes, nuclei and organelles, protein fibers, lipid droplets, and ISF, mainly consisting of water. Moreover, the cellular cytoplasm also mainly consists of water, introducing optical heterogeneity already at the intracellular level[26], [35], [36]. The relative refractive index (RRI) of the skin *m*, calculated as the ratio of the refractive index of the skin scatterers $n_{scatter}$ to the refractive index of the interstitial fluid n_{ISF}, makes it possible to estimate the degree of skin scattering. Thus, at a wavelength of 589.6 nm, the n_{ISF} value varies from 1.35 to 1.37[204], while for collagen, which makes up the bulk of the connective tissue, the refractive index depends on its degree of hydration and was measured as 1.474[205]. The refractive index of skin melanin is 1.6[204], which is even higher than that of collagen. On the example of these two scatterers, it already becomes noticeable that the value of *m* for the skin exceeds unity. Since the heterogeneous structure of the skin contains a huge number of such local scatterer/ISF interfaces, the probability of scattering due to refractive index mismatch at the interface boundary is very high for photons of optical radiation propagating in the skin. Reduction of skin scattering is possible if the value of *m* is equal to or close to 1. Since it is difficult to reduce the refractive indices of skin scatterers to the level of the ISF, Tuchin proposed a technology for immersion optical clearing (OC) of biological tissues[35], which consists in changing the refractive index of the interstitial fluid n_{ISF}. This method makes it possible to effectively match the RI in the skin, which leads to a decrease in the skin scattering coefficient ($\mu_s(\lambda)$=0), as well as to an increase in the direction of single scattering events (g=1).

1.3.1. Principle of action

This method is based on the use of biocompatible, often hyperosmotic chemical agents called Optical Clearing Agents (OCA). When skin samples are immersed *ex vivo* in such a substance, or when applied topically (applicable to *in vivo* skin), it exerts osmotic pressure on the skin, changing the natural water concentration gradient in the SC of the skin. Due to this osmotic pressure, free water molecules located in the intercellular space are forced to go outside. Thus, the flow of water out of the skin into the external environment is organized. Due to the release of water from the skin sample, its thickness decreases, and it becomes possible to observe a more compact organization of skin scatterers[26], [36], [204], [206], [207]. The expected increase in the concentration of scatterers per unit volume in this case should lead to an increase in skin scattering, however, because of a decrease in skin thickness in combination with a more regular packing of scatterers, the transmittance through the skin increases, as does its transparency[204], [207]. This is due to the fact that with the loss of water, the volume fraction of skin scatterers f_s increases, since the absolute volume of scatterers V_s remains constant, but at the same time the sample volume V changes (so-called skin shrinking). As a result, there is an increase in the constructive interference of forward scattered light and destructive interference in the direction perpendicular to the direction of light propagation in the skin, which leads to an increase in the signal of collimated transmittance through the skin[204]. The described mechanism of dehydration is one of the three main mechanisms of skin OC[27], [204], [208]–[212]. Similar changes in the internal configuration of skin scatterers are also characteristic of skin mechanical compression and stretching[213], [214]. Osmotic pressure is also the main mechanism responsible for OCA toxicity. Despite the generation of fluid flows into and out of the skin, strong osmotic pressure can lead to irreversible destruction of the tissue structure[215].

The second mechanism of skin OC is the RI matching of the skin structural components and ISF. It occurs in parallel with the process of skin dehydration, since in the process of water outflow from the skin into the external environment the molecules of the hyperosmotic agent also begin to diffuse into the skin[26], [28]–[30], [208]–[210], [216]–[219]. The stronger the degree of skin dehydration, the more OCA molecules penetrate into the intercellular space, replacing water. Since the RI of the OCAs used is higher than that of water, this leads to a decrease in the value of m, thereby causing a RI matching of the scatterers and the ISF[206], [207], [214], [220]–[222]. A key feature of these mechanisms is their reversibility, since the

skin water content can be restored either by its immersion in saline (*ex vivo*) or by OCA flushing out by adjacent, well-hydrated *in vivo* skin areas. For fibrous tissues, such as the skin dermis, the second mechanism is dominant over the first, since severe dehydration is possible only with the use of hyperosmotic agents, while the size of OCA molecules is much smaller than the average value of the interfibrillar space[30], [216], [223], [224].

At the same time, it has been shown that some hygroscopic agents, such as glycerol, can cause swelling or edema of the skin due to the binding of water molecules in the intercellular space. These water molecules reduce the initial RI of the OCA, preventing a high level of RI matching in the skin from being achieved. As a result, there is an increase in the skin scattering coefficient $\mu_s(\lambda)$ and a decrease in the signal of collimated transmittance through the skin[36].

The third mechanism of skin OC is directly related to the molecular features of some hyperosmotic agents and their ability to interact with the molecular structure of skin scatterers[26], [36]. One of the main scattering structures in the skin is collagen, which is organized into complex fiber structures. Hydrogen bonds are the main binding force in collagen triple helices. The use of OCA with a large number of hydroxyl groups makes it possible to screen hydrogen bonds in collagen helices. This non-covalent destabilization of hydrogen bonds leads to temporary dissociation of collagen fibers (**Figure 16**)[225]. By reducing the size of the main scattering components of the skin in this way, a reduction in skin scattering is achieved.

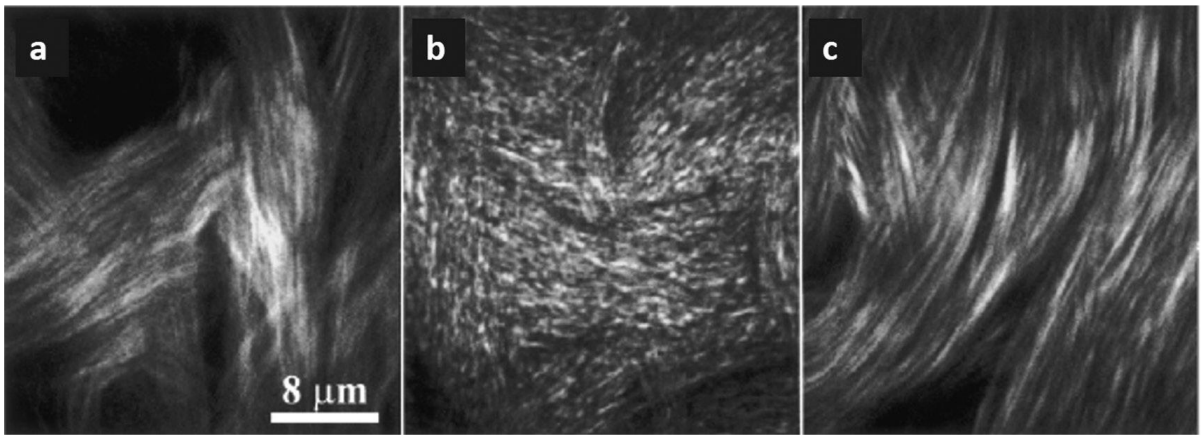

Figure 16. Reversible effect of glycerol on the dermis of rodents. SHG images (a) before glycerol application, (b) after glycerol application, (c) after rehydration with phosphate-buffered saline (PBS)[225].

However, it was shown in the work[211] that the effect of glycerol during optical clearing of skin samples *in vivo* did not cause dissociation of collagen fibers. It was only possible to observe a decrease in the diameter of the collagen fibers, which was also reflected in the

reduced skin scattering and, together with a decrease in the sample thickness, became the main mechanism of optical clearing *in vivo*.

Thus, the triple combination of effect of dehydration, caused by the high osmolarity of the OCA used, the RI matching of skin scatterers and ISF due to the penetration of OCA into the intercellular space, and the reversible dissociation of skin structural proteins are the main mechanisms of optical immersion clearing of the skin.

1.3.2. Optical Clearing Agents (OCA)

The effectiveness of OC depends on the RI of the agents used, their osmolarity and physicochemical properties, and at the same time depends on physiological characteristics, such as Ph and temperature[226] of biological tissues, which directly affects the diffusion rate of OCA[26].

Currently, OCAs used for OC can be roughly divided into 5 main groups (**Table 2**): Sugars (glucose, fructose, sucrose, dextrose, ribose)[209], [224], [227]–[235]; polyatomic alcohols (propylene glycol (PG), glycerol, polyethylene glycols of various molecular weights (PEG), mannitol, xylitol, sorbitol)[211], [220], [223], [231], [232], [236]–[246]; Fatty acids such as linoleic and oleic[1], [247]; Organic solvents (dimethyl sulfoxide (DMSO) and thiazone)[1], [3], [210], [247]–[256]; electrolyte contrast agents (Trazograph™, Verografin™, Hypaque™ and Omnipaque™)[28]–[30]. Typical release form of the latter is of 60% and 76% solution of mixture of diatrizoate sodium (635.89 g/mol) and/or diatrizoate meglumine (809.13 g/mol)

Table 2. Main chemicals used as OCA. Data taken from own measurements and works[26], [35], [36].

Group	OCA	Molecular weight (g/mol)	RI (λ=589 nm)
Sugars	Glucose	180.2	1.4148 (54%-solution)
	Fructose	180.2	1.4141 (48%-solution)
	Sucrose	342.3	1.4906 (80%-solution)
Polyatomic alcohols	Propylene glycol (PG)	76.1	1.4326
	Glycerol	92.1	1.4747
	Polyethylene glycol – 400 (PEG-400)	380-420	1.4558
	Sorbitol	182.2	1.375
Fatty acids	Linoleic acid	280.4	1.4699
	Oleic acid	282.46	1.4583
Organic solvents	Dimethyl sulfoxide (DMSO)	78.13	1.4731
	Thiazone	162.3	1.5383
Electrolyte contrast agents	Trazograph™-76	635.89/809.13	1.460
	Verografin™-76	635.89/809.13	1.485

	Hypaque™	635.89/809.13	1.437

Based on the available scientific publications[28]–[30], [35], [36], [167], [204], [208], [219], [248], [252], [257], [258], it can be concluded that glycerol, glucose, PG, and PEG are the most commonly used OCA for OC of biological tissues. Moreover, it was shown in the works[242], [243] that the efficiency of OC does not directly depend on the RI of the OCA used, but depends on the features of the molecular structure that determines the interaction of the OCA with skin components.

OCAs from the group of alcohols are typical polyhydric alcohols and have similar molecular structural features in the form of the presence of more than one hydroxyl group. Their hydrophilic properties, combined with hyperosmotic properties, cause dehydration and skin shrinking, which leads to a decrease in scattering[26], [28]–[30], [36]. Moreover, the work[243] showed that the effectiveness of OC directly depends on the number of hydroxyl groups in the OCA used, which is explained by their ability to disrupt the high-level structure of skin proteins such as collagen. And in the work[228] it was found that alcohols whose hydroxyl groups are located far enough apart in the carbon chain have a greater potential for OC than those alcohols whose hydroxyl groups were located next to each other.

OCAs from the group of sugars are represented by monosaccharides, whose distinguishing feature is also hydrophilicity and the presence of more than one hydroxyl group. Due to this, they are able to form hydrogen bonds and bridges, affecting the organization of the skin structural protein[26], [36]. It was demonstrated in the work[235] that solutions of glucose, fructose, and ribose have an OC potential similar to that of polyhydric alcohols; however, the main problem for their penetration into the skin is the natural barrier of the SC, which permeability enhancement methods will be discussed in the next subsection.

Unsaturated fatty acids, due to their lipophilic properties, can interact with the lipid domains of the SC and change their permeability, which is why initially these acids, considered to be completely biocompatible[259], were used to deliver drugs to the skin[260], [261]. However, subsequently, they began to be used in skin OC as a biocompatible OCA capable of RI matching and reducing skin scattering by replacing the ISF[26], [28]–[30], [36].

The general principle of action of OCA, belonging to the category of organic solvents, is the interaction with proteins and lipid domains of the SC[40]. DMSO, for example, can change the intercellular conformation of keratin, as well as interact with the polar heads of the skin lipid bilayer, disrupting its geometry and reducing skin scattering[35]. In the study of skin OC using

DMSO[210], it was shown that, like alcohols and sugars, it is able to interact with the structural proteins of the skin dermis, which led to a decrease in scattering and an increase in the collimated transmittance signal. Moreover, this signal directly depended on the concentration of DMSO in the skin.

Electrolyte contrast agents are classified as a separate category of OCA due to their chemical properties. Initially hydrophilic colorless liquids, they also have RI significantly higher than that of the ISF, which allows them to be used for skin OC. Iohexol, also known as Omnipaque™, can also be used in *in vivo* studies as it has a low osmolarity compared to other commonly used OCAs, avoiding potential cytotoxic effects and structural deformities. The low viscosity ensures rapid penetration of this type of agents deep into the skin[28], [35], [36].

For experiments related to skin OC, it is desirable to use such combinations of OCAs whose spectral characteristics do not have obvious absorption bands and have high transmittance in the spectral range under study. Currently, various combinations of OCAs from various groups are being investigated in order to find the most effective combinations[35], [36].

When planning *in vivo* experiments on skin OC, it is necessary to take into account the potential OCA toxicity. Almost all the listed OCAs, classified into the main 5 groups, are positioned in the scientific literature as generally non-toxic. However, the high concentrations of agents commonly used in *ex vivo* experiments and the long application time of OCA can cause undesirable effects under *in vivo* conditions, such as hemostasis[208], shrinking, and even necrosis of skin[262]. Numerous studies have also reported local side effects of OCA use, such as irritation and edema[211], [223], [224], [229], [230]. Although most of these effects are reversible and resolve shortly after OCA exposure ends, *in vivo* clinical use of these substances can often be associated with skin lesions. In this regard, the habitually high concentrations of OCA reported in the scientific literature must be reduced when moving to the clinical setting in order to meet the clinical requirements of applicability and biocompatibility[36].

Also, it is worth mentioning that for the purposes of studying biological tissues *in vitro* and *ex vivo* in biology and molecular analysis, more complex compositions of OCA are used in combination with specialized protocols, such as 3DISCO (3D imaging of solvent-cleared organs), uDISCO, SeeDB (see deep brain), ScaleS, Clear T2, and PACT (passive CLARITY technique). These methods imply full clearing using chemical solvents for a long period of time (from hours to several days/weeks) of various organs, including full clearing of the brain

tissue[28], [30], [35], [36], [263]. However, these technologies are unsuitable for *in vivo* biocompatible skin OC due to irreversible chemical changes in the processed samples, such as, for example, delipidation and decalcification[36].

1.3.3. Penetration Enhancers

When optically clearing the skin, the main way to achieve a non-invasive biocompatible effect of OCA is to apply agents to the skin surface. However, the barrier properties of SC limit the penetration of chemicals (including OCA, which are mostly hydrophilic chemical agents) into the skin. At present, methods for enhancing the diffusion of OCA into the skin are actively used to reduce the time at which RI matching is achieved, as well as to achieve a similar effect when using reduced concentrations of OCA, which is useful when transferring the OC technique to clinical conditions.

One way to increase skin permeability for OCA is to use so-called chemical penetration enhancers (CPEs)[28]–[30], [35], [36], [40]. In combination with OCA, they make it possible to accelerate the diffusion of the latter through the stratum corneum into the deeper layers. Ethanol, PG, DMSO, azone, thiazon, oleic acid, and hyaluronic acid[2], [3], [30], [31], [210], [235], [249]–[251], [253], [255], [256], [258], [264]–[273] have recently been the main chemical enhancers of epidermal permeability.

Ethanol is a hydrophilic solvent widely used in various chemical transdermal preparations. Its principle of action is to change the barrier properties of the stratum corneum and enhance the percutaneous diffusion of OCA, mainly by dissolving the SC lipids[267], [268].

DMSO, in addition to being used as an independent OCA, is able to enhance the SC permeability for hydrophilic OCA by changing the structural integrity of the lipid bilayer, thereby changing the solubility properties of skin SC[270]. The combined use of ethanol and DMSO as CPE makes it possible to achieve a much greater effect than when using these agents separately and in high concentrations[274].

PG is used as a permeability enhancer, since it is able to dissolve the keratin of skin SC and integrate into the structure of the lipid bilayer, enhancing the diffusion of hydrophilic OCAs[40], [275]. In addition, the work[31] demonstrated the effectiveness of PG specifically as a CPE, since its own OC potential was lower than that of the other OCAs used.

Azone and its derivatives such as thiazone have been used in some studies as a skin permeation enhancer for OCA[29], [31]. Their principle of action seems to be the formation of a separate phase within the lipid bilayer in the SC[40]. However, these substances have not

yet been approved by the FDA for use on the skin, probably due to their use as insecticides, herbicides, and also because of the antiviral activity found (which does not allow them to be classified as inactive chemical ingredients).

Oleic acid, like other fatty acids, is able to disrupt the structure of the SC due to the integration of its long curved molecular structure into it, increasing skin permeability for hydrophilic OCAs[32], [40], [247].

Hyaluronic acid (HA) has recently been used to enhance the diffusion of OCA through the skin due to its natural biocompatibility, biodegradability and non-immunogenicity - it is a linear polysaccharide naturally produced by the human body. Several theories were proposed to explain its permeability enhancing effect[276]–[278]. One of them is the hydrophilic interaction of HA - hydration and loosening of the SC due to the interaction of a large number of water molecules in the skin with the polymer base of hyaluronic acid. Another theory was also proposed that the lipophilic domains of HA can alter the structure of keratin by interaction and thus lead to the appearance of disordered regions of lipid bilayers[278], increasing the rate of OCA diffusion through the SC.

In contrast to chemical methods of epidermal permeability enhancement, various physical methods to increase transdermal diffusion of OCA used in experimental approaches offer some advantages in the form of no interaction between OCA and enhancer, and the risk of additional skin irritation is reduced due to the absence of additional chemical interaction with the skin[30]. Among these methods, one can single out the removal of the stratum corneum[279]–[282], irradiation of the skin surface with laser radiation of various intensities[283], [284], mechanical and photothermal skin microperforation[285], [286], laser ablation[287], [288], fractional microablation[289], iontophoresis[290], sonophoresis[291], [292] and the use of microneedles[293], [294].

Removal of the stratum corneum partially distorts the main skin barrier that prevents OCA from diffusing into skin and can be performed using a variety of methods, including tape stripping[279], medical grade adhesive[280], sandpaper rubbing[281], or microdermabrasion[282]. For example, the work[291] showed an increase in the amplitude of the OCT signal up to 15%, recorded from the deep layers of the skin, after the removal of the SC layer.

Heating of the skin SC layer in combination with photomechanical waves, which leads to a violation of its barrier function, makes it possible to use laser radiation as an enhancer for skin

OCA diffusion. In work[284] it was demonstrated that the percutaneous diffusion of OCA when using laser radiation increased several times compared to diffusion into intact skin.

Violation of the SC integrity, achieved with microperforation, makes it possible to create microscopic channels in the skin superficial layer's structure, through which OCA can directly penetrate into the deeper skin layers. Such channels can be obtained both optically, using a lamp[285], and mechanically, using, for example, a microneedle roller[286].

Microablation using laser radiation sources allows achieving an effect similar to microperforation. Moreover, laser radiation allows to adjust the depth and shape of the channels created in the skin[289]. However, optomechanical damage to the epidermis caused by laser radiation can lead to various negative effects, such as edema[288], [289], and hinder the process of RI matching using OCA.

In iontophoresis, an electrical current applied to the skin surface induces a diffuse transdermal ion flux, allowing charged or hydrophilic molecules such as OCA to be delivered deep into the skin. Iontophoresis does not directly change the permeability of the stratum corneum: molecules entrained by a diffuse flow of ions or an electroosmotic waterflow (in the presence of electrolytes) choose the path of least resistance (for example, hair follicles), while penetrating deep into the skin[40]. In the work[290] the volumetric flow of OCA through the skin when using iontophoresis increased by about 20 times compared with passive diffusion.

The use of ultrasound (US) with a frequency of 1-1.5 MHz on the skin (sonophoresis) causes the effect of cavitation, which consists in the formation, oscillation, and subsequent collapse of microbubbles inside the skin layers. The oscillation of bubbles exerts shear stress on the skin, and as a result of their collapse, local shock waves cause a violation of the stratum corneum integrity, increasing the skin permeability for OCA[36], [40], [295]–[297]. In addition, cavitation causes a change in the ordered structure of collagen fibers, reducing skin scattering[291], [295]. The study[298] demonstrated a 1.5-fold and 1.6-fold increase, respectively, in the efficiency of OC with 60% glycerol and PEG-400 solutions when exposed to ultrasound compared to their effect without using ultrasound.

Also, significant results have been obtained in OC enhanced by a multimodal combination of chemical and physical penetration enhancers[2], [255], [299], [300] or by a combination of several physical penetration enhancers[280], [289], [291], [301]–[303].

1.3.4. The use of optical clearing in skin optical diagnostic methods

Recently, a large number of scientific publications have demonstrated the potential of using the OC technique to reduce skin scattering, which allows increasing the contrast and probing depth of various optical skin diagnostic methods[28]–[30], [35], [36].

The improved performance of the multiphoton microscopy technique when combined with OC was shown in a study[304] where various concentrations of glycerol and Omnipaque™ were topically applied to the skin of a pig's ear for 60 minutes. As a result, a significant increase in contrast and imaging depth was achieved.

The work[225] demonstrated the effect of glycerol solution application to the skin of rodents, expressed in an increase in tissue transparency for the multiphoton microscopy method due to the reversible dissociation of collagen fibers. This process was reversible, as the reassociation of collagen fibers was demonstrated when saline was applied to the skin.

Cicchi *et al.*[257] reported a significant increase in contrast and penetration depth (2-fold) in *ex vivo* two-photon microscopy of the human dermis with short-term application of hyperosmotic OCAs (glycerol, PG, sucrose).

The effect of OC of human skin *in vivo* on the imaging depth of the OCT method, as well as on artifacts caused by skin scattering, was investigated in[305]. Both OCAs used (glycerol and ultrasonic gel) made it possible to reduce the intensity of artifacts in OCT images and increase the probing depth by 1.5 times.

The surface application of a PG solution on human skin *in vivo* made it possible to observe an increase in the contrast and probing depth of images obtained by OCT[306].

Optical clearing of skin melanoma *in vivo* with a mixture of PEG-400 and butanediol was studied by OCT and diffuse reflectance spectroscopy in the work[307]. As a result, it was shown that the skin diffuse reflectance signal decreased by 90% after 45 minutes of OC, and the probing depth of the OCT method increased by 2.5 times, allowing to image melanoma microvasculature at a depth of 750 μm.

In the work[308], He *et al.* investigated the effect of *in vivo* skin OC with various OCAs on blood glucose monitoring by OCT. Surface application of a 50% glycerol solution showed the best results, in which the correlation coefficient between the slope of the OCT signal and the concentration of glucose in the blood improved by 7.1% on average. The mannitol solution showed similar but less pronounced results.

In recent work[309], salicylic acid was used as an OCA in combination with a chemical epidermal permeability enhancer (azone) to investigate their synergistic effect on the skin *in vivo* using OCT and diffuse reflectance spectroscopy. An increase in the concentration of salicylic acid led to a stronger decrease in the skin reflectance signal. In addition, the best synergistic effect on OCT probing depth (~32% increase) was obtained with 1% salicylic acid and 1% azone.

The same optical methods of skin diagnostics were used in a study[255] where combined optical clearing of human skin *in vivo* with a mixture of thiazone and PEG-400, enhanced by ultrasound, led to an increase in the depth of light penetration into the skin by 41%. The diffuse reflectance signal decreased by up to 15.5% already after 10 minutes of clearing.

In the work[291], a combined OC protocol consisting of the use of lipophilic OCA (oleic acid) in combination with microdermabrasion and sonophoresis was applied to dark skin (phototype IV) *in vivo*. At a depth of 400 μm, the amplitude of the OCT signal increased by 34% as a result of clearing, which significantly improves the potential clinical analysis of highly pigmented skin.

Numerous works, including recent ones, on the spectroscopic studies of the effect of skin OC of laboratory animals reported similar results, consisting in a decrease in the overall level of the skin diffuse reflectance signal[231], [244], [310]–[312] and an increase in the fluorescence signal recorded from deeply located fluorophores[313], [314].

In the work[315], Pena *et al*. demonstrated using double correlation OCT approach that the topical application of OCA reduces the tissues' electro-kinetic response, thus providing a new application in bioelectrical impedance analysis, allowing to estimate the electric properties of biological tissues.

Darwin *et al.* in their recent study[316] demonstrated the effectiveness of OC in the analysis of the concentration of various dyes contained in human skin *in vivo* using Raman microscopy. This technology has shown its potential to improve the method of laser tattoo removal, since the combination of superficial application of glycerin and removal of the stratum corneum with tape stripping allowed increasing the depth of analysis by Raman microscopy from 50 to 400 μm.

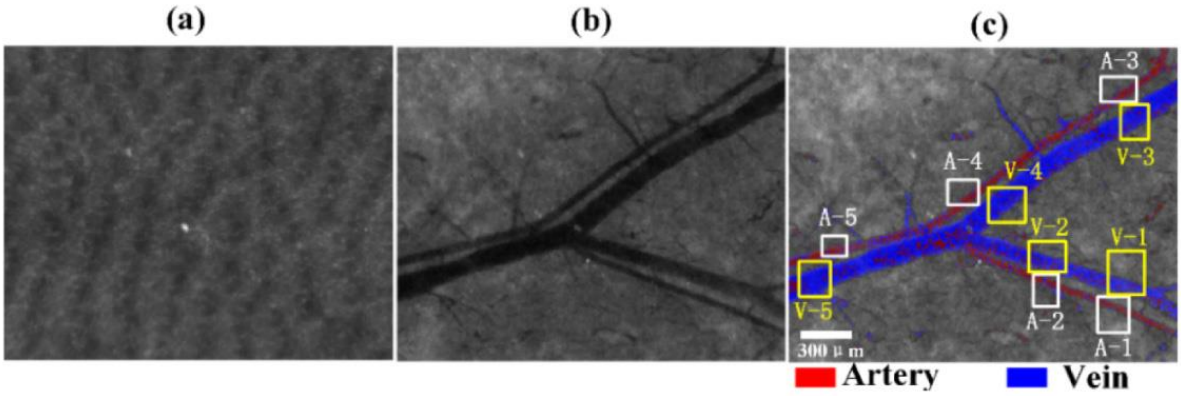

Figure 17. Skin images before and after OC, obtained with hyperspectral imaging. (a) Image of intact skin taken at 540 nm. (b) Skin image taken at 540 nm after OCA treatment. (c) The structure of veins and arteries extracted from hyperspectral images (Labeled (A-1 - A-5, V-1 - V-5) white and yellow boxes represent the regions of interest of arteries and veins, respectively, for subsequent statistical analysis of microvessels saturation with oxygen)[317].

The efficacy of *in vivo* skin OC has also been demonstrated for hyperspectral imaging in recent work[317]. The structure of the skin veins and arteries was obtained after skin treatment with OCA (**Figure 17**), which improved the non-invasive assessment of microvascular oxygen saturation, which is an important analytical parameter in the clinical study of the skin pathologies development.

2. Experimental study of optical clearing effect combined with multimodal optical diagnostic technique

2.1. Introduction

As was described in the previous chapter, optical methods of skin diagnostics are an effective alternative to traditional invasive diagnostic methods. They allow obtaining information about the structural and biochemical skin tissue structure *in vivo* in real time, which led to their extensive implementation in the clinical practice of skin lesions analysis. In the above review of the scientific literature, it was demonstrated that the skin scattering and absorption properties, which are the main reason for the limitation of the use of optical methods in skin diagnostics, can be changed using the method of skin optical clearing.

However, despite the numerous studies of skin OC, described in the previous chapter, by combined (multimodal) optical methods, which allow obtaining complementary information about the skin optical properties[15]–[19], a multimodal spectroscopic analysis of the skin optical parameters with spatial resolution (i.e., with layer-by-layer probing, which makes it possible to separately investigate the spectral data obtained from different skin layers) under the OCA action in combination with CPEs, which offers the practical possibility of a more accurate structural analysis and determination of the boundaries of pathological skin changes, has not been previously studied. In addition, the probe-induced mechanical pressure effect on the skin optical parameters in such measurements was not taken into account or was studied separately.

Thus, the aim of our experimental study presented in this chapter was twofold: (i) to investigate the effect of the OC process applied to *ex vivo* human skin samples on SR DR and AF spectra using two combinations of OCA and CPE, and (ii) to quantify the clearing-like effect of drying and of spectroscopic probe pressure on skin. These two complementary experimental protocols were conducted at CRAN laboratory (University of Lorraine, France) in collaboration with the Metz-Thionville regional hospital for the human skin grafts and at Saratov State University (Saratov, Russia) for the rat skin grafts, respectively. Because we needed several standardized skin samples, *ex vivo* rat skin strips were used also for this study.

2.2. Materials and methods

2.2.1. Chemical agents used for optical clearing

In this study, two mixtures of combined OCA and CPE were chosen from literature data[256] and preliminary own studies[318], [319] for their good OC capacity and low toxicity (possible usable on patients). The first OCA mixture (OCA 1) was made of Polyethylene Glycol 400 (PEG 400, Ref. 202398, Sigma-Aldrich, USA), Propylene Glycol (PG, Ref. P4347, Sigma-Aldrich, USA) and aqueous 3M-sucrose solution (Ref. 59378, Sigma-Aldrich, USA): volume fractions were 45%, 5% and 50% (v/v), respectively. The second OCA mixture (OCA 2) was made of PEG 400 and Dimethyl sulfoxide (DMSO, Ref. 276855-1L, Sigma-Aldrich, USA): volume fractions were 80% and 20% (v/v), respectively. Refractive indices were measured as 1.448 for OCA 1 and 1.466 for OCA 2 using Abbe refractometer DR-M2/1550 (Atago, Japan) at 480 nm and at room temperature (24 ℃).

2.2.2. Skin samples preparation

For the measurement protocol performed on *ex vivo* human skin samples, 13 skin stripes were harvested on skin wastes using an Acculan 3Ti Dermatome (Aesculap®, Chaumont, France) during aesthetic surgery (arm inner side lifting after massive body loss) and after agreement was obtained from the patient. Skin thickness was afterwards measured on histological slides using a conventional optical microscope. Skin sample thickness was determined for each sample as the average of 10 measurements obtained from evenly distributed points on Hematoxylin and Eosin-stained histological slides (using the Piximetre open access software). Mean value over the 13 skin grafts was 900±280 µm. Authorization to use skin wastes for the current study was obtained from the INSERM Ethical committee, IRB 00003888 (opinion #17-400). Two complementary studies are described in this chapter. Indeed, the first study performed on *ex vivo* human skin raised questions that required a second study to be answered. The second study was performed on rat skin grafts as many homogeneous skin grafts were needed.

For the experimental protocol conducted on *ex vivo* rat skin samples, 17 laboratory outbred male rats with a body mass of 200±50 g were used. The use of rat skin for the experiments is justified by the fact that it is often used as a more affordable replacement for human skin in permeation experiments[26]. Moreover, its uniformity and small difference in stratum corneum thickness between samples and individuals give a lower inter-individual

standard deviation of skin permeability compared to human skin[320]. Also, rat skin shows a similarity with human skin in optical properties at wavelengths close to those used in the spectroscopic experiment (at 400 nm wavelength μ_a, μ_s' and refractive index values are 3,7 / 3,8 cm^{-1}, 70 / 71 cm^{-1}, and ~1,45 / 1,42, for human / rat skin respectively)[26], [310], [321].

Skin samples were taken from the thigh area of each animal. All animals were kept in the Shared Services Center of the Saratov State Medical University named after V.I. Razumovsky under the standard vivarium conditions with fixed illumination regime. Animals were treated in accordance with the rules of the European Convention for the Protection of Vertebrate Animals used for Experimental and Other Scientific Purposes (Strasbourg, 1986) and the International Guiding Principles for Biomedical Research Involving Animals.

2.2.3. Hybrid model of ex vivo skin and fluorescent gel

It has been demonstrated in the literature[322] that using a hybrid model consisting of a skin sample placed on a fluorescent film gives the possibility to evaluate the dynamics of skin scattering for a spectroscopic approach by tracking changes in the signal intensity emitted by the fluorescent bottom layer. In this study the top layer of our hybrid model was an *ex vivo* human graft skin, and the bottom layer was a fluorescing, absorbing and scattering gel-based substrate made of agarose (Ref. 16500-500, Invitrogen, USA) as gel material (1% w/v), intralipids-20% (Ref. I141-100ML, Sigma-Aldrich, USA) (5% v/v) as scatterer, Indian Ink (Ref. 45807073, Lefranc & Bourgeois, France) (0.02% v/v) as absorber and Chlorin e6 (Ref. POR0001, Advanced BioChemicals, USA) (Ce6, 500 µM) as exogenous fluorophore (with absorption and emission peaks at ~400 and ~665 nm, respectively (**Figure 18**)). This bottom layer was 10 mm thick; its reduced scattering (μ_s') and absorption (μ_a) coefficients were 5.8 mm^{-1}[323] and 0.08 mm^{-1}[324] at 663 nm, respectively.

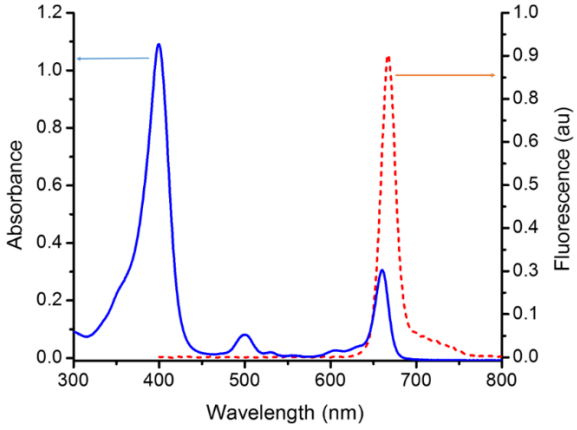

Figure 18. Absorption (solid line) and fluorescence (dashed line) spectrum of Chlorin e6 in methanol[325].

2.2.4. Spatially Resolved multi-modal spectroscopy measurements combined with optical clearing

2.2.4.1. Multimodal spectroscopic device

The SpectroLive® device was used to acquire SR DR and multiply excited AF intensity spectra (see Refs.[326], [327] for detailed technical and metrological features). Briefly, the multiple fiber optics probe used consisted of one central (600 µm - core diameter, Numerical Aperture NA=0.22) excitation fiber that delivered excitation light onto the skin surface, and four rings of six collecting fibers each (200 µm - core diameter, NA=0.22), located at four various distances from the source fiber, i.e., different Source-Detector Separations (SDS): D_1=400 µm, D_2=600 µm, D_3=800 µm and D_4=1000 µm, respectively. SR AF emission spectra were measured consecutively for five different bandpass filtered LED sources (Full Width at Half-Maximum, FWHM ~ 10 nm) centered at λ_1 = 365 nm, λ_2 = 385 nm, λ_3 = 395 nm, λ_4 = 405 nm and λ_5 = 415 nm, respectively. A broadband (350–800 nm) Xenon flash lamp light source was used to obtain the SR DR spectra. The acquisition of the AF and DR spectra were performed using four HRS-BD1 spectrometers (Mightex, USA) (one per SDS), in the 350-800 nm spectral range, with optical resolutions of 1.7, 4.1, 4.1, 9.7 nm-FWMH for D_1, D_2, D_3, D_4 detection channels, respectively.

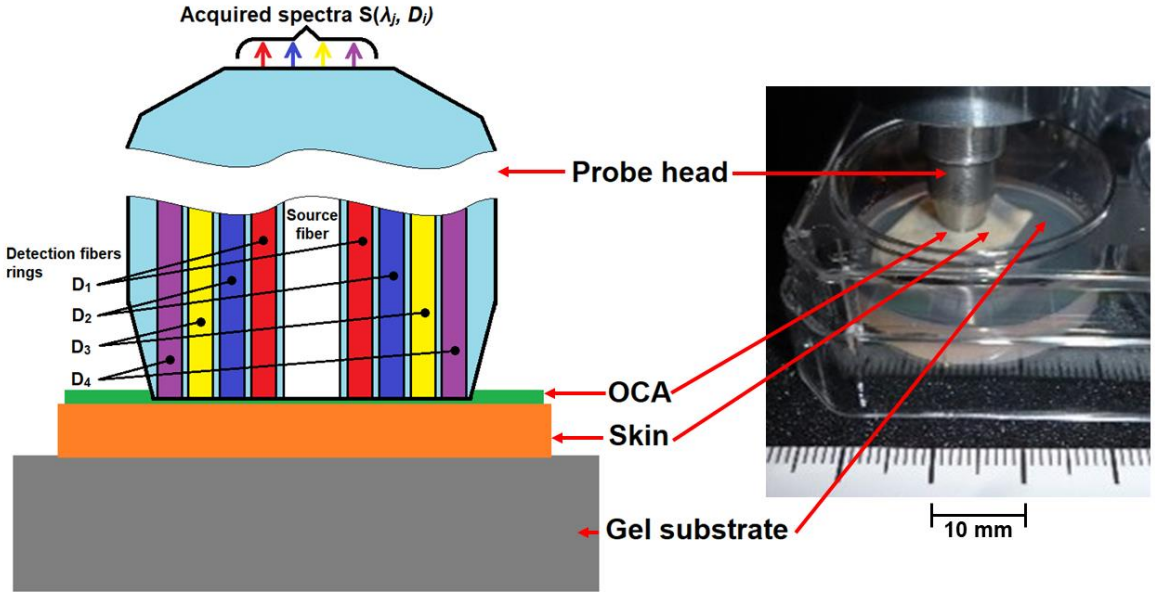

Figure 19. Schematic representation (left) and photo (right) of the hybrid skin-gel experimental model and setup configuration. Spectrolive® device's multifiber optics probe head placed in contact onto the outer surface of the *ex vivo* skin sample, lying on the fluorescing gel substrate. The topically applied OCA is represented in green. S(λ_j, D_i) are the spectra collected by the detection rings of fibers at the four corresponding SDS D_i with D_1=400 µm, D_2=600 µm, D_3=800 µm and D_4=1000 µm.

2.2.4.2. Experimental protocol

The optical clearing and spectroscopic measurement protocol was as follows: at initial time point t0, 0.3 mL of a chosen OCA was applied on the epidermis outer surface of the skin sample lying on the gel substrate of the hybrid model. Then, the optical probe tip was placed in tight contact with the skin epidermis (**Figure 19**) and the spectroscopic data acquired that are, 5 AF intensity spectra (corresponding to the five aforementioned excitation wavelength peaks λ_j) and one DR spectrum at each SDS, resulting in a total of 24 spectra for each time point. To get the time kinetics information, these spectroscopic data were collected every 4 minutes for 36 minutes, that is every t=t0+4k minutes (with k = {0,1,2,3,4,5,6,7,8,9}). Although the complete process of OCAs diffusion into the skin takes several hours, it was decided to track changes only during the first half hour, since the potential clinical use of the immersion clearing technique does not require the completion of the process due to its duration. Only the initial effect of the applied OCA was therefore considered. Four experimental conditions were considered: conditions 1 and 2 for application of OCA 1 and OCA 2, condition 3 for control measurements with saline solution instead of OCA, and condition 4 for "dry" condition (neither saline nor OCA solutions). Three skin samples were tested under each condition except the control measurements where four skin samples were used. For each measured spectrum, three acquisitions in a row were performed and averaged in order to improve its signal-to-noise ratio.

2.2.4.3. Fluorescence and diffuse reflectance spectra preprocessing and exploitation

Raw intensity spectra acquired by the spectrometers were first median filtered to eliminate possible high amplitude spike artifacts and the background spectrum measured on the same day with the light sources turned off was subtracted from all the acquired spectra. The latter background-corrected spectra were then smooth filtered using a Savitzky-Golay polynomial filter with a 20 nm–width spectral window. Then, for the AF spectra, these preprocessed spectra were normalized by corresponding spectral correction coefficients in order to compensate for the different transfer function of each acquisition channel and multiplied by the incident illumination power to allow for amplitude comparison on consistent normalized relative intensity scale (arbitrary units).

Data analysis consisted in Area Under the Curve (AUC) calculation, that is the sum of the intensities within a given bandwidth of the spectra. The main purpose of using AUC instead of

fluorescence or absorption peaks was that the AUC analysis allows to level out possible artifacts inherent in a narrow spectral band (amplitude fluctuation, etc.), as well as to track the overall change corresponding to the quantum yield region (in the case of fluorescence) or the absorption region of a particular chromophore[26].

MATLAB software (R2018a, The Mathworks) was used for all spectral data preprocessing functions and AUC calculations. For the skin AF spectra, the spectral range 425–525 nm was chosen to calculate AUC_{skin_AF}, representing the region of emission of the main skin fluorophores[26]. For the Chlorin e6 (Ce6) contained in the gel layer of our hybrid model, AUC_{Ce6_F} was calculated over the spectral emission bandwidth of this exogenous fluorophore (**Figure 20**) in the 650–700 nm range (Figure 20(a)). In this illustrative graph, the Ce6 emission peak is clearly visible. This allows to conclude that even the short SDS, such as D2, surpass the skin thickness in their depth of probing.

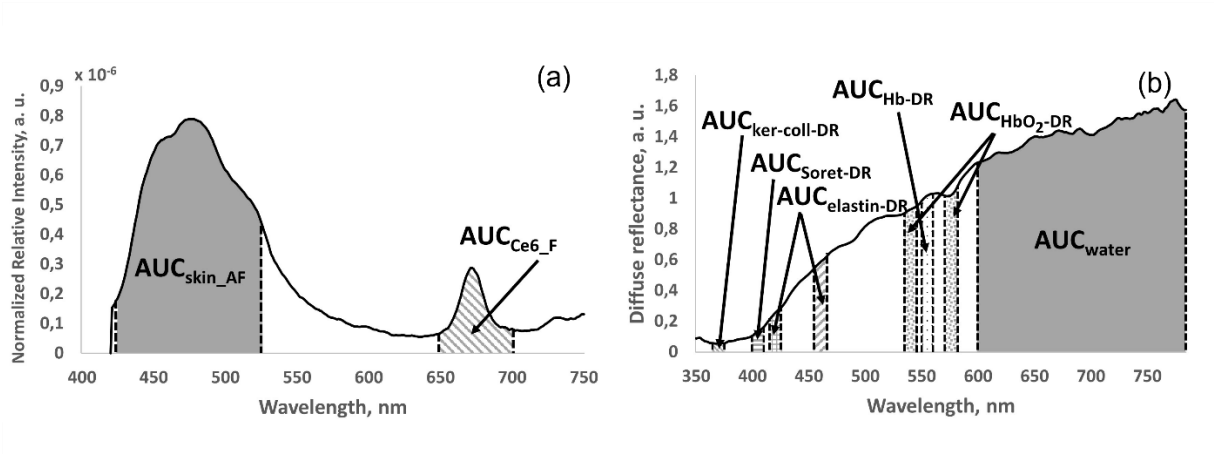

Figure 20. Example of (a) a fluorescence normalized relative intensity spectrum (excited at λ_2=385 nm) collected at SDS D2 with corresponding spectral ranges of calculated Areas Under the Curve $AUC_{skin\text{-}AF}$ for skin autofluorescence (425-525 nm) and $AUC_{Ce6\text{-}F}$ for Chlorin e6 fluorescence (650-700 nm); (b) a DR intensity spectrum collected at SDS D2 with corresponding spectral ranges of calculated $AUC_{ker\text{-}coll\text{-}DR}$ for keratin and collagen cross-links absorption peaks (365-375 nm), $AUC_{Soret\text{-}DR}$ for Soret band of hemoglobin (400-410 nm), $AUC_{elastin\text{-}DR}$ for two peaks of elastin absorption (415-425 nm and 455-465 nm), $AUC_{HbO2\text{-}DR}$ for two peaks of oxyhemoglobin absorption (535-545 nm and 572-582 nm), $AUC_{Hb\text{-}DR}$ for deoxygenated hemoglobin absorption peak (550-560 nm) and AUC_{water} for one of the spectral ranges of water absorption (600-784 nm).

In order to compare the time course of the AUC values obtained for all skin samples in the 4 different experimental conditions, all AUC values were normalized to their initial values (t0) so as to represent the time variations *ΔAUC* (in %) defined as:

$$\Delta AUC(t) = 100 \times \frac{AUC(t) - AUC(t0)}{AUC(t0)} \quad (4)$$

For the DR spectra, the values of AUC were calculated for four bandwidths, corresponding to the absorption range of several skin chromophores (Figure 20(b)): 365-375, 415-425, 455-

465 and 600-784 nm, respectively corresponding to (i) keratin and collagen absorption, (ii and iii) two elastin peaks[328] and (iv) water absorption (water content determines scattering properties of skin in 600-800 nm spectral range)[26]. Also, four bandwidths corresponding to the hemoglobin absorption peaks were calculated: 535-545 nm and 572-582 nm bandwidths related to oxyhemoglobin absorption peaks, 550-560 nm bandwidth related to deoxygenated hemoglobin and the 400-410 bandwidth related to Soret band of hemoglobin (oxyhemoglobin absorption band)[26], [204]. To estimate the overall impact of the experimental protocol on acquired DR spectra, a 365-784 nm bandwidth that corresponds to the entire area of observation was also calculated.

Normalized averaged changes in skin AF and Ce6 fluorescence after 36 minutes of experiment corresponding to each excitation wavelength λ_j and each distance D_i were calculated for each condition using Equation 5:

$$c(\lambda j, Di) = \frac{1}{n}\sum_n \frac{AUC_{t=t0+36}(\lambda j,Di)}{AUC_{t=t0}(\lambda j,Di)} \qquad \text{with} \quad i \in \{1..4\}\ and\ j \in \{1..5\}, \tag{5}$$

where Σ_n is the sum among the n=3 skin samples (for the control condition using saline solution, n=4), $AUC_{t=t0+36}$ is the AUC value after 36 minutes of experimental protocol, $AUC_{t=t0}$ is the initial AUC value.

2.2.5. Pressure effect investigation

To investigate the pressure effect caused by the spectroscopic probe in contact with skin, the following protocol was performed. The fat layer of seven (n=7) *ex vivo* samples (2×2 cm^2) of rat skin was previously removed. Then, each sample was placed on a 15 mm-thick layer of 3%-agarose fluorescent gel (as described in Section 2.2.3). The mean initial (i.e., unloaded) thickness of all used skin samples was measured as 738±66 μm. A 6.35 mm diameter optical probe (R400-7-VIS/NIR, Ocean Optics, USA) was placed in contact with the skin in the center of the test sample (**Figure 21**). Unlike the probe described in Section 2.2.4.1., this probe consisted of one central (400 μm - core diameter, Numerical Aperture NA=0.22) collecting fiber that acquired light emitted by the surrounding ring of six excitation fibers (400 μm - core diameter, NA=0.22) located at SDS of ~500 μm. The peak excitation wavelength was 405±10 nm, and the optical power at the probe tip was 5 mW. The spectra of fluorescence were recorded using a QE65000 spectrometer (Ocean Optics, USA) as a function of the pressure applied by the probe onto the skin. Twelve different loads were added onto the special holder integrated into the probe in order to apply an increasing (total) pressure (ranging) from 82 kPa

(initial time, intrinsic weight of the probe) to 269 kPa. The spectroscopic measurements were performed after 1 minute application of a new load in order to consider relaxation time for the viscoelasticity behavior of the skin samples.

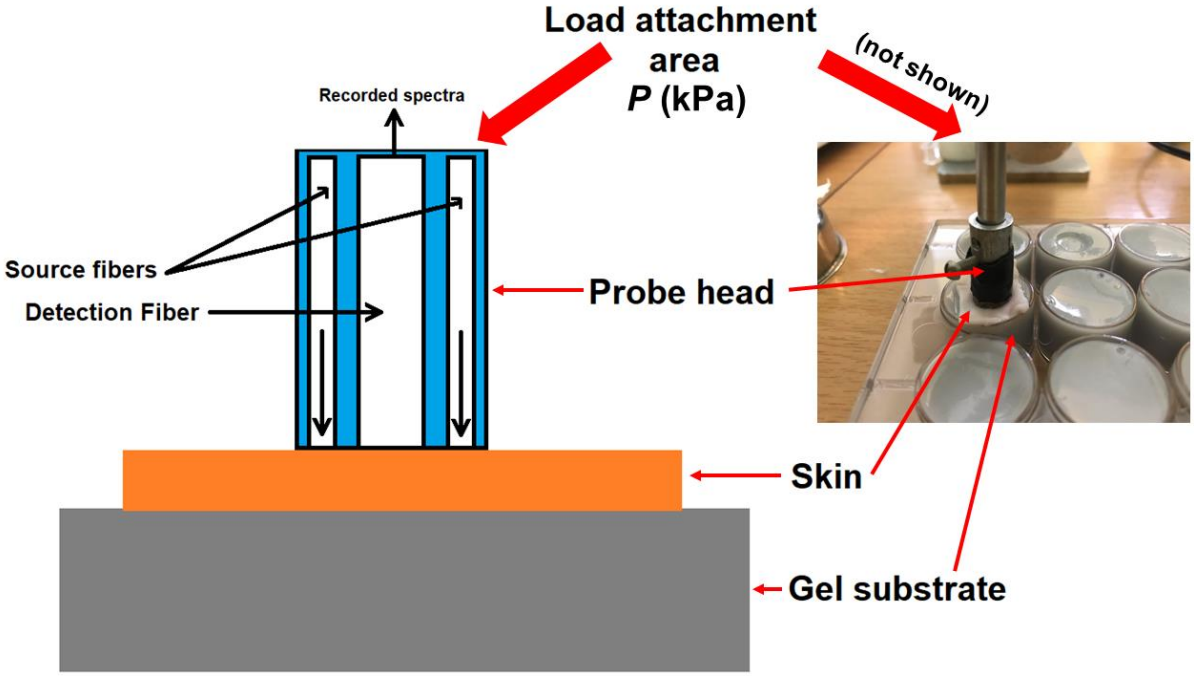

Figure 21. Schematic (left) and photo (right) of the experimental setup. Optical probe head with load attachment area is in contact with the center of skin sample placed on top of a fluorescent gel substrate.

2.2.6. Study of the ex vivo skin dehydration effect on the spectroscopic measurements

To investigate the changes observed in the spectroscopic signals during our experimental protocols on human skin, possibly related to the "natural" dehydration of the *ex vivo* skin samples, ten (n=10) *ex vivo* rat skin samples (2×2 cm^2) with fat layer removed were mounted on a dedicated sample holder and glued around the perimeter of the 1×1 cm^2 square window in the dedicated holder illustrated in **Figure 22**. The latter mounted skin sample was positioned perpendicularly to the collimated beam of a broadband halogen light source HL-2000 (Ocean Optics, USA) using a 400 µm–core diameter and NA=0.22 optical fiber (QP400-1-VIS-NIR, Ocean Optics, USA) coupled to an achromatic collimating lens (74-ACR, Ocean Optics, USA). The light transmitted throughout the skin sample was collected by a similar fiber with collimating lens and converted to intensity spectra in two complementary UV-VIS and VIS-NIR spectral ranges using spectrometers USB4000-UV-VIS and USB4000-VIS-NIR (Ocean Optics, USA), respectively. Two aperture diaphragms were installed midway between the emitting fiber and the sample, and between the collecting fiber and the sample. Spectroscopic data

were acquired every 10 minutes during 40 minutes of "natural" drying of the sample. In order to speed up the latter dehydration process, a warm air flux (~36°C) was directed towards the dermal site of the skin sample for the entire duration of the experimental protocol. In parallel, skin sample thickness measurements were performed before the spectroscopic acquisitions began and at each of the five acquisition time points from start t0 to t0+40 min. For each skin sample, the initial and the final weights were also measured in order to quantify the water loss due to dehydration.

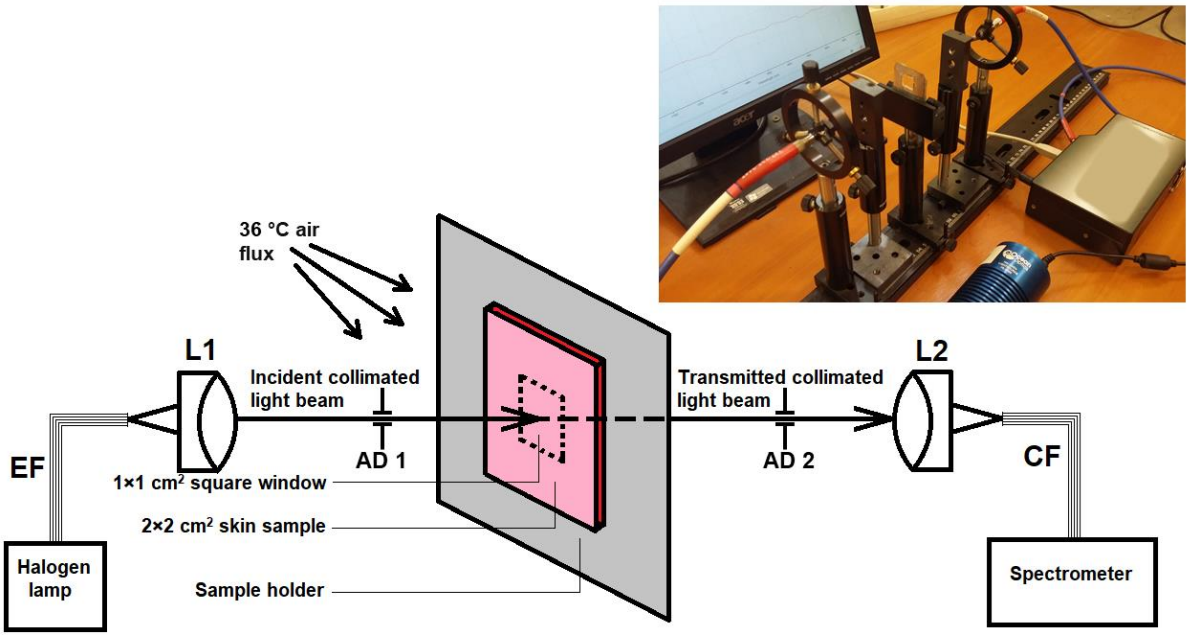

Figure 22. Schematic representation of the experimental setup for studying the *ex vivo* skin dehydration-related modifications of spectral absorbance. Incident collimated light beam delivered from the light source with the emission fiber (EF) and collimating lens (L1) passed through the skin sample mounted on the square hole on the sample holder. Transmitted light was collected onto spectrometers through the collimating lens (L2) and collecting fiber (CF). Two aperture diaphragms (AD 1 and AD 2) were installed midway between the emitting fiber and the sample, and between the collecting fiber and the sample.

2.3. Results and discussion

2.3.1. Optical clearing impact on ex vivo human skin monitored with optical spectroscopy

2.3.1.1. Fluorescence data analysis

Illustrative time curves of AUC variations calculated from the AF ($\Delta AUC_{skin\text{-}AF}$) and Ce6 fluorescence ($\Delta AUC_{Ce6\text{-}F}$) intensity spectra excited at 385 nm on 13 human skin samples are plotted with standard deviation bars in **Figure 23** for OCA 1 (*n*=3), OCA 2 (*n*=3), control (*n*=4) and "dry" (*n*=4) conditions. OCA caused clearing of skin as gel fluorescence acquired from

underneath the skin sample constantly increased from t0 to t0+36 minutes. Clearing of the skin sample may also be deduced from the constant decrease of the skin sample AF intensity[26] over the 36 minutes time delay. After 36 minutes of OCA 1 or OCA 2 application, enhanced light penetration can be observed through an increase of $AUC_{Ce6\text{-}F}$ with time (arising from bottom gel layer) of 50% and 95%, respectively (Figure 23(b)), and a decrease of $AUC_{skin\text{-}AF}$ (from upper skin layer of the hybrid model) of 28% and 15%, respectively (Figure 23(a)). Obtained results have a relatively high SD values due to the small statistical sampling and large biological variations of human skin samples (variations in thickness and morphology). But the mean value of SD for all experimental conditions and time points was 11%.

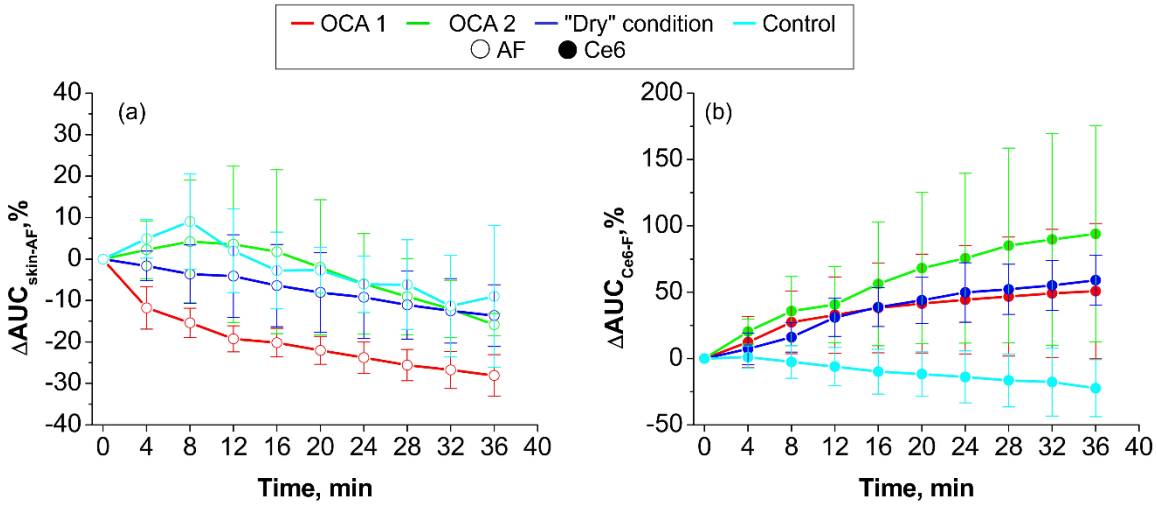

Figure 23. Normalized AUC variations kinetics with standard deviation bars of (a) human *ex vivo* skin AF (empty circles) and (b) gel fluorescence (filled circles) intensity at each time point from 0 to 36 minutes, for OCA 1 (red color, PEG/PG/Sucrose), OCA 2 (green color, PEG/DMSO), control saline solution (blue color) and "dry" (cyan color) conditions, and for excitation wavelength λ=385 nm and distance D_1.

As expected, control measurements using saline solution did not lead to any increase in Ce6 fluorescence intensity collected, i.e., it did not induce noticeable clearing process. However, surprisingly the dry condition induced the same type of results as under the OCA application: 14%-decrease of $\Delta AUC_{skin\text{-}AF}$ and 60%-increase of $\Delta AUC_{Ce6\text{-}F}$. This is the reason why we decided to further investigate the dry condition using more easily accessible skin samples i.e., rat skin samples (see Section 2.3.3).

Representative time curves for all D_i of $\Delta AUC_{skin\text{-}AF}$ and $\Delta AUC_{Ce6\text{-}F}$ excited at 365 nm on *n*=13 human skin samples are presented in **Figure 24** for OCA 1, OCA 2, control and "dry" conditions. Similar graphs, but for excitation at 385 nm, 395 nm, 405 nm and 415 nm are presented, respectively, in **Figure 25**, **Figure 26**, **Figure 27** and **Figure 28**. Standard deviation

(SD) bars were removed from these figures to keep the picture curves legible (the mean value of SD was 11%).

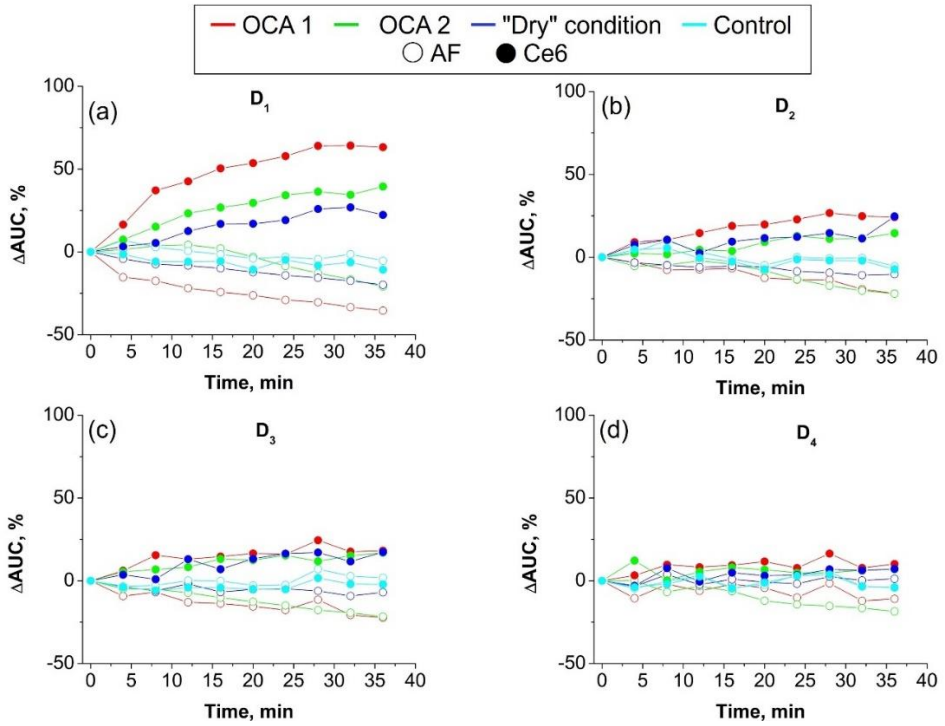

Figure 24. Normalized AUC mean variations kinetics of human *ex vivo* skin AF (empty circles) and gel Ce6 (filled circles) spectra for OCA 1 (red color, PEG/PG/Sucrose), OCA 2 (green color, PEG/DMSO), control saline solution (blue color) and "dry" (cyan color) conditions, and for excitation wavelength λ=365 nm at each distance: (a) D_1, (b) D_2, (c) D_3 and (d) D_4.

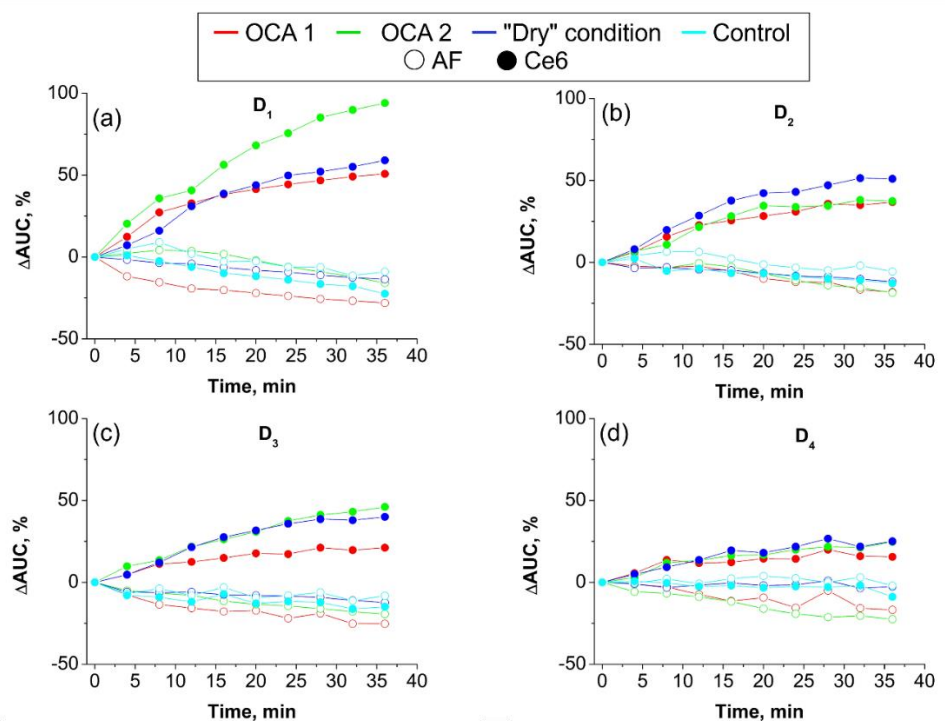

Figure 25. Normalized AUC mean variations kinetics of human *ex vivo* skin AF (empty circles) and gel Ce6 (filled circles) spectra for OCA 1 (red color, PEG/PG/Sucrose), OCA 2 (green color, PEG/DMSO), control saline solution (blue color) and "dry" (cyan color) conditions, and for excitation wavelength λ=385 nm at each distance: (a) D_1, (b) D_2, (c) D_3 and (d) D_4.

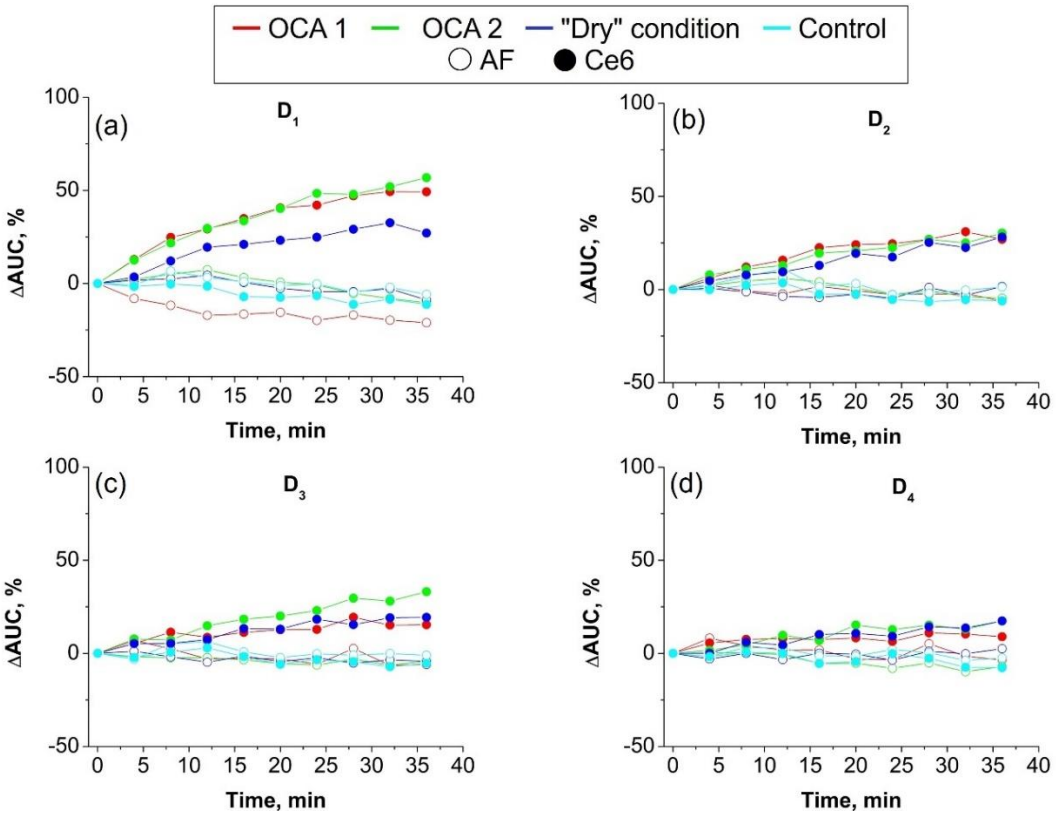

Figure 26. Normalized AUC mean variations kinetics of human *ex vivo* skin AF (empty circles) and gel Ce6 (filled circles) spectra for OCA 1 (red color, PEG/PG/Sucrose), OCA 2 (green color, PEG/DMSO), control saline solution (blue color) and "dry" (cyan color) conditions, and for excitation wavelength λ=395 nm at each distance: (a) D_1, (b) D_2, (c) D_3 and (d) D_4.

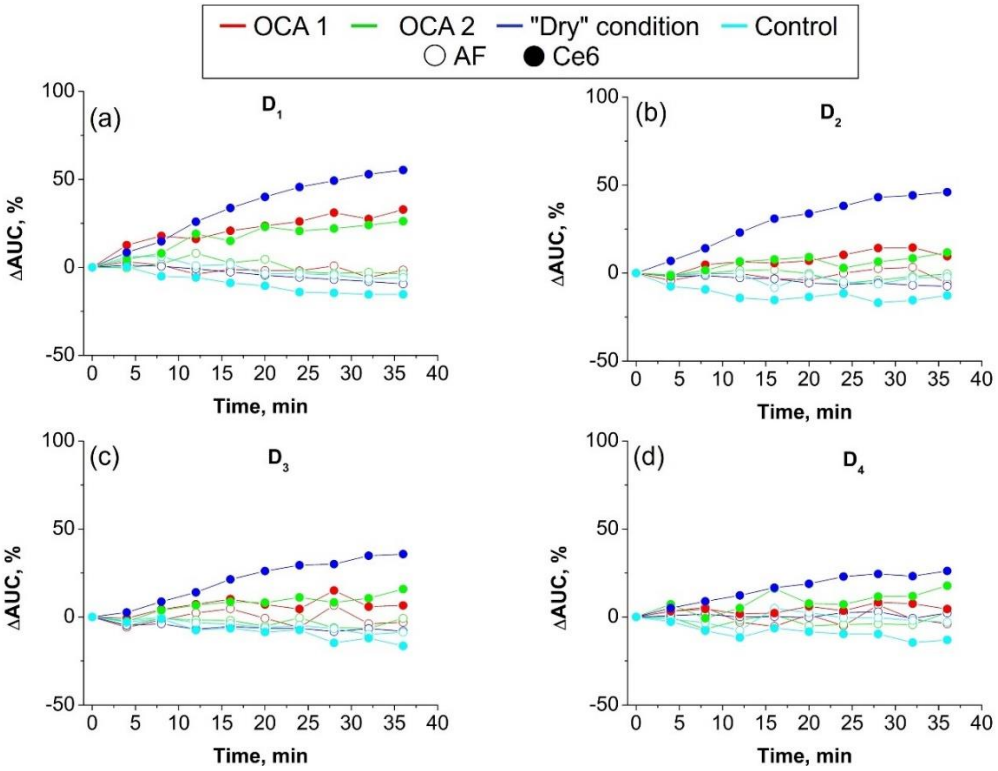

Figure 27. Normalized AUC mean variations kinetics of human *ex vivo* skin AF (empty circles) and gel Ce6 (filled circles) spectra for OCA 1 (red color, PEG/PG/Sucrose), OCA 2 (green color, PEG/DMSO), control saline solution (blue color) and "dry" (cyan color) conditions, and for excitation wavelength λ=405 nm at each distance: (a) D_1, (b) D_2, (c) D_3 and (d) D_4.

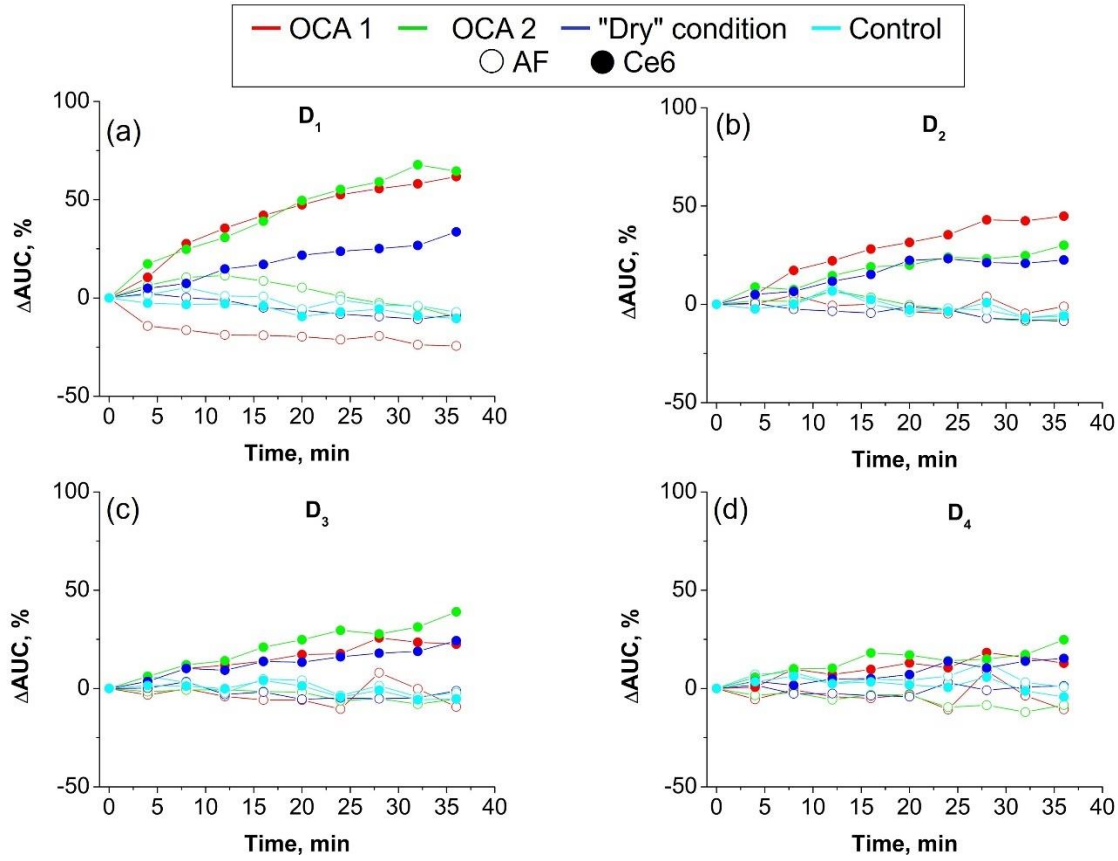

Figure 28. Normalized AUC mean variations kinetics of human *ex vivo* skin AF (empty circles) and gel Ce6 (filled circles) spectra for OCA 1 (red color, PEG/PG/Sucrose), OCA 2 (green color, PEG/DMSO), control saline solution (blue color) and "dry" (cyan color) conditions, and for excitation wavelength λ=415 nm at each distance: (a) D_1, (b) D_2, (c) D_3 and (d) D_4.

Figures 24, 25, 26, 27 and 28 show that OCA 2 in general has a greater clearing impact than OCA 1 when considering the Ce6 fluorescence intensity increase at D_1 clearly but also D_2, D_3 and D_4: for example, 25%-increase at D_4 excited at 385 nm (vs 15%-increase for OCA 1) or 39%-increase at D_3 excited at 415 nm (vs 22%-increase for OCA 1). The only noticeable exception (63%-increase for OCA 1 vs 39%-increase for OCA 2) was observed for 365 nm-excited Ce6 fluorescence at D_1 (Figure 24(a)). For both OCA, osmotic effect of applied OCA followed by a refractive index matching after their diffusion within skin layer caused reduction in skin scattering. As the result, less photons are scattered in the skin: more photons propagate deeper throughout and within the skin and can be collected at a longer distance after 36 minutes[26], [28]–[30]. On the contrary, when considering skin AF, OCA 1 seems to have the same level of clearing as OCA 2 or even a slightly greater one as 385 nm-excited skin AF intensity, for example, displays a 28%-decrease at D_1 (vs 18%-decrease for OCA 2). For D_2, D_3 and D_4 excited at all λ_j, the mean skin AF intensity decrease is slightly constant after 36 minutes and quite similar (11%-decrease) for both OCA 1 and OCA 2.

The “dry” condition shows that the *ex vivo* skin samples experience compaction and shrinking of cutaneous layers inducing clearing-like effect[22], [26], [329], [330]. It is worth noting that the 405-nm excited Ce6 fluorescence increase under the “dry” condition at all D_i is obviously greater than that of both OCA 1 and OCA 2, which is apparently due to the skin dehydration and the fact that the main absorption peak of Chlorin e6 is located approximately at 403 nm.

Normalized averaged variations of $AUC_{skin\text{-}AF}$ and $AUC_{Ce6\text{-}F}$ after 36 minutes of experiment for each excitation wavelength λ_j and each distance D_i are presented in **Figure 29**. From this figure spatial resolution reveals that clearing has a greater impact on all spectra intensities at shorter distances than at longer ones: the signal increase (respectively decrease) is greater at D_1 than at D_4 for Ce6 (skin AF respectively). Since shorter distances are mostly sensitive to upper cutaneous layer, this was expected as the main optical barrier is epidermis and even more the upper layer of epidermis, i.e., stratum corneum.

To observe the general effect of each experimental condition on the acquired spectra and to compare the results between the conditions, boxplots were built for normalized averaged variations of $AUC_{skin\text{-}AF}$ and $AUC_{Ce6\text{-}F}$ after 36 minutes, grouping all variations values at all five λ_j, for each condition and each distance D_i and presented in **Figure 30**.

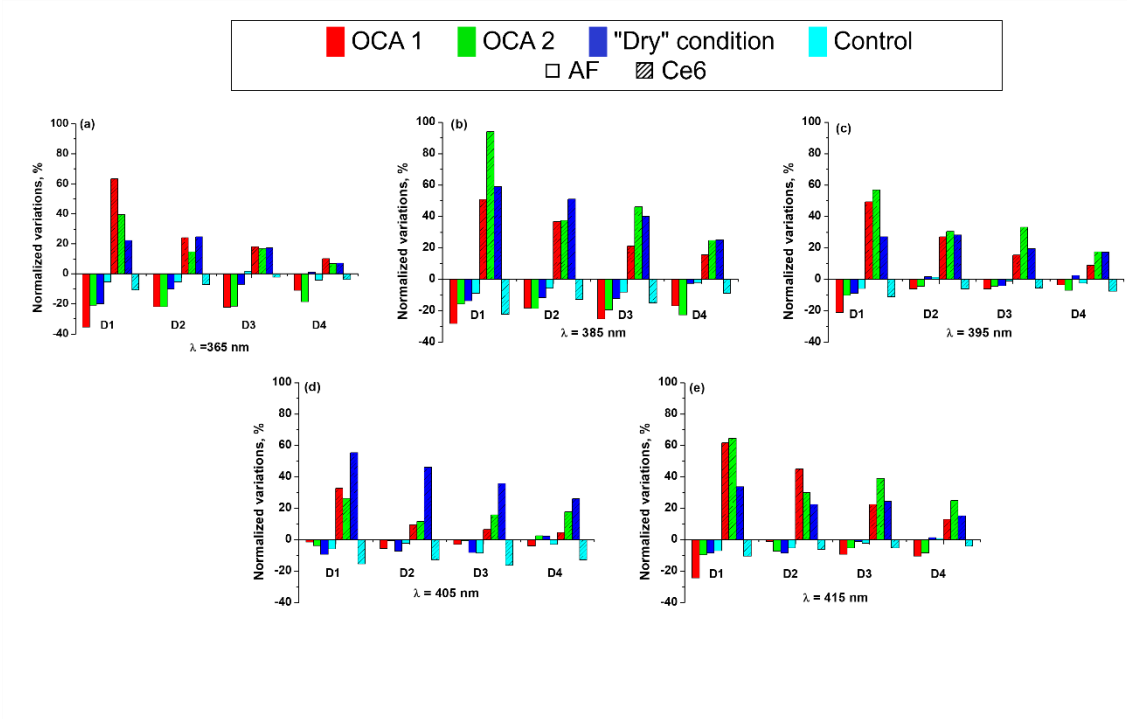

Figure 29. $AUC_{skin\text{-}AF}$ and $AUC_{Ce6\text{-}F}$ normalized variations (%) after 36 minutes of experimental protocol application for all four experimental conditions (OCA 1, OCA 2, dry and control) for each distance (D_1, D_2, D_3 and D_4) and each excitation wavelength λ_j: (a) 365 nm, (b) 385 nm, (c) 395 nm, (d) 405 nm and (e) 415 nm.

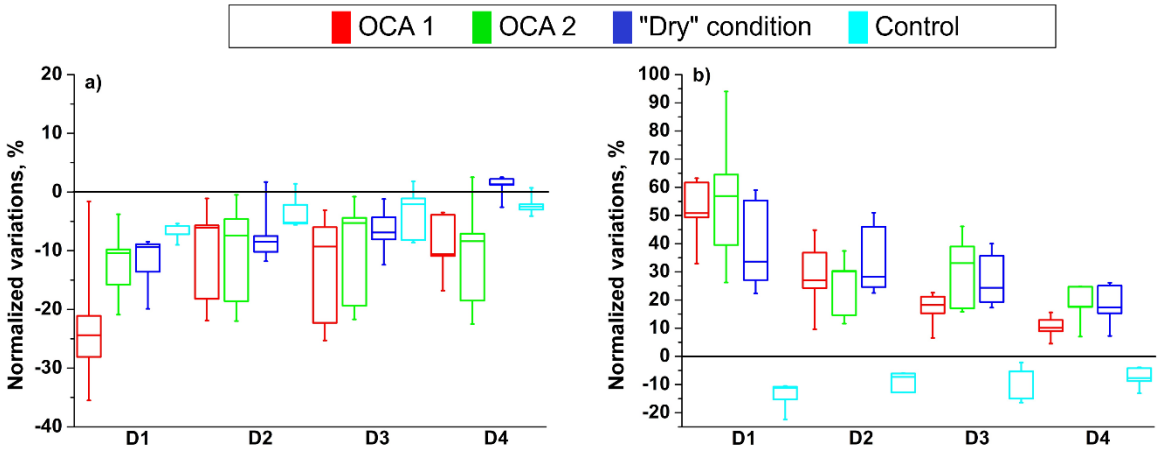

Figure 30. (a) $AUC_{skin\text{-}AF}$ and (b) $AUC_{Ce6\text{-}F}$ boxplot graphs of normalized variations (%) of spectra intensity after 36 minutes of experimental protocol application grouped among all five λ_j for each experimental condition (OCA 1, OCA 2, dry and control) and each distance (D_i). Boxes values are first quartile, median and third quartile, whiskers are the minimum and maximum of data, respectively.

For OCA 1 (PEG/PG/Sucrose mixture), a mean 24% decrease of $AUC_{skin\text{-}AF}$ for all λ_j was observed at D_1, what is ~2 times greater than that of OCA 2 (PEG/DMSO mixture) (11% mean decrease). This is probably due to the presence of Sucrose in OCA 1, that has strong hyperosmotic properties[29]. The free water extraction from epidermal and dermal layers leads to skin AF intensity decrease. According to the literature, PG is widely used as a penetration enhancer that can solubilize the intercellular lipids of SC, thus facilitating the dehydration process[331]. As a result, the superficial skin layers were probably affected stronger than by OCA 2 after 36 minutes. But on the other hand, analysis of spectra acquired by a more distant collection fibers (D_3 and D_4) gives an opposite result. Here, the decrease of $AUC_{skin\text{-}AF}$ and increase of $AUC_{Ce6\text{-}F}$ is more prominent for OCA 2. This difference in the values from more distant SDS is probably due to DMSO impact, that is the hydrophilic solvent capable of changing the intercellular keratin conformation from α helical to a β sheet and interact with lipid bilayer of human skin SC, thus facilitating and increasing the rate of OCA diffusion deeper within the skin[26], [30], [332]. In comparison with OCA 1, where PG is used as an enhancer, the volume concentration of DMSO as an enhancer was 4 times greater in OCA 2. This fact probably resulted to a deeper diffusion of the PEG/DMSO (OCA 2) mixture within the skin and to more significant interaction with the collagen and elastin fibers, giving a better optical clearing effect after 36 minutes.

2.3.1.2. DR data analysis

Normalized variations of human skin *ex vivo* AUC_{DR} after 36 minutes (end of protocol) for the absorption spectral bandwidths of keratin, elastin/collagen and water are presented in **Figure 31**. We propose to focus DR analysis here on data acquired (i) at D_1 for keratin (365-375 nm) as keratin is found in the upper layer (SC) and shorter distances are sensitive to upper layer optical properties (Figure 31(a)), and (ii) at D_4 for water (600-784 nm spectral range) and elastin/collagen as both elastin and collagen are found in deeper layers (Figure 31(b)) to which longest distances are most sensitive.

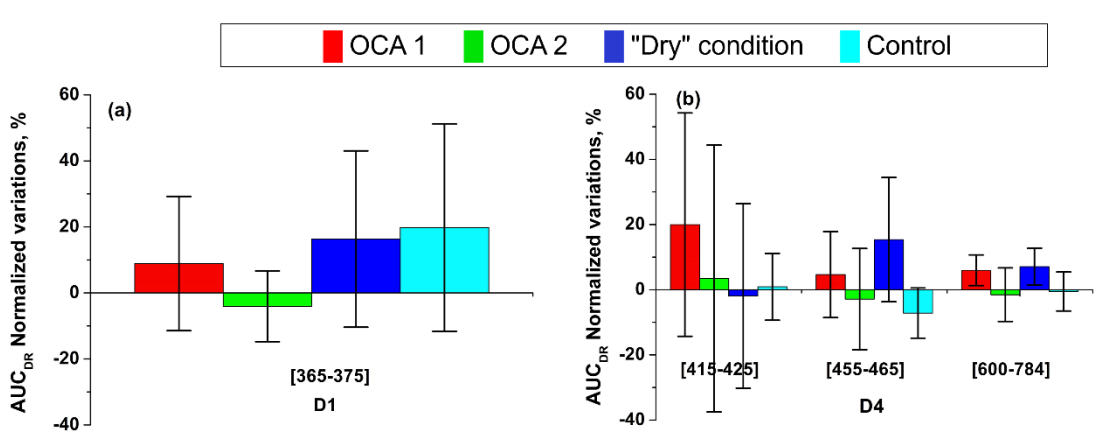

Figure 31. AUC_{DR} normalized variations (%) after 36 minutes of experimental protocol application for all four experimental conditions (OCA 1, OCA 2, dry and control) for (a) keratin spectral bandwidth (365-375 nm) at D_1 and (b) water (600-784 nm) and elastin/collagen spectral bandwidths (415-425 nm and 455-465 nm) at D_4.

OCA 2 has a higher clearing effect than OCA 1 as the DR signal tends to decrease/increase when OCA 2/OCA 1 is applied. DR signal decrease is due to cutaneous layers scattering coefficient lowering. Moreover, analysis of normalized variations of AUC_{DR} after 36 minutes for the spectral bandwidths of blood absorption, presented in **Figure 32**, allows to suggest that OCA 1 application even caused an increase in skin scattering of the upper layers (epidermis and dermis). As we can see, application of OCA 1 causes significant increase of DR at D_1 (Figure 32(a)) for all observed spectral bandwidths related to blood absorption. At D_2 distance (Figure 32(b)), the changes in DR caused by OCA 1 are not so pronounced (except for Soret band), but still noticeable. At longer distances (D_3 and D_4 (Figure 32(c,d))), such a noticeable OCA 1 effect is no longer observed. For OCA 2, a decrease at D_2 and D_3 was observed for all four blood-related bandwidths, that is probably due to clearing effect.

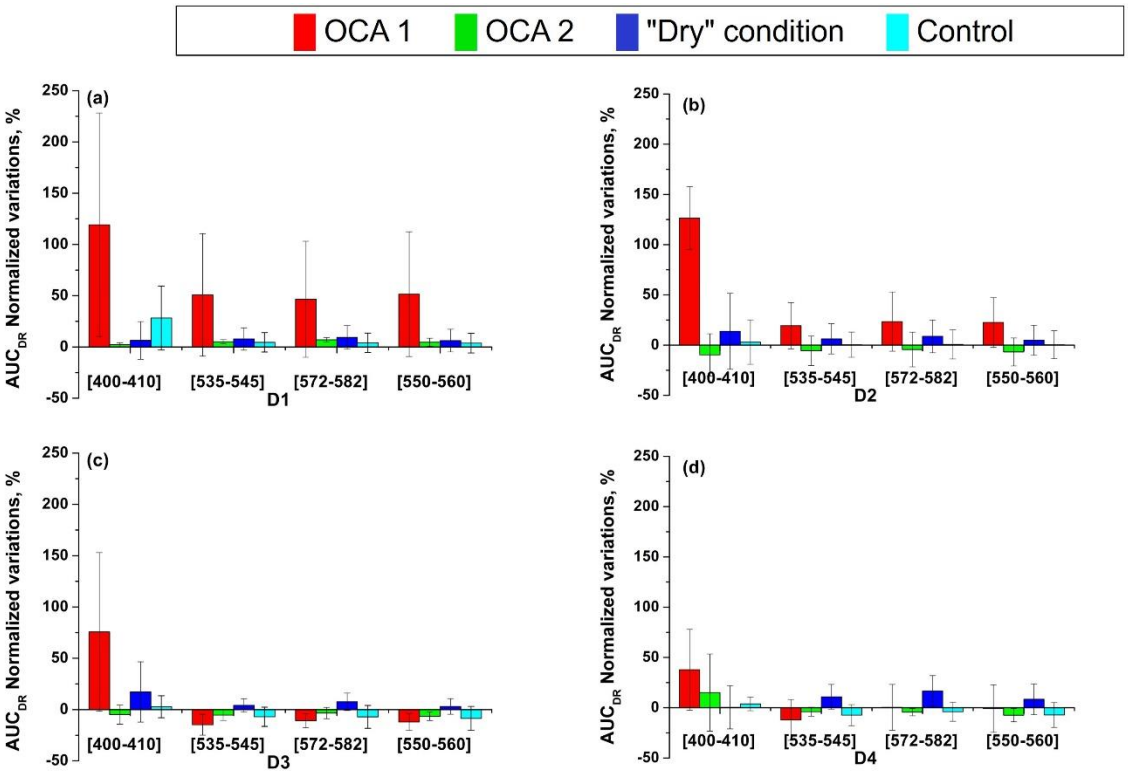

Figure 32. AUC_{DR} normalized variations (%) after 36 minutes of experimental protocol application for all four experimental conditions (OCA 1, OCA 2, dry and control) for Soret band (400-410 nm), oxyhemoglobin spectral bandwidths (535-545 nm and 572-582 nm) and deoxygenated hemoglobin spectral bandwidth (550-560 nm) at D_1 (a) and D_2 (b).

Considering the whole spectral range that is presented in **Figure 33**, we can notice a very stable increase of DR signal for all distances under dry conditions after 36 minutes of protocol, that is consistent with the literature data[26]. Within this spectral range, water absorption decrease caused by dehydration contributes to an increased DR intensity.

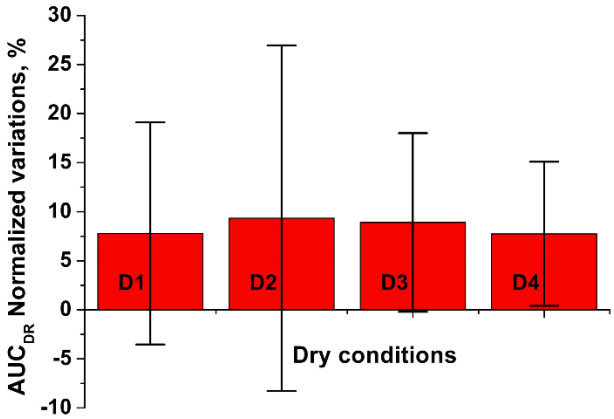

Figure 33. AUC_{DR} normalized variations (%) after 36 minutes of experimental protocol for dry condition for whole spectral bandwidth (365-784 nm) for each distance (D_1, D_2, D_3, D_4).

2.3.2. Probe pressure effect investigation

Because the results obtained at the previous experiment using human skin raised questions about the impact of probe pressure on skin samples and about skin drying during the experiment, additional measurements were performed on rat skin, thus providing a more "homogeneous" (in terms of thickness mainly) set of skin samples. To investigate these unexpected results of the dry condition, we proposed 2 hypotheses to the clearing-like results: probe pressure and dehydration effects.

The variations of AUC values normalized to the initial pressure level ΔAUC(P) were calculated as a function of the optical probe pressure P(kPa) applied onto rat *ex vivo* skin sample for the 450-550 nm skin AF spectral range and for the 650-700 nm gel Ce6 fluorescence spectral range (hybrid model). Then, corresponding ΔAUC_{skin_AF} and ΔAUC_{Ce6_F} were averaged among seven (*n*=7) *ex vivo* rat skin samples. Resulting curves are presented in **Figure 34**.

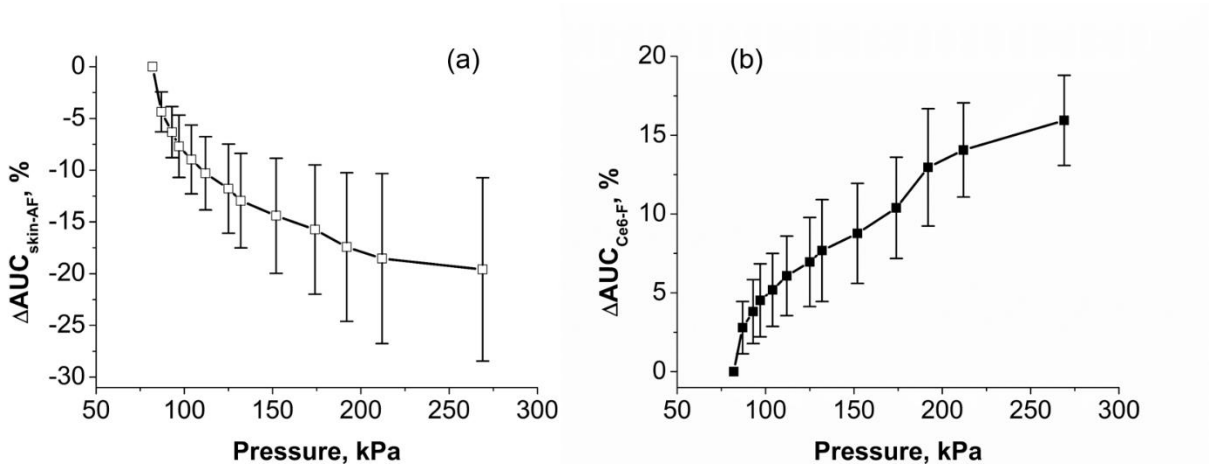

Figure 34. Normalized AUC variations dependence on the applied pressure for the (a) rat skin *ex vivo* AF and (b) Ce6 fluorescence. Mean values and SD were calculated for the results obtained from 7 skin samples (*n*=7).

A non-parametric two-sided Wilcoxon signed rank test was applied to the corresponding groups of AUC both for AF and Ce6 values to test the significance of kinetic differences. At a 5%-significance level, all the differences between paired groups were considered to be statistically significant ($p < 0.05$).

The results of the probe pressure experiment showed that an increase in the load applied by the spectroscopic probe led to an increase in the Ce6 fluorescence intensity detected through skin sample and to a decrease of the skin AF intensity. The results are consistent with data from the literature[329], [330], [333]–[337]. General observation is that under compression, absorption and scattering coefficients increase. Water displacement causes thinning of the skin samples that results into increased transmittance. It allows a greater

volume of excitation (and emission respectively) photons to reach the fluorescing gel layer (the detector respectively).

The clearing-like effect of the probe pressure is here confirmed.

2.3.3. Measurements of a dehydration effect on a light propagation through the skin

As shown in **Figure 35**, mean thickness of ten (*n*=10) rat *ex vivo* skin samples was measured every 10 minutes for 40 minutes. A 15-% decrease of mean skin thickness is observed after a 40 minute-drying protocol.

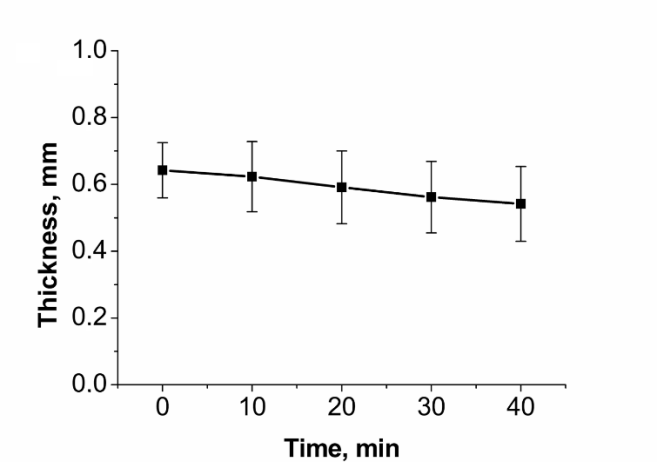

Figure 35. Mean thickness of ten (*n*=10) rat *ex vivo* skin samples as a function of drying time.

Depending on the specific skin samples and initial thickness, the corresponding collimated transmittance signal was increased by up to 8 times with drying. An illustrative graph of collimated transmittance kinetic measured at λ=600 nm for 10 skin samples data points is presented in **Figure 36**. The latter shows an overall increasing transmittance tendency of about 2-fold after 40 minutes (fitted curve T=0.11 to T=0.22). For the 500-750 nm spectral range, an increase of transmittance intensity was observed over the 40 minute-drying protocol.

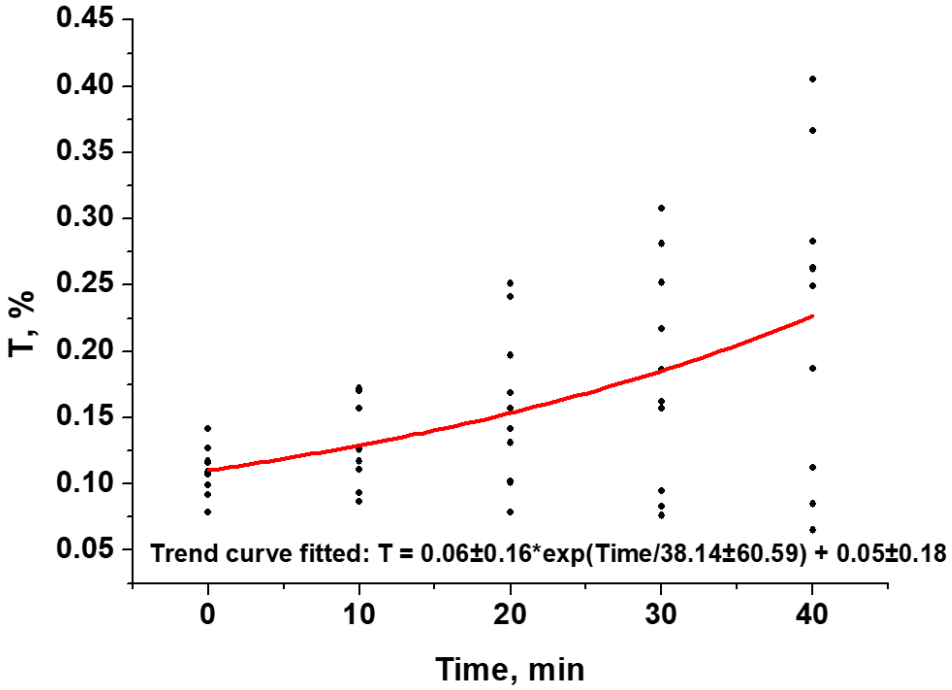

Figure 36. Kinetic data points (black dots) of collimated transmittance for ten (*n*=10 skin) rat *ex vivo* samples acquired at λ=600 nm with the trend curve fitted (exponential growth, in red).

To test the significance of observed differences and to dispel possible doubts about the significance of the transmittance change, a Wilcoxon signed rank test was applied to the groups of mean values of collimated transmittance within the 500-750 nm bandwidth. As seen in **Figure 37**, considering a 5%-significance level, transmittance measured at any time point appeared to be significantly different compared to transmittance measured at any other time point (except for t=t0+20 vs t=t0+30 which is the only pair that displays no statistically significant difference).

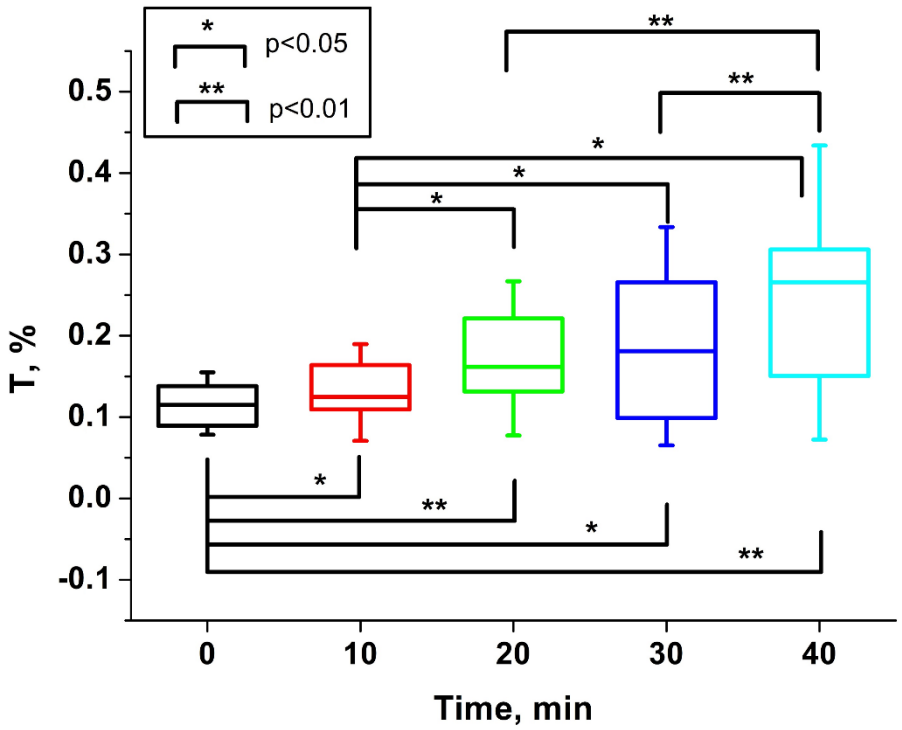

Figure 37. Boxplot of collimated transmittance (mean values over the 500-750 nm bandwidth) kinetic groups (*n*=10) and corresponding results of a two-sided Wilcoxon signed rank test of significance of collimated transmittance differences (pairwise comparison brackets). Boxes values are first quartile, median and third quartile, whiskers are the minimum and maximum of data, respectively.

As noted in Section 2.3.3, dehydration caused an increase of collimated transmittance signal through skin with time. Simultaneous thickness measurements proved that observed increase might be related to the skin thinning with time which takes place because of the water displacement and evaporation. At the same time, skin structural modifications (more scatterers and absorbers per unit volume) may cause increase of scattering and absorption coefficients from one hand and also better tissue components compactness (collagen and elastin fibers ordering) from the other hand. The latter will lead to scattering waves constructive interference with better overall light transmittance through the sample[26]. Together with tissue layer thinning these two mechanisms for sure will overcome some increase of scattering and absorption coefficients, which was demonstrated experimentally.

Ex vivo hybrid model that was tested in this study showed a good applicability for spectroscopy as it allows to test spectral contribution of different fluorophores located at the various depths and their kinetic. However, some limitations are also applied. Unlike *in vivo* conditions, this model does not possess neither blood nor lymph flows (only residual hemoglobin is present inside vessels and capillaries): therefore, effect of hemoglobin on acquired spectra is low, and skin dehydration is observed. However, this two-layer model suits

well the study of clearing using spatially resolved spectroscopy as different distances of photons collection are sensitive to different depths allowing to discriminate different clearing processes at different skin depths.

A bulk signal (like optical spectra acquired *in vivo*), mixing contributions from all cutaneous layers, would not be open to such interpretation.

Moreover, this model has previously been used[322] with non spatially resolved fluorescence spectroscopy. We demonstrated this model was also suited for studying the impact of topically applied OCA on skin samples over time using spatially resolved spectroscopy and also combining fluorescence spectroscopy and DR to investigate the depth dependency of the OC process.

On the hybrid model, DMSO allowed a greater clearing impact when considering the underneath gel fluorescence intensity increase compared to sucrose as OCA. Results obtained with DR showed that the clearing process was mainly due to the dissolution of the lipid layer, due to which DMSO has long and successfully been used as an enhancer of skin permeability for drugs.

Our study also raised the question of methodology and more specifically about control conditions, thus two control conditions were used: using saline solution and using “nothing” (neither saline nor any type of solution), i.e., dry condition.

Dehydration appeared as a new effect to take into account in the dry condition which was avoided when using saline solution. To our knowledge, such process has rarely been described in the literature so far[30], [36].

2.4. Conclusion

The current study was carried out using *ex vivo* skin samples (human and rat). Experimental results presented in this chapter indirectly confirm that the improvement of the depth sensitivity of the spatially resolved DR and AF spectroscopy is related not only to the refractive indices matching under OCA effect, but also to the mechanical clearing effect due to probe pressure. In case of absence of any liquids applied on the skin sample, an increase in spectroscopic signal could be also related to the water loss by the *ex vivo* skin that cannot maintain its properties and getting thinner with the exposure time. Also, a great potential of the multiple excitation wavelengths combined with DR has been demonstrated, allowing to

distinguish different spectral contributions, related to the various skin fluorophores, located in different skin depths.

The clearing-like results obtained in dry condition also allowed us to investigate the optical probe pressure effect which indeed by inducing compaction of cutaneous layers also contributes to the clearing process along with dehydration and refractive index matching induced by OCA.

3. Experimental study of biocompatible enhanced optical clearing effect of human skin *in vivo* by the LC-OCT imaging technique

3.1. Introduction

Section 1.3.4 of Chapter 1 demonstrated that currently there are many examples of using OC technology to improve the contrast of OCT skin images *in vivo*[35], [36], [305], [306], [308] and, in particular, its application for skin cancer characterization[307]. However, when translating these methods into clinical use, there is a need to comply with established regulations, including the use of chemicals on healthy and pathologically changed skin of patients. At high concentrations, OCA show significant results, however, in clinical settings, the concentrations of the substances used may need to be reduced in order to pass the threshold of clinical utility and biocompatibility[338].

The penetration of most chemicals is hindered, as they are stopped by the SC layer, which acts as a natural barrier of human body[40], [339], [340]. Most of the used OCAs are hydrophilic and are used in high concentrations, that hinders their penetration through the stratum corneum into the living epidermis[341], but at the same time they may cause damage and even necrosis of the skin when injected under the dermis[262], [342]. On the other side, a low concentration of OCA does not allow to achieve a noticeable clearing effect. Thus, the use of OCA at biocompatible concentrations should be combined with the use of CPE, which, even at relatively low allowed concentrations, can disrupt the impermeable structure of the SC and facilitate the penetration of OCA. Additionally, the physical permeation enhancement methods can be combined with CPE for more efficient biocompatible clearing.

Considering this, the aim of our next experimental study presented in this chapter, according to the list of objectives addressed in this PhD work, was to experimentally evaluate using Line-field Confocal OCT (LC-OCT) technique the efficacy of optical clearing of human skin *in vivo* with biocompatible OCA combined with chemical and physical permeability enhancers.

3.2. Materials and methods

3.2.1. Chemical agents

In this study, nine different combinations of OCA and CPE were studied as potential clinically-biocompatible mixtures. The latter were chosen based on the literature data

including our own preliminary studies[26], [29], [30], [36]. Three chemicals, most often referred to as OCA in the scientific literature, were selected: Polyethylene Glycol 400 (PEG, Sigma-Aldrich, USA) as an OCA from the group of alcohols and two aqueous 3M- solutions of sugars – Sucrose (Sigma-Aldrich, USA) and Glucose (Sigma-Aldrich, USA). As CPE compounds mentioned in the scientific literature[26], [30], three other chemicals were considered: Propylene Glycol (PG, Sigma-Aldrich, USA) as an alcohol group representative, Dimethyl sulfoxide (DMSO, Sigma-Aldrich, USA) as an organic solvent and Oleic acid (OA, Sigma-Aldrich, USA) as the fatty acid. For the sake of biocompatibility, the concentrations of each of the aforementioned substances in the present experimental study did not exceed their maximum allowed concentration, established by the FDA and contained in the inactive ingredients database, for topical application in the form of a solution[338]. The resulting compositions of OCA and CPE, as well as their volume fractions and maximum allowed concentrations from FDA database are shown in **Table 3**. As there is no information about maximum FDA-allowed concentration for topical application of glucose and sucrose, the concentration of 50% was established for use in this experiment because it was reported as the most effective concentration of glucose for optical clearing[343]. In the case of OA and DMSO, it was not possible to mix them only with any of the three OCA, since in this case the maximum allowed concentration for these chemicals would be exceeded. For this purpose, PG or distilled water was additionally mixed to their solutions as the second CPE to compensate for the allowed concentrations.

Table 3. Concentration values of the nine mixtures of OCA and CPE with corresponding FDA-allowed maximal concentrations for topical application in the form of solution and volume fractions (%, v/v) of resulting mixtures.

Concentration (%, v/v)		OCA			CPE			Distilled water
		Glucose	PEG-400	Sucrose	DMSO	OA	PG	
	Max *c*. (FDA)	-	4 (w/v)	-	45,5 (w/w)	7,4 (w/w)	99,98 (w/v)	-
Glucose/DMSO		50			45.5			4,5
Glucose/OA/PG		50				7.44	42.56	
Glucose/PG		50					50	
PEG/OA/PG			3.52			7.44	89.04	
PEG/PG			3.52				92.48	
PEG/PG/DMSO			3.52		45.5		50.98	
Sucrose/DMSO				50	45.5			4.5
Sucrose/OA/PG				50		7.44	42.56	
Sucrose/PG				50			50	

Also, a 36 g/L hyaluronic acid (HA) aqueous solution (Evalar, Russia) was used to treat specific skin areas in order to determine the potential effect of hyaluronic acid as a CPE without being included in the mixtures. It was decided not to include hyaluronic acid in the composition of OCA, but to use it separately, since the literature mentions an increase in skin permeability for hydrophilic and lipophilic OCA after preliminary treatment of the skin with an aqueous solution of hyaluronic acid[264].

3.2.2. Anatomical skin sites

The human skin sites under investigation were the areas of left- and right-hand dorsum skin *in vivo* between the thumb and forefinger of healthy volunteers. Three volunteers aged between 25 and 31 years with the skin phototype of 2 and 3 were enrolled in this study. All skin areas were subjected to the experimental protocol repeatedly due to the number of mixtures and experimental conditions. To prevent residual effects of the previous protocol, each skin area remained intact for a week before the beginning of the next exposure. All volunteers gave their informed consent for topical application of OCAs mixtures, dermabrasion, sonophoresis of skin dorsum of their hand and the acquisition of LC-OCT images, for the kinetics study. Volunteers' safety was guaranteed thanks to FDA-approved concentrations of OCAs and to CE-marked LC-OCT, dermabrasion and sonophoresis medical device.

3.2.3. Technical equipment

3.2.3.1. LC-OCT

Line-field Confocal Optical Coherence Tomography (LC-OCT) device “deepLive” (Damae Medical, France) was used for the image acquisition. Operating at a 650-950 nm spectral range emitted by a supercontinuum laser, it provides a unique 3D imaging modality, allowing to switch from a histology-like vertical mode to a confocal-like horizontal mode, and to record a 3D stack of tissue volumes *in situ* with a maximum axial and lateral resolution of less than 1.3 µm and a penetration depth about 500 µm[176]. Such a resolution allows to estimate the contrast changes of the tested skin caused by optical clearing at a cellular level (**Figure 38**).

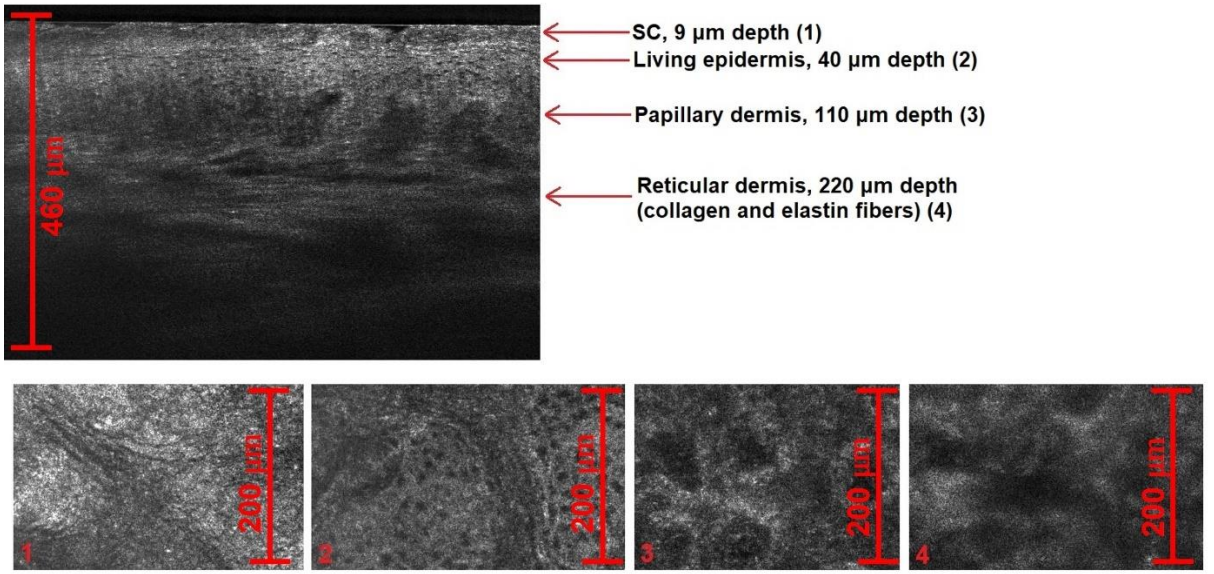

Figure 38. (top) Histology-like B-scan extracted from LC-OCT acquired 3D-image, displaying visible distinguishing between different skin layers; (bottom) 4 different skin layers images, extracted as confocal-like horizontal scans from the 3D-image: SC layer, acquired at 9 µm depth (1), Living epidermis, acquired at 40 µm depth (2), Papillary dermis, acquired at 110 µm depth (3), Reticular dermis, acquired at 220 µm depth (4).

3.2.3.2. Physical permeation enhancers

Therapeutic ultrasound (Pulson 100, Gymna, Belgium) was used as a physical permeability enhancer in experiments with OCT since this technique helps to increase the permeability of the skin[291], [292], [295]. The duty cycle was 100%, frequency was 1 MHz, and the power density was 1 W/cm^2. The second physical permeability enhancer was microdermabrasion (Philips VisaCare, Philips, Netherlands). This procedure is widely used in cosmetology and involves the abrasion / removing of the stratum corneum that leads then to an increase in the permeability of the skin for OCA.

3.2.4. Experimental protocol

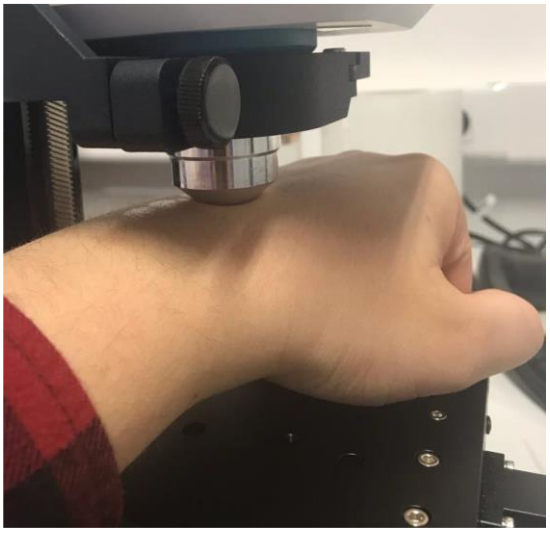

Figure 39. Photograph of the tested skin site in a gentle contact with LC-OCT probe.

Each of listed OCA was used separately, and, for comparison, after pretreatment of skin areas with a solution of hyaluronic acid. The skin sites were treated with ethanol before testing. Then a 3D image was taken using LC-OCT (**Figure 39**). After that, the investigated area was treated for 1 minute using a dermabrasion device to disrupt the integrity of the stratum corneum for enhanced penetration of OCA. Then, after taking another 3D image, the selected skin site was processed with ultrasound twice for 5 minutes. For each OCA, 2 skin sites were examined on each volunteer. For the first area, during both 5-minute intervals of ultrasound treatment, OCA was topically applied on the skin. For the second area of the skin, during the first 5 minutes of ultrasound treatment, a water solution of hyaluronic acid was applied to the skin instead of the OCA. In the second 5 minutes of ultrasound treatment, the selected OCA was applied to the skin, as in the case of the first skin area. Between ultrasound treatments, and then for 30 minutes with an interval of 5 minutes, 3D images of the selected area were taken using LC-OCT. For each imaging, the OCA used in each particular case was used as the immersion liquid for the LC-OCT probe. In control measurements, 2 skin sites of each volunteer were used. Paraffin oil was used as an immersion liquid. At the first site, the skin was not exposed to any of the external influences described in the protocol for OCA. 10 consecutive 3D images were acquired at the same time intervals as if the OCA protocol was applied to the skin. At the second site, the standard protocol described for OCA using hyaluronic acid pretreatment in the first 5 minutes of US sonication was performed. In the

next 5 minutes of US treatment, paraffin oil was applied to the skin instead of OCA. The rest of the steps exactly repeated the described protocol for OCA.

3.2.5. Data analysis

From the obtained 3D images, the entire volume of in-depth data was taken for analysis, except for the superficial 36 µm-thick layer. This was done in order to ignore the superficial areas of high contrast caused by reflection from the glass interface of the LC-OCT probe, which is configured with a slight slope. Thus, the 20 µm-thick SC layer[33] was mostly not included in the analysis, and the surface of the resulting image was represented by the stratum granulosum.

For data analysis, the pixel intensity distribution was calculated for each horizontal sections (1224 × 500 pixels) of the 1224 × 500 × 460 µm 3D image (**Figure 40**) along the z-axis with a depth step of 10 µm.

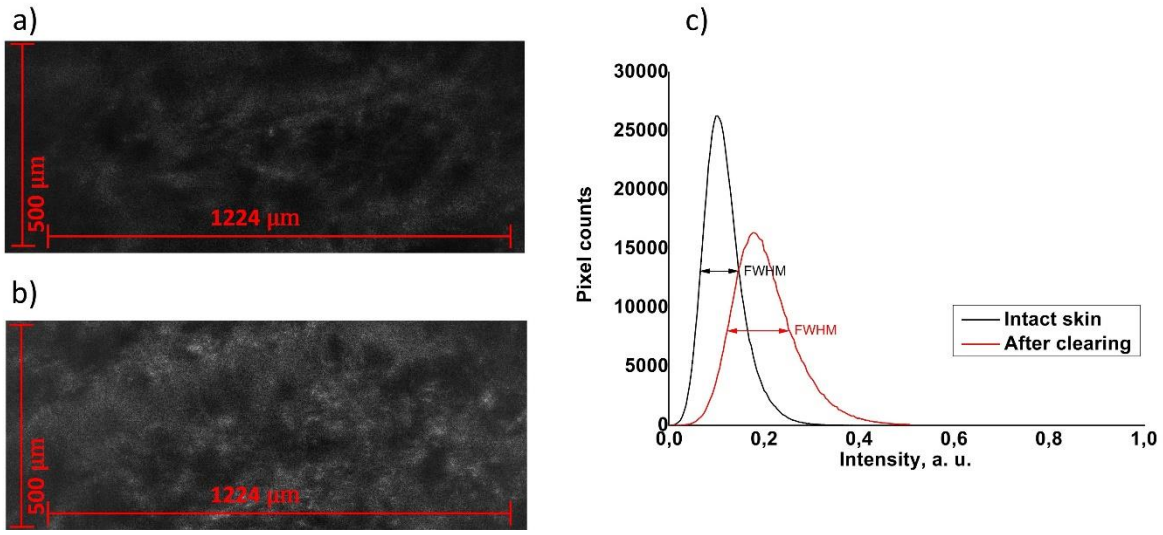

Figure 40. Examples of individual horizontal sections extracted from LC-OCT 3D images at 200 µm depth from intact skin *in vivo* (a) and skin after optical clearing (b); (c) Corresponding graphs of the pixel intensity distribution for intact skin (black) and skin after optical clearing (red) at 200 µm depth. Corresponding arrows show the full width at half maximum (FWHM) for each curve.

It is to be noticed that the pixel intensity histograms obtained for most of the individual horizontal sections of 3D images had the form of a normal distribution, except for the uppermost skin layer images where secondary peaks appeared due to hollow black areas on images related to the skin relief (**Figure 41**). The peak intensity and the full width at half maximum (FWHM) values of such a distribution make it possible to estimate, respectively, the average intensity and image contrast of an individual horizontal section. To simultaneously

assess the effect of optical clearing on the overall intensity and contrast of the horizontal section, the ratio *R* between mean intensity I_{mean} and FWHM was calculated as:

$$R = \frac{I_{mean}}{1-FWHM}, \quad (6)$$

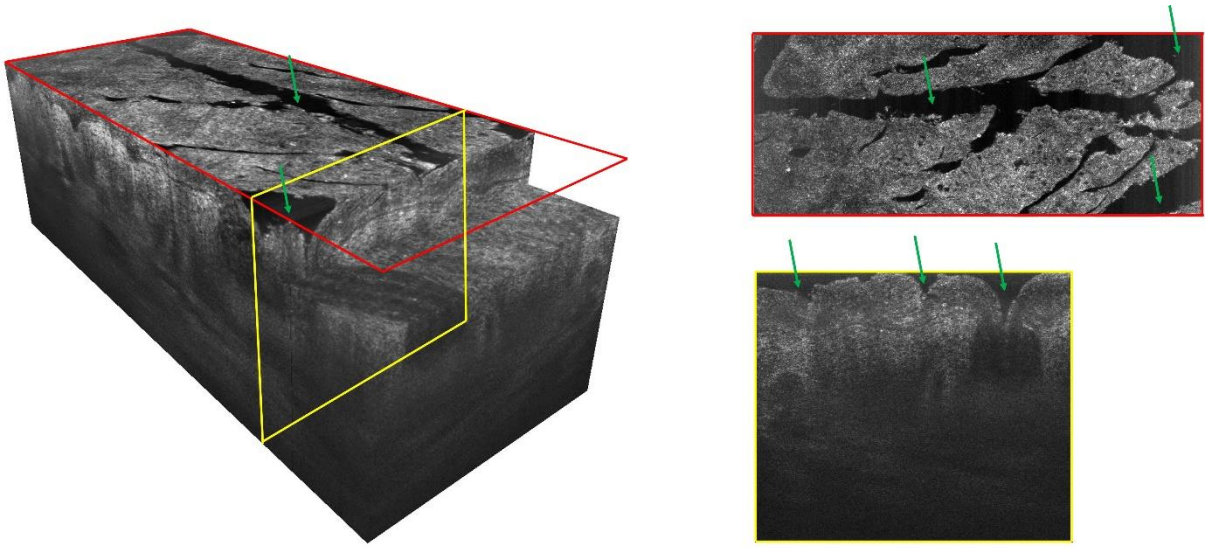

Figure 41. Illustration of a typical 1224 × 500 × 460 µm 3D image of skin (left), acquired by LC-OCT (deepLive, Damae Medical, France) in the current study and corresponding "slices" of a surface (top right) and in-depth sections (bottom right) showing the presence of the skin relief-related hollow dark regions (green arrows).

To estimate the ability and rate of OCA penetration into the superficial and deep layers of the skin, the relative changes in percentages of *R* compared to the initial values were calculated for measurement steps t=6, 11 and 26 min (**Figure 42**), where t=6 is LC-OCT measurement after 5 minutes of US-assisted OC (OC+US), t=11 – after 10 minutes of OC+US, t=26 – 15 minutes after optical clearing. These ratios were calculated at 70, 250 and 350 µm depths, in the midst of the living epidermis, the upper dermis and the deep reticular dermis layers, respectively. Then, these ratios were averaged among the volunteers.

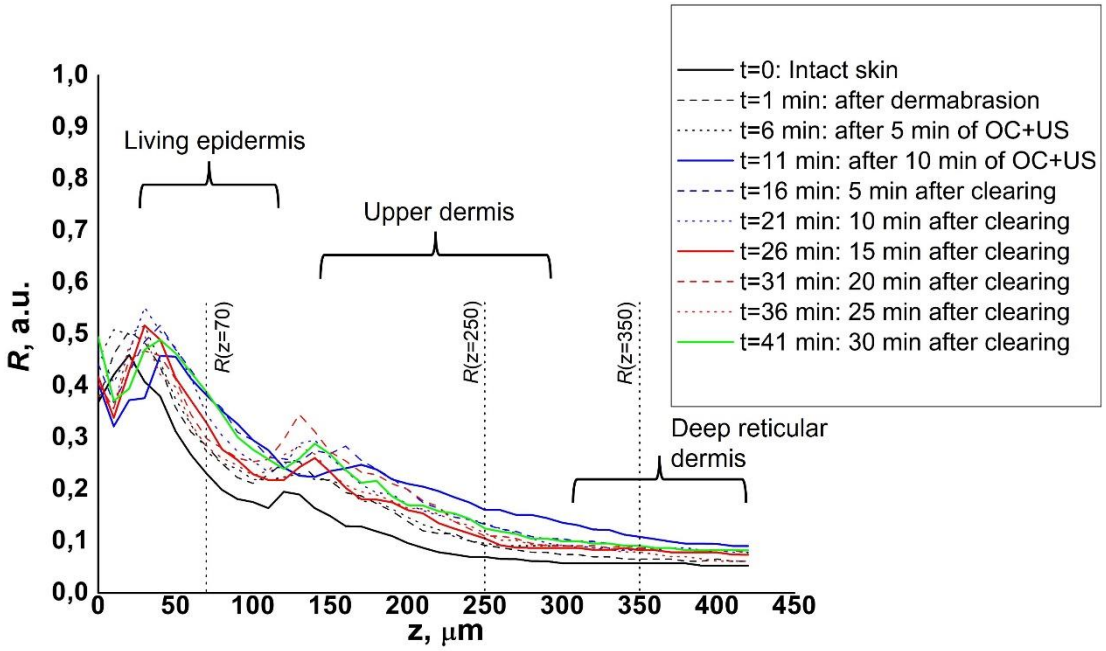

Figure 42. Illustration of depth dynamic of ratio *R* for different experimental protocol steps for one OCA, measured on one volunteer. The 3 vertical dotted black lines indicate the depths within the 3 different skin layers (shown with curly brackets) at which the changes of *R* were calculated.

Then, the Area Under Curve (AUC(70-400)) was calculated for the depth dependent graphs of *in vivo* skin *R* ratio in the range 70-400 µm. This value allows to evaluate the overall increase in contrast and intensity of the 3D image [26]. The range between 0 and 70 µm was excluded from AUC calculation because in the upper skin areas artifacts in the *R*-values were observed, caused by the presence of the hollow areas in the horizontal sections described above. The obtained AUC values were averaged between the volunteers with respect to time points and OCA mixture. In order to compare the effectiveness of the different OCAs to each other as well as with control results, average AUC values previously calculated were all normalized to their corresponding initial values (at t=0) i.e., AUC relative values. Image processing and calculations were performed on MATLAB (R2018a, The Mathworks).

3.2.6. Exponential fitting of AUC data

The experimental protocol conducted in this study can be nominally divided in time by two phases. The first phase corresponds to the “active part” of the protocol, in which all external manipulations (dermabrasion, US treatment) and, consequently, a major OC contribution were performed, and takes a time range t from 0 to 11 minutes. The rest of the protocol

involved only “passive” observation and measurements for 30 minutes (from t = 11 minutes to t = 41 minutes), thus, the active manipulations here have already been completed and any changes in AUC(70-400) can be mainly associated only with passive diffusion of OCA into the skin. To estimate the overall completion of the OC process after the end of the active phase, which would be an undoubted advantage of a specific OCA since in this case additional “passive” phase is not required, the experimental data were fitted. Taking into account the nominal separation of the experimental protocol into two phases described above, the Biphasic Exponential Association was chosen as an appropriate model. It is described by the function

$$y = \begin{cases} Y_b & x < TD_1 \\ Y_b + A_1\left(1 - e^{-\frac{x-TD_1}{Tau_1}}\right) & TD_1 \le x < TD_2 \\ Y_b + A_1\left(1 - e^{-\frac{x-TD_1}{Tau_1}}\right) + A_2\left(1 - e^{-\frac{x-TD_2}{Tau_2}}\right) & x \ge TD_2 \end{cases} \quad (7)$$

where Y_b is the *y* value at which exponential begins, A_1 and A_2 are the first and the second exponential amplitudes, respectively, TD_1 and TD_2 are the first and the second time offset, respectively, Tau_1 and Tau_2 are the first exponential and the second exponential time constants, respectively.

Since we assumed the hypothesis that the “passive” phase of our experimental protocol is a logical continuation of the “active”, and, therefore, its amplitude should remain unchanged or increase (an insufficient time will pass for a significant reversal of the OC effect due to the *in vivo* physiological response), we determined for this model the lower bound of the A_2 parameter not lower than zero ($A_2 \ge 0$). Y_b parameter was fixed as 1 for our model, as the fitted AUC(70-400) data was normalized to initial value for all OCA. TD_1 and TD_2 parameters were manually fixed as 0 min and 11 min, respectively, as the “active” phase starts at t=0 timepoint and the “passive” phase of our hypothesized biphasic model starts right after all the manipulations are done (t=11 min). The fitting was performed in Origin 2018 (OriginLab Corporation).

To compare simultaneously the amplitude and the time constant of the fitted kinetic AUC(70-400) data, two ratios were calculated for each dataset. The first one is the slope at Origin fitted curve for the first phase (SAO_1), defined as $SAO_1 = A_1/Tau_1$. For the second “passive” exponential, a SAO_2 ratio was defined as $SAO_2 = A_2/Tau_2$.

3.3. Results and discussion

The average relative changes of *R* values at 3 different skin depths for each experimental condition (each OCA) and for the control condition are presented in **Figure 43**. The SD bars represent the Standard Deviation due to the biological variation of *in vivo* skin samples and also due to the fact that individual horizontal sections were used without averaging over the skin volume.

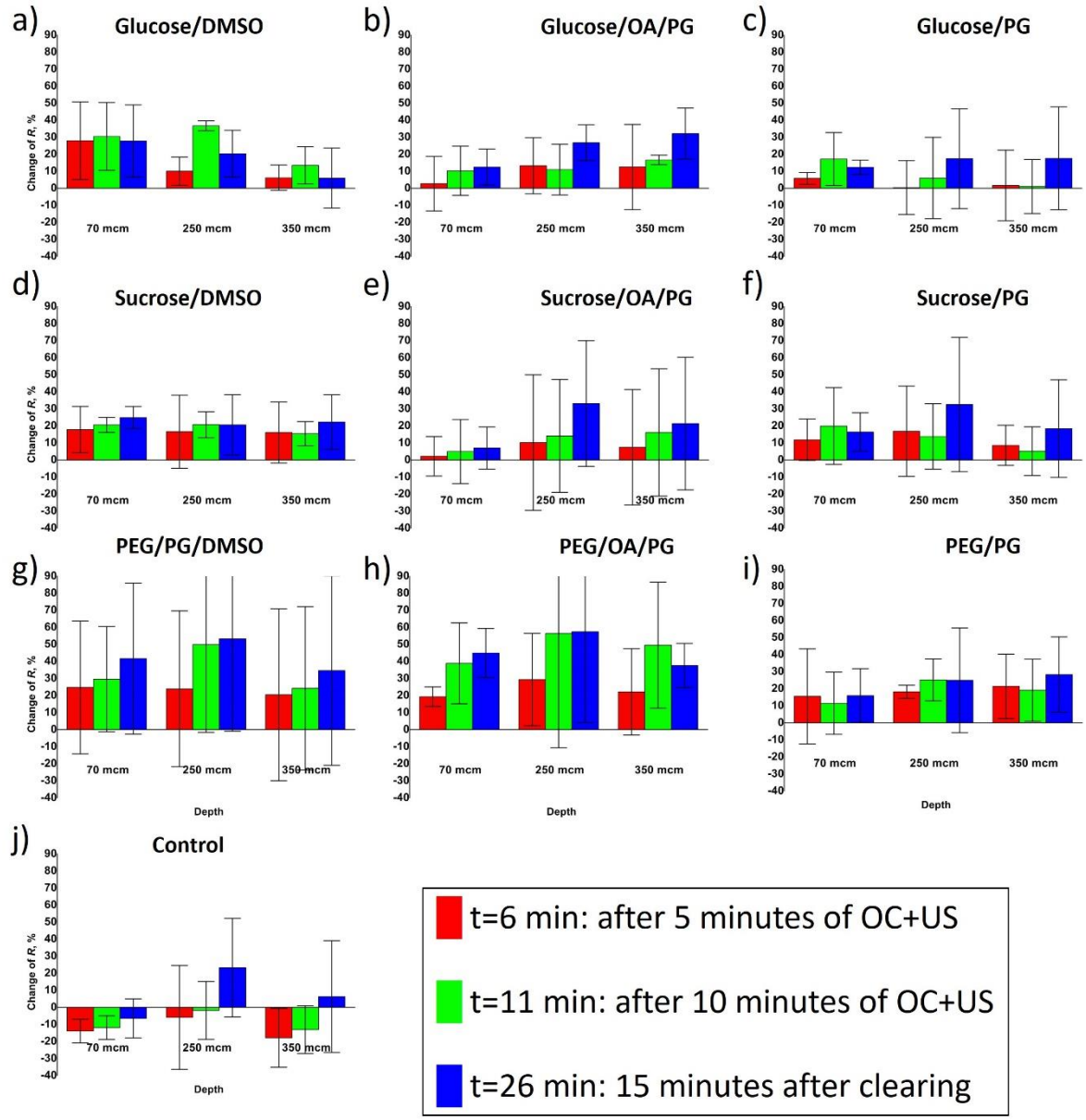

Figure 43. Percentages of R relative changes (with reference to initial value at t=0): after 5 minutes of OC and US (red), after 10 minutes of OC and US (green) and 15 minutes after OC (blue). Average ±SD values are given among the volunteers for the 10 different OC mixtures: (a) Glucose/DMSO, (b) Glucose/OA/PG, (c) Glucose/PG, (d) Sucrose/DMSO, (e) Sucrose/OA/PG, (f) Sucrose/PG, (g)PEG/PG/DMSO, (h) PEG/OA/PG, (i) PEG/PG and for (j) control (1st skin site) condition.

From the plots shown in Figure 43 it can be observed that the control experiment (Fig. 43(j)), as expected, did not cause any significant increase in *R* whatever the analyzed depth: mean change of R at t=11 min is -9%. The use of DMSO (Fig. 43(a,d and g) as a CPE resulted in an increase in *R* at 70 μm depth (mean 27% increase at t=11 min). For mixtures of DMSO with both sugars, there was a rise in *R* after the first 5 minutes of US-assisted OC (28% and 18%- *R* increase for mixtures of Glucose/DMSO and Sucrose/DMSO, respectively), and then no significant increase in subsequent time periods (for Glucose/DMSO, the ratio *R* did not change 15 minutes after OC, for Sucrose/DMSO we observed a 7%-increase). Nevertheless, the use of PEG with DMSO in combination with PG as an additional CPE resulted in a 25%- *R* increase after 5 minutes of OC, and at 15 minutes after clearing it was still possible to observe a 17%-*R* increase (up to a total 42%-increase). A similar trend was observed in the deeper layers of the skin. At 250 and 350 μm-depths, the PEG/PG/DMSO mixture resulted in 24% and 20%-*R* increase, respectively, after 5 minutes of US clearing. Then, 15 minutes after clearing, the *R* ratio rose again to 53% and 35%, respectively. The Sucrose/DMSO mixture here also caused a clearing effect, expressed as an increase of the *R* parameter, but on a smaller scale and without any increase with time. Remarkably, the Glucose/DMSO mixture showed a very slight *R* increase at a 350 μm-depth, however, at a 250 μm-depth, the *R* ratio was modified (27% increase) after the second 5-minute US clearing compared to the first one. This allows to conclude that the dynamics of Glucose/DMSO penetration into the deep layers of *in vivo* skin is lower compared to the PEG/PG/DMSO mixture.

This is an interesting observation, since the volume concentration of both sugars in OCA was several times higher than that of PEG. DMSO as CPE can interact with the lipid layers of the SC and thus facilitate the penetration of hydrophilic OCAs such as sugars and PEG[26], [30], [332]. It is likely that in our case the effect of DMSO on the increase in permeability *in vivo* was limited, which did not lead to a strong subsequent long-term increase in OC. PG used in the PEG/PG/DMSO mixture is also able to interact with and dissolve SC lipids, accelerating skin dehydration under the action of hyperosmotic agents and increasing the rate of OC[36], [331]. Probably, the combination of these two CPE made it possible to obtain an enhanced in-depth clearing effect that continued with time, even when using lower concentrations of the hyperosmotic agent. Moreover, PG and DMSO cannot be strictly classified as CPE, since they also possess the properties of OCA[30], [36].

With the use of PG as CPE, the clearing effect for Glucose and Sucrose mixtures was mainly limited by the upper skin layers and did not increase much with time (at a 70 µm depth, the change in *R* 15 minutes after OC compared to the first 5 minutes of US clearing was 6% and 4% for mixtures of Glucose/PG and Sucrose/PG, respectively). Compared to sugar mixtures, the PEG/PG mixture showed a marked clearing effect even in the deep reticular dermis. At a 350 µm depth, the *R* parameter increased by 21% after 5 minutes of US-assisted clearing and then, after 15 minutes, it continued to slightly increase to 28%. Compared to the PEG/PG/DMSO mixture results described above, the PEG/PG mixture showed clearing potential in the deep layers of *in vivo* skin, albeit on a smaller scale. This is probably due to the lack of penetration enhancing properties of DMSO[332], although PG was used in this case at a high (92% vol./vol,) concentration.

Mixtures of sugars with a paired OA/PG used as CPE showed a better clearing effect in depth than with the other CPE (mixed with DMSO). Even though the change in *R* in the epidermal layer at a 70 µm depth was not as significant as the one obtained with the other sugar/CPE mixtures, at a 250 µm depth, the mixtures of Glucose/OA/PG and Sucrose/OA/PG showed a steady increase during the experiment. For the Glucose/OA/PG mixture, this ratio continued to increase by 15% 15 minutes after the end of clearing compared to this value 5 minutes after US clearing. The similar increase for the Sucrose/OA/PG mixture was observed with a value of 22%. Moreover, this trend was also found in the deep layers of the dermis. At 350 µm depth, the relative change in the *R* ratio for the Glucose/OA/PG mixture increased by a factor of almost 2.5 from 13% after 5 minutes of OC and US to 32% 15 minutes after the end of US-assisted clearing that is 25 minutes after OC start. The same values for a mixture of Sucrose/OA/PG showed a 3-fold increase from 7% to 21%. This difference from the results obtained without the use of oleic acid (OA) as CPE indicates the advantage of using it with the sugars to clear the “deep” layers of *in vivo* skin. OA, as well as DMSO and PG, can increase the permeability of the SC for OCA by disrupting the organization of its lipid layer[32], [247], [300]. However, OA does not have hyperosmotic properties, and therefore does not cause much dehydration of the skin, unlike other CPEs. This fact, as well as, probably, a larger permeability increase of the SC layer, lead to a deeper penetration of the OCA into the skin and, as a result, a better increase in the contrast and intensity of images throughout the depth.

Based on the results presented in Figure 40, the best optical clearing effect across the depth of *in vivo* skin was achieved using a mixture of PEG/OA/PG. In the epidermal layer at a

70 µm depth, the relative change between *R* 15 minutes after OC and *R* after 5 minutes of OC + US clearing was 26% (from 19% to 45%). This is the highest value of *R* change achieved at this depth under the observed parameters. At the same time, in the dermis layer at depths of 250 and 350 µm, the change in *R* reached its maximum value already after 10-minutes of US-assisted clearing and amounted to 56% and 50%, respectively.

Averaged (*n*=3 volunteers) AUC kinetic curves of ratio *R*(70-400 µm) and normalized to the corresponding initial values for each OC and control protocol are presented in **Figure 44**. SD bars were removed to keep the curves legible: the mean SD value is 10% of non-normalized initial values.

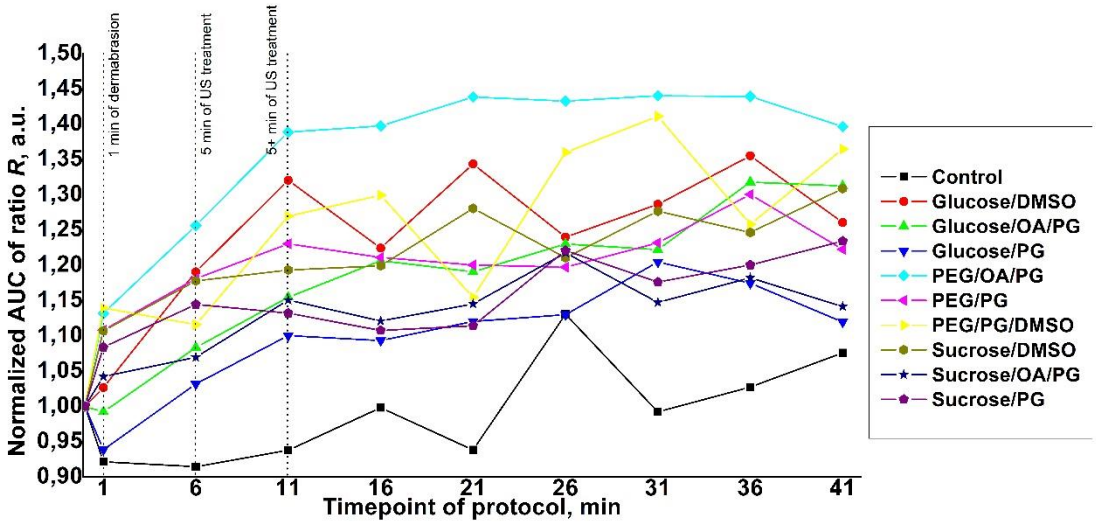

Figure 44. Normalized mean AUC (*n*=3) variation kinetics of the *R* ratio for the 9 different OCA mixtures and for the control (1st skin site) condition.

These results confirm the conclusions from Figure 43. The PEG/OA/PG mixture showed the most confident kinetics and reached an AUC value of ~1.4 (corresponding to a 40%-increase) already at the end of the 10 minute-OC+US treatment. Then the changes were insignificant, which indicates the completion of the clearing process. The Glucose/DMSO mixture showed a similar value at the same time point (~1.32), but as shown in Figure 43, the clearing effect in the deeper skin layers was more pronounced when PEG/OA/PG was used as the OCA. These results are in good agreement with the modeling studies of confocal microscopy probing depth and contrast increase under the action of OCA[344]–[346] and the results referenced in[291], where the combined use of microdermabrasion, US-treatment and oleic acid as an

OCA on *in vivo* human skin resulted in more than a twofold increase in OCT probing depth and more than a threefold increase in OCT signal amplitude.

Figure 45 displays a similar to the Figure 44 averaged (*n*=3 volunteers) normalized AUC kinetic curves of ratio R(70-400 µm), but for the skin sites subjected to the HA pretreatment followed by OC protocol (described in Sec. 3.2.4.), for each OC and control protocol (conducted at the 2nd skin site).

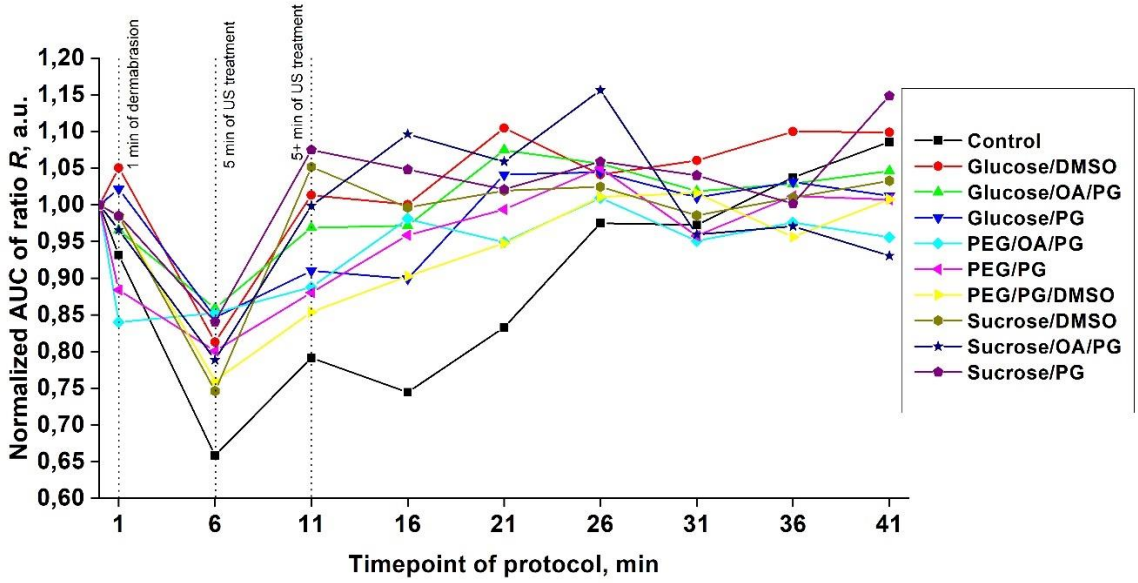

Figure 45. Normalized mean AUC (*n*=3) variation kinetics of the *R* ratio, calculated from the HA pretreatment OC protocol for the 9 different OCA mixtures and for the control (2nd skin site) condition.

Figure 45 shows that the pretreatment of experimental areas with HA for 5 minutes led to a significant decrease in AUC (t=6 min), which could only return to values close to the initial ones due to subsequent manipulations. These results are apparently due to the excess of the HA optimal concentration, which led to a shielding effect. Thus, these results cannot be called meaningful in terms of tracking changes in the intensity and contrast of OCT images. Further research should focus on determining the optimal concentration of HA solution used for skin treatment. However, in this work, a more detailed analysis of the results obtained on skin areas with HA pretreatment was not carried out.

Kinetics of AUC(70-400) of ratio *R* (obtained from the OC protocol results) fitted with a biphasic exponential model showed high values of the coefficient of determination r^2. Depending on the OCA used, r^2 took values in the range from 0.69 to 0.97 (**Figure 46**).

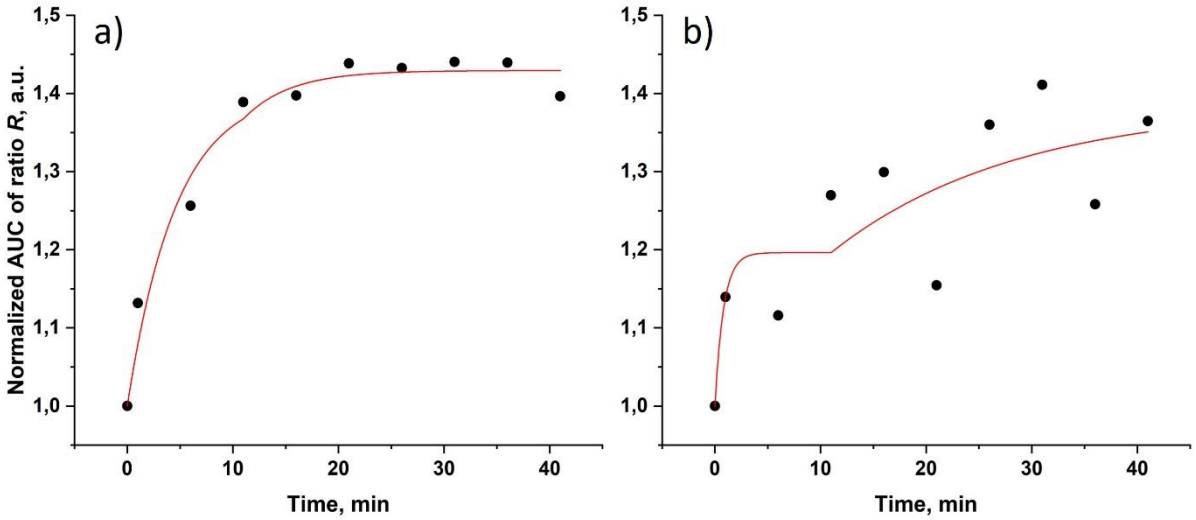

Figure 46. Experimental data (black circles) of the AUC(70-400) of ratio *R* time dependence and the corresponding fitted curves (red line) of the biphasic exponential model for the mixture of (a) PEG/OA/PG, which showed the highest r^2 value (0.97) and for the mixture of (b) PEG/PG/DMSO, which showed the lowest r^2 value (0.69).

The results of the biphasic exponential model-derived parameter analysis are presented in **Figure 47**.

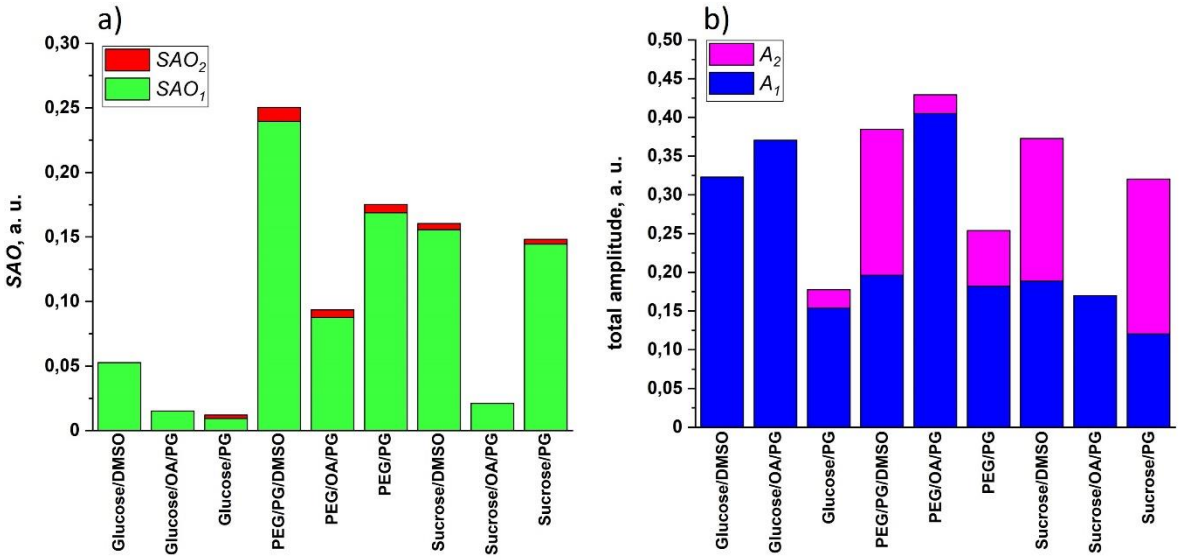

Figure 47. Stacked histograms of (a) calculated SAO_1 and SAO_2 parameters and (b) derived A_1 and A_2 parameters of fitted curves of biphasic exponential association model.

These results largely agree with the results presented in Figures 43 and 44. The PEG/PG/DMSO mixture shows the highest stacked value of the *SAO* parameter; moreover, the main contribution to the column is made by the SAO_1, which indicates the greatest efficiency of this OCA during the "active" phase of the biphasic exponential model in terms of the balance between achieved amplitude and the time spent on this. Quite similar results were achieved using the PEG/PG, Sucrose/DMSO and Sucrose/PG mixtures. However, when looking at the

stacked histograms of the exponential curves total amplitude, it becomes noticeable that for the above OCAs, a significant contribution to the amplitude is made by the parameter A_2, which corresponds to the amplitude of the "passive" phase. Thus, their relatively small SAO_2 values and corresponding significant A_2 values indicate a long "passive" phase before the OC reaches its final plateau, which is not the optimal expected result.

On the contrary, mixtures of Glucose/DMSO, Glucose/OA/PG and PEG/OA/PG showed the highest values of the total amplitude, and the main contribution to the amplitude was made by parameter A_1, which indicates their effectiveness in terms of the duration of the process - OC was for the most part completed within 11 minutes of the "active" phase, when all the manipulations described in the experimental protocol were completed. Comparison of the actual results of the AUC(70-400) of ratio *R* kinetics and the amplitudes of the exponential curve of the hypothesized biphasic model clearly shows that the PEG/OA/PG mixture has the best values of the increase in contrast and intensity of the signal obtained by LC-OCT in terms of the process time.

Thus, we have experimentally shown the potential of optical clearing of human skin *in vivo*, enhanced by chemical and physical methods of permeability enhancement, by biocompatible OCA, which makes it possible to safely use this technique for the diagnosis and treatment of healthy and pathologically altered skin areas.

3.4. Conclusion

We presented the results of a comparative study of the OC effect by biocompatible mixtures of OCA and CPE. Polyethylene glycol-400 (PEG) as well as aqueous solutions of Glucose and Sucrose were used as OCA. Propylene glycol (PG), Oleic acid (OA), and dimethyl sulfoxide (DMSO) were used as CPE. To enhance the clearing effect, physical permeation methods, such as dermabrasion and sonophoresis, were used. By analyzing the *R* ratio, which contains information about the average intensity and contrast of the images obtained by LC-OCT method, we determined the in-depth effectiveness of skin *in vivo* OC using various OCA. The results showed that the overall level of the *R* ratio in the 70-400 μm skin depth region, calculated as the AUC, showed the best increase (40%) after 10 minutes of US-assisted clearing using a mixture of PEG/OA/PG. The other eight OCA also showed an increase in the overall *R* level with depth. The results of the experimental data fitting with the hypothesized biphasic exponential association model are in a good agreement with experimental results. Thus, the

effectiveness of OC with biocompatible concentrations of OCA was proven through an increase in the overall intensity and contrast of the obtained LC-OCT images over the entire depth of the examined skin *in vivo*.

4. Conclusion and perspectives

The main objective of the first experimental part presented in Chapter 2 of this thesis manuscript was (i) to investigate the effect of the optical clearing (OC) process applied to *ex vivo* human skin samples on spatially resolved (SR) DR and AF spectra using two combinations of Optical Clearing Agents (OCA) and Chemical Permeation Enhancers (CPE), and (ii) to quantify the clearing-like effect of drying and of spectroscopic probe pressure on skin.

For the OC process investigation, the *ex vivo* hybrid model was tested in combination with spatially resolved spectroscopy. Hybrid configuration of tested samples, consisted of ex vivo skin and the fluorescent gel, allowed to analyze a spectral contribution of different fluorophores located at the various depths and their kinetic during optical clearing. As different distances of multimodal spectroscopy' collection fibers are sensitive to different depths, it allowed to discriminate different clearing processes at different skin depths. Topical application of 2 combinations of OCA and CPE demonstrated their applicability in increased intensity of fluorescence and DR signal acquired from the gel layer underneath the skin. At the same time, a scattering reduction of a skin layer under the OCA action caused a decrease in detected AF spectra intensity and better photons propagation within the skin. Thus, OC was demonstrated to be an efficient technique in improved detection of a spectroscopic signal produced by the deeper layers of skin.

Also, it has been experimentally confirmed that the improvement of the depth sensitivity of the spatially resolved DR and AF spectroscopy is related not only to the OCA effect. The clearing-like results obtained in dry condition allowed us to prove the optical probe pressure effect which also contributed to the clearing process along with refractive index matching induced by OCA and dehydration.

In case of absence of any liquids applied on the skin sample, an increase in spectroscopic signal was also related to the water loss by the *ex vivo* skin that cannot maintain its properties and getting thinner with the exposure time.

Finally, the main objective of the last experimental part presented in Chapter 3 was to experimentally evaluate using Line-field Confocal OCT (LC-OCT) technique the efficacy of optical clearing of human skin *in vivo* with biocompatible OCA combined with chemical and physical permeability enhancers. To make this study possibly transferable to the real clinic conditions and to satisfy the biocompatible concentration requirements, we developed the

mixtures of OCA and CPE according to the FDA inactive ingredients database. Polyethylene glycol-400 (PEG) as well as aqueous solutions of Glucose and Sucrose were used as OCA. Propylene glycol (PG), Oleic acid (OA), and dimethyl sulfoxide (DMSO) were used as CPE. To enhance the clearing effect, physical permeation methods were also used. By analyzing the average intensity and contrast of the images obtained by LC-OCT method, we determined the in-depth effectiveness of skin in vivo biocompatible OC. The results showed that the best increase in image intensity and contrast after 10 minutes of US-assisted clearing was achieved using a mixture of PEG/OA/PG. The results of the experimental data fitting with the hypothesized biphasic exponential association model are in a good agreement with experimental results. Thus, the effectiveness of OC with biocompatible concentrations of OCA was demonstrated.

Further prospects for research in this direction could imply optimization of the biocompatible OCA and CPE mixture composition by expanding the list of chemicals under study, as well as the inclusion of this technique in real clinical studies of neoplastic skin lesions. To improve the diagnostic ability of the optical method of skin analysis, it also makes sense to use a multimodal approach that combines OCT imaging technique and various methods of optical spectroscopy. In the future studies, it may be helpful for skin carcinoma *in vivo* diagnosis and characterization. An additional way to improve the diagnostic potential of multimodal spectroscopy can be the analysis of spectra using machine learning techniques.

Bibliography

[1] Y. Liu, X. Yang, D. Zhu, R. Shi, and Q. Luo, "Optical clearing agents improve photoacoustic imaging in the optical diffusive regime", *Opt. Lett*. **38**(20), 4236–4239 (2013).

[2] E. A. Genina, A. N. Bashkatov, E. A. Kolesnikova, M. V. Basko, G. S. Terentyuk, and V. V. Tuchin, "Optical coherence tomography monitoring of enhanced skin optical clearing in rats in vivo", *JBO* **19**(2), 021109 (2013).

[3] J. Wang, R. Shi, and D. Zhu, "Switchable skin window induced by optical clearing method for dermal blood flow imaging", *JBO* **18**(6), 061209 (2012).

[4] H. J. C. M. Sterenborg, M. Motamedi, R. F. Wagner, M. Duvic, S. Thomsen, and S. L. Jacques, "In vivo fluorescence spectroscopy and imaging of human skin tumours", *Laser. Med. Sci*. **9**(3), 191–201 (1994).

[5] Y. P. Sinichkin, S. R. Utz, A. H. Mavliutov, and H. A. Pilipenko, "In vivo fluorescence spectroscopy of the human skin: experiments and models", *JBO* **3**(2), 201–212 (1998).

[6] I. Georgakoudi, B. C. Jacobson, J. Van Dam, V. Backman, M. B. Wallace, M. G. Müller, Q. Zhang, K. Badizadegan, D. Sun, G. A. Thomas, L. T. Perelman, and M. S. Feld, "Fluorescence, reflectance, and light-scattering spectroscopy for evaluating dysplasia in patients with Barrett's esophagus", *Gastroenterology* **120**(7), 1620–1629 (2001).

[7] J. B. Dawson, D. J. Barker, D. J. Ellis, E. Grassam, J. A. Cotterill, G. W. Fisher, and J. W. Feather, "A theoretical and experimental study of light absorption and scattering by in vivo skin", *Phys. Med. Biol*. **25**(4), 695–709 (1980).

[8] S. L. Jacques, "The Role of Skin Optics in Diagnostic and Therapeutic Uses of Lasers", in *Lasers in Dermatology*, Berlin, Heidelberg, 1–21 (1991).

[9] C. Reble, I. Gersonde, S. Schanzer, M. C. Meinke, J. Helfmann, and J. Lademann, "Evaluation of detection distance-dependent reflectance spectroscopy for the determination of the sun protection factor using pig ear skin", *J. Biophotonics* **11**(1), e201600257 (2018).

[10] H. Hou, M. Dong, Y. Wang, L. Shu, Z. Ma, and Y. Liu, "Rapid and Noninvasive Detection of Skin Cholesterol with Diffuse Reflectance Spectroscopy Technology", *Spectrosc. Spect. Anal*. **36**(10), 3215–3221 (2016).

[11] Y. Zhang, A. J. Moy, X. Feng, H. T. M. Nguyen, K. R. Sebastian, J. S. Reichenberg, M. K. Markey, and J. W. Tunnell, "Diffuse reflectance spectroscopy as a potential method for nonmelanoma skin cancer margin assessment", *Translational Biophotonics* **2**(3), e202000001 (2020).

[12] E. Borisova, D. Ivanov, B. Kolev, T. Genova, V. Mircheva, S. Ilyov, L. Zaharieva, I. Lihachova, A. Lihachovs, J. Spigulis, and P. Troyanova, "Autofluorescence spectroscopy of cutaneous neoplasia under ultraviolet, visible and near infrared excitation", in *Tissue Optics and Photonics* **11363**, 113630Z (2020).

[13] E. G. Borisova, I. A. Bratchenko, Y. A. Khristoforova, L. A. Bratchenko, T. I. Genova, A. I. Gisbrecht, A. A. Moryatov, S. V. Kozlov, P. P. Troyanova, and V. P, Zakharov, "Near-infrared autofluorescence spectroscopy of pigmented benign and malignant skin lesions", *Opt. Eng*. **59**(6), 061616 (2020).

[14] E. Borisova, T. Genova-Hristova, P. Troyanova, I. Terziev, E. A. Genina, A. N. Bashkatov, O. Semyachkina-Glushkovskaya, V. V. Tuchin, and L. Avramov, "Optical UV-VIS-NIR spectroscopy of benign, dysplastic and malignant cutaneous lesions ex vivo", in *Biophotonics: Photonic Solutions for Better Health Care VI* **10685**, 106853T (2018).

[15] L. Lim, B. Nichols, M. R. Migden, N. Rajaram, J. S. Reichenberg, M. K. Markey, M. I. Ross, and J. W. Tunnell, “Clinical study of noninvasive in vivo melanoma and nonmelanoma skin cancers using multimodal spectral diagnosis”, *JBO* **19**(11), 117003 (2014).

[16] M. Amouroux, G. Díaz-Ayil, W. C. P. M. Blondel, G. Bourg-Heckly, A. Leroux, and F. Guillemin, “Classification of ultraviolet irradiated mouse skin histological stages by bimodal spectroscopy: multiple excitation autofluorescence and diffuse reflectance”, *JBO* **14**(1), 014011 (2009).

[17] V. V. Tuchin, J. Popp, and V. Zakharov, *Multimodal Optical Diagnostics of Cancer*, 1st ed., Springer, Cham (2020).

[18] V. Narayanamurthy, P. Padmapriya, A. Noorasafrin, B. Pooja, K. Hema, A. Khan, K. Nithyakalyani, and F. Samsuri, “Skin cancer detection using non-invasive techniques”, *RSC Adv*., **8**(49), 28095–28130 (2018).

[19] F. Abdat, M. Amouroux, Y. Guermeur, and W. Blondel, “Hybrid feature selection and SVM-based classification for mouse skin precancerous stages diagnosis from bimodal spectroscopy”, *Opt. Express* **20**(1), 228–244 (2012).

[20] S. K. Chang, Y. N. Mirabal, E. N. Atkinson, D. Cox, A. Malpica, M. Follen, and R. Richards-Kortum, “Combined reflectance and fluorescence spectroscopy for in vivo detection of cervical pre-cancer”, *JBO* **10**(2), 024031 (2005).

[21] R. A. Schwarz, W. Gao, D. Daye, M. D. Williams, R. Richards-Kortum, and A. M. Gillenwater, “Autofluorescence and diffuse reflectance spectroscopy of oral epithelial tissue using a depth-sensitive fiber-optic probe”, *Appl. Opt*, **47**(6), 825–834 (2008).

[22] V. V. Tuchin, J. P. Culver, C. Cheung, S. A. Tatarkova, M. A. DellaVecchia, D. A. Zimnyakov, A. A. Chaussky, A. G. Yodh, and B. Chance, “Refractive index matching of tissue components as a new technology for correlation and diffusing-photon spectroscopy and imaging”, in *Coherence Domain Optical Methods in Biomedical Science and Clinical Applications III* **3598**, 111–120 (1999).

[23] M. Niwayama, “Voxel-based measurement sensitivity of spatially resolved near-infrared spectroscopy in layered tissues”, *JBO* **23**(3), 1–4 (2018).

[24] M. C. Meinke, S. B. Lohan, W. Köcher, B. Magnussen, M. E. Darvin, and J. Lademann, “Multiple spatially resolved reflection spectroscopy to monitor cutaneous carotenoids during supplementation of fruit and vegetable extracts in vivo”, *Skin. Res. Technol*. **23**(4), 459–462 (2017).

[25] Z. Kovacsova, G. Bale, S. Mitra, I. de Roever, J. Meek, N. Robertson, and I. Tachtsidis, “Investigation of Confounding Factors in Measuring Tissue Saturation with NIRS Spatially Resolved Spectroscopy”, *Adv. Exp. Med. Biol*. **1072**, 307–312 (2018).

[26] V. V. Tuchin, *Tissue Optics: Light Scattering Methods and Instruments for Medical Diagnosis*, 3rd ed., SPIE Press, Bellingham (2015).

[27] D. A. Boas, “A fundamental limitation of linearized algorithms for diffuse optical tomography”, *Opt. Express* **1**(13), 404–413 (1997).

[28] A. Yu. Sdobnov, M. E. Darvin, E. A. Genina, A. N. Bashkatov, J. Lademann, and V. V. Tuchin, “Recent progress in tissue optical clearing for spectroscopic application”, *Spectrochimica Acta Part A: Molecular and Biomolecular Spectroscopy* **197**, 216–229 (2018).

[29] D. Zhu, K. V. Larin, Q. Luo, and V. V. Tuchin, “Recent progress in tissue optical clearing”, *Laser. Photon. Rev*. **7**(5), 732–757 (2013).

[30] E. A. Genina, A. N. Bashkatov, and V. V. Tuchin, “Tissue optical immersion clearing”, *Expert Rev. Med. Devices* **7**(6), 825–842 (2010).

[31] Z. Zhi, Z. Han, Q. Luo, and D. Zhu, “Improve optical clearing of skin in vitro with propylene glycol as a penetration enhancer”, *J. Innov. Opt. Health Sci*. **2**(3), 269–278 (2009).

[32] J. Jiang and R. K. Wang, “How different molarities of oleic acid as enhancer exert its effect on optical clearing of skin tissue in vitro”, *J. X-Ray Sci. Technol*. **13**(3), 149–159 (2005).

[33] V. V. Tuchin, “Tissue Optics and Photonics: Light-Tissue Interaction", *JBPE* **1**(2), 98-134 (2015).

[34] T. B. Fitzpatrick, *Dermatology in general medicine*, Mcgraw-Hill Book Co., New York (1993).

[35] L. M. C. Oliveira and V. V. Tuchin, “Optical Clearing and Tissue Imaging”, in *The Optical Clearing Method: A New Tool for Clinical Practice and Biomedical Engineering*, L. M. C. Oliveira and V. V. Tuchin, Eds., 107–138, Springer, Cham (2019).

[36] V. V. Tuchin, D. Zhu, and E. A. Genina, *Handbook of Tissue Optical Clearing: New Prospects in Optical Imaging*, 1st ed., Routledge & CRC Press, Boca Raton (2022).

[37] T. Vo-Dinh, *Biomedical Photonics Handbook: Biomedical Diagnostics*, 2nd ed., Routledge & CRC Press, Boca Raton (2019).

[38] A. Bashkatov, E. Genina, and V. Tuchin, “Optical properties of skin, subcutaneous, and muscle tissues: A review”, *J. Innov. Opt. Heal. Sci*. **4**(1), 9-38 (2011).

[39] S. L. Jacques, “Optical properties of biological tissues: a review”, *Phys. Med. Biol*. **58**(11), R37-61 (2013).

[40] R. Yang, T. Wei, H. Goldberg, W. Wang, K. Cullion, and D. S. Kohane, “Getting Drugs Across Biological Barriers”, *Adv. Mater*. **29**(37), 1606596 (2017).

[41] V. V. Tuchin, “Tissue Optics and Photonics: Biological Tissue Structures”, *JBPE* **1**(1), 3-21 (2015).

[42] “Epidermis”, *Wikipedia*, Retrieved 16 December 2021, https://en.wikipedia.org/w/index.php?title=Epidermis&oldid=1054898144

[43] M. Heisig, R. Lieckfeldt, G. Wittum, G. Mazurkevich, and G. Lee, “Non steady-state descriptions of drug permeation through stratum corneum. I. The biphasic brick-and-mortar model”, *Pharm. Res*. **13**(3), 421–426 (1996).

[44] V. V. Tuchin, *Lasers and Fiber Optics in Biomedical Science*, 2nd ed., Saratov University Press, Saratov (2010).

[45] R. F. Reinoso, B. A. Telfer, and M. Rowland, “Tissue water content in rats measured by desiccation”, *J. Pharmacol. Toxicol. Methods* **38**(2), 87–92 (1997).

[46] L. M. Oliveira, A. L. V. S. Lage, M. P. P. Clemente, and V. V. Tuchin, “Rat muscle opacity decrease due to the osmosis of a simple mixture”, *JBO* **15**(5), 055004 (2010).

[47] G. J. Tearney, M. E. Brezinski, J. F. Southern, B. E. Bouma, M. R. Hee, and J. G. Fujimoto, “Determination of the refractive index of highly scattering human tissue by optical coherence tomography”, Opt. Lett. 20(21), 2258–2260 (1995).

[48] M. Sand, T. Gambichler, G. Moussa, F. G. Bechara, D. Sand, P. Altmeyer, and K. Hoffmann, “Evaluation of the epidermal refractive index measured by optical coherence tomography”, *Skin. Res. Technol*. **12**(2), 114–118 (2006).

[49] H. Schaefer and T. E. Redelmeier, *Skin Barrier: Principles of Percutaneous Absorption*, 1st ed., S. Karger, Basel (1996).

[50] T. L. Troy and S. N. Thennadil, “Optical properties of human skin in the near infrared wavelength range of 1000 to 2200 nm”, *JBO* **6**(2), 167–176 (2001).

[51] S. L. Jacques, “Optical assessment of cutaneous blood volume depends on the vessel size distribution: a computer simulation study*”, J. Biophotonics* **3**(1–2), 75–81 (2010).

[52] L. A. Goldsmith, *Physiology, biochemistry, and molecular biology of the skin*, 2nd ed., Oxford University Press, Oxford (1991).

[53] J. Marks and J. Miller, *Lookingbill and Marks’ Principles of Dermatology*, 6th ed., Elsevier, Amsterdam (2017).

[54] E. Claridge, S. Cotton, P. Hall, and M. Moncrieff, “From colour to tissue histology: Physics-based interpretation of images of pigmented skin lesions”, *Med. Image Anal*. **7**(4), 489–502 (2003).

[55] C. S. Sinnatamby, *Last’s Anatomy: Regional and Applied*, 12th ed., Churchill Livingstone, London (2011).

[56] Blausen.com staff, “Medical gallery of Blausen Medical 2014”, *WikiJournal of Medicine* **1**(2), 2014.

[57] W. E. Allen, “Terminologia anatomica: international anatomical terminology and Terminologia Histologica: International Terms for Human Cytology and Histology”, *J. Anat*. **215**(2), 221 (2009).

[58] A. Bykov, V. Tuchin, and I. Meglinski, “Multiplexed spatially-focused localization of light in adipose biological tissues”, *Sci. Rep*. **12**, 9711 (2022).

[59] E. V. Salomatina, B. Jiang, J. Novak, and A. N. Yaroslavsky, “Optical properties of normal and cancerous human skin in the visible and near-infrared spectral range”, *JBO* **11**(6), 064026 (2006).

[60] G. Muller*, Laser-Induced Interstitial Thermotherapy*, SPIE Press, Bellingham (1995).

[61] F. P. Bolin, L. E. Preuss, R. C. Taylor, and R. J. Ference, “Refractive index of some mammalian tissues using a fiber optic cladding method”, *Appl. Opt*. **28**(12), 2297–2303 (1989).

[62] Y. Zhou, J. Yao, and L. V. Wang, “Tutorial on photoacoustic tomography”, *JBO* **21**(6), 061007 (2016).

[63] R. L. P. van Veen, H. J. C. M. Sterenborg, A. Pifferi, A. Torricelli, E. Chikoidze, and R. Cubeddu, “Determination of visible near-IR absorption coefficients of mammalian fat using time- and spatially resolved diffuse reflectance and transmission spectroscopy”, *JBO* **10**(5), 054004 (2005).

[64] A. N. Bashkatov, E. A. Genina, V. I. Kochubey, A. A. Gavrilova, S. V. Kapralov, V. A. Grishaev, V. V. Tuchin, “Optical properties of human stomach mucosa in the spectral range from 400 to 2000nm: Prognosis for gastroenterology”, *Medical Laser Application* **22**(2), 95–104 (2007).

[65] I. Yariv, G. Rahamim, E. Shliselberg, H. Duadi, A. Lipovsky, R. Lubart, and D. Fixler, “Detecting nanoparticles in tissue using an optical iterative technique”, *Biomed. Opt. Express* **5**(11), 3871–3881 (2014).

[66] A. N. Bashkatov, E. A. Genina, M. D. Kozintseva, V. I. Kochubei, S. Yu. Gorodkov, and V. V. Tuchin, “Optical properties of peritoneal biological tissues in the spectral range of 350–2500 nm”, *Opt. Spectrosc*. **120**(1), 1–8 (2016).

[67] J. Weissman, T. Hancewicz, and P. Kaplan, “Optical coherence tomography of skin for measurement of epidermal thickness by shapelet-based image analysis”, *Opt. Express* **12**(23), 5760–5769 (2004).

[68] D. J. Carpenter, M. B. Sajisevi, N. Chapurin, C. S. Brown, T. Cheng, G. M. Palmer, D. S. Stevenson, C. L. Rao, R. P. Hall, and C. R. Woodard, “Noninvasive optical spectroscopy for identification of non-melanoma skin cancer: Pilot study”, *Lasers Surg. Med*. **50**(3), 246–252 (2018).

[69] E. Drakaki, C. Dessinioti, A. J. Stratigos, C. Salavastru, and C. Antoniou, “Laser-induced fluorescence made simple: implications for the diagnosis and follow-up monitoring of basal cell carcinoma”, *JBO* **19**(3), 30901 (2014).

[70] V. H. Maciel, W. R. Correr, C. Kurachi, V. S. Bagnato, and C. da Silva Souza, “Fluorescence spectroscopy as a tool to in vivo discrimination of distinctive skin disorders”, *Photodiagnosis Photodyn. Ther*. **19**, 45–50 (2017).

[71] D. J. Leffell, M. L. Stetz, L. M. Milstone, and L. I. Deckelbaum, “In vivo fluorescence of human skin. A potential marker of photoaging”, *Arch. Dermatol*. **124**(10), 1514–1518 (1988).

[72] W. Lohmann and E. Paul, “In situ detection of melanomas by fluorescence measurements”, *Naturwissenschaften* **75**(4), 201–202 (1988).

[73] W. Lohmann, W. B. Schill, D. Bucher, T. Peters, M. Nilles, A. Schulz, and R. Bohle, “Elastosis and cancer”, *Z. Naturforsch. C. J. Biosci*. **49**(3–4), 223–229 (1994).

[74] H. Zeng, C. MacAulay, D. I. McLean, B. Palcic, and H. Lui, “The dynamics of laser-induced changes in human skin autofluorescence--experimental measurements and theoretical modeling”, *Photochem. Photobiol*. **68**(2), 227–236 (1998).

[75] R. Richards-Kortum and E. Sevick-Muraca, “Quantitative optical spectroscopy for tissue diagnosis”, *Annu. Rev. Phys. Chem*. **47**, 555–606 (1996).

[76] N. Kollias, R. Gillies, C. Cohén-Goihman, S. B. Phillips, J. A. Muccini, M. J. Stiller, and L. A. Drake, “Fluorescence photography in the evaluation of hyperpigmentation in photodamaged skin”, *J. Am. Acad. Dermatol*. **36**(2), 226–230 (1997).

[77] N. Kollias, R. Gillies, M. Moran, I. E. Kochevar, and R. R. Anderson, “Endogenous skin fluorescence includes bands that may serve as quantitative markers of aging and photoaging”, *J. Invest. Dermatol*. **111**(5), 776–780 (1998).

[78] R. Gillies, G. Zonios, R. Rox Anderson, and N. Kollias, “Fluorescence Excitation Spectroscopy Provides Information About Human Skin In Vivo”, *J. Invest. Dermatol*. **115**(4), 704–707 (2000).

[79] N. Kollias and G. N. Stamatas, “Optical non-invasive approaches to diagnosis of skin diseases”, *J. Invest. Derm. Symp. P*. **7**(1), 64–75 (2002).

[80] M. A. Calin, S. V. Parasca, R. Savastru, M. R. Calin, and S. Dontu, “Optical techniques for the noninvasive diagnosis of skin cancer”, *J. Cancer. Res. Clin. Oncol*. **139**(7),1083–1104 (2013).

[81] E. Borisova, P. Pavlova, E. Pavlova, P. Troyanova, and L. Avramov, “Optical Biopsy of Human Skin - A Tool for Cutaneous Tumours’ Diagnosis”, *Int. J. Bioautomation* **16**(1), 53-72 (2012).

[82] Q. Liu, “Role of optical spectroscopy using endogenous contrasts in clinical cancer diagnosis”, *World Journal of Clinical Oncology* **2**(1), 50–63 (2011).

[83] E. Borisova, E. Carstea, L. Cristescu, E. Pavlova, N. Hadjiolov, P. Troyanova, and L. Avramov, “Light-Induced Fluorescence Spectroscopy And Optical Coherence Tomography Of Basal Cell Carcinoma”, *J. Innov. Opt. Heal. Sci*. **2**(3), 261-268 (2009).

[84] N. Rajaram, J. S. Reichenberg, M. R. Migden, T. H. Nguyen, and J. W. Tunnell, “Pilot clinical study for quantitative spectral diagnosis of non-melanoma skin cancer”, *Laser. Surg. Med*. **42**(10), 876–887 (2010).

[85] D. Y. Churmakov, I. Meglinski, S. A. Piletsky, and D. A. Greenhalgh, “Analysis of skin tissues spatial fluorescence distribution by the Monte Carlo simulation”, *J. Phys. D: Appl. Phys*. **36**(14), 1722-1728 (2003).

[86] R. Na, I. M. Stender, and H. C. Wulf, “Can autofluorescence demarcate basal cell carcinoma from normal skin? A comparison with protoporphyrin IX fluorescence”, *Acta Derm. Venereol*. **81**(4), 246–249 (2001).

[87] A. J. Thompson, S. Coda, M. B. Sørensen, G. Kennedy, R. Patalay, U. Waitong-Brämming, P. A. A. De Beule, M. A. A. Neil, S. Andersson-Engels, N. Bendsøe, P. M. W. French, K. Svanberg, and C. Dunsby, “In vivo measurements of diffuse reflectance and time-resolved autofluorescence emission spectra of basal cell carcinomas”, *J. Biophotonics* **5**(3), 240–254 (2012).

[88] M. Panjehpour, C. E. Julius, M. N. Phan, T. Vo-Dinh, and S. Overholt, “Laser-induced fluorescence spectroscopy for in vivo diagnosis of non-melanoma skin cancers”, *Laser. Surg. Med*. **31**(5), 367–373 (2002).

[89] L. Brancaleon, A. J. Durkin, J. H. Tu, G. Menaker, J. D. Fallon, and N. Kollias, “In vivo Fluorescence Spectroscopy of Nonmelanoma Skin Cancer”, *Photochem. Photobiol*. **73**(2), 178–183 (2001).

[90] H. Zeng, D. I. M. M.d, C. E. MacAulay, B. Palcic, and H. L. M.d, “Autofluorescence of basal cell carcinoma”, in *Lasers in Surgery: Advanced Characterization, Therapeutics, and Systems VIII* **3245**, 314–317 (1998).

[91] E. Borisova, P. Troyanova, P. Pavlova, and L. Avramov, “Diagnostics of pigmented skin tumors based on laser-induced autofluorescence and diffuse reflectance spectroscopy”, *Quantum Electron*. **38**(6), 597 (2008).

[92] A. O. Ustinova, I. A. Bratchenko, D. N. Artemyev, “Monte Carlo simulation of skin multispectral autofluorescence”, *JBPE* **5**(2), 020306 (2019).

[93] S. Neus, T. Gambichler, F. G. Bechara, S. Wöhl, and P. Lehmann, “Preoperative assessment of basal cell carcinoma using conventional fluorescence diagnosis”, *Arch. Dermatol. Res*. **301**(4), 289–294 (2009).

[94] S. K. Kamrava, M. Behtaj, Y. Ghavami, S. Shahabi, M. Jalessi, E. E. Afshar, and S. Maleki, “Evaluation of diagnostic values of photodynamic diagnosis in identifying the dermal and mucosal squamous cell carcinoma”, *Photodiagnosis Photodyn. Ther*. **9**(4), 293–298 (2012).

[95] M. M. Kleinpenning, E. W. Wolberink, T. Smits, W. A. M. Blokx, P. C. M. van De Kerkhof, P. E. J. van Erp, and R. M. J. P. Gerritsen, “Fluorescence diagnosis in actinic keratosis and squamous cell carcinoma”, *Photodermatol. Photoimmunol. Photomed*. **26**(6), 297–302 (2010).

[96] N. van der Beek, J. de Leeuw, C. Demmendal, P. Bjerring, and H. A. M. Neumann, “PpIX fluorescence combined with auto-fluorescence is more accurate than PpIX fluorescence alone in fluorescence detection of non-melanoma skin cancer: an intra-patient direct comparison study”, *Lasers Surg. Med*. **44**(4), 271–276 (2012).

[97] E. A. Edwards and S. Q. Duntley, “The pigments and color of living human skin”, *Am. J. Anat*. **65**(1), 1–33 (1939).

[98] N. Kollias and A. Baqer, “On the assessment of melanin in human skin in vivo”, *Photochem. Photobiol*. **43**(1), 49–54 (1986).

[99] N. Kollias and A. H. Baqer, “Quantitative assessment of UV-induced pigmentation and erythema”, *Photodermatol*. **5**(1), 53–60 (1988).

[100] G. Zonios, J. Bykowski, and N. Kollias, “Skin melanin, hemoglobin, and light scattering properties can be quantitatively assessed in vivo using diffuse reflectance spectroscopy”, *J. Invest. Dermatol*. **117**(6), 1452–1457 (2001).

[101] L. Wang, S. L. Jacques, and L. Zheng, “MCML—Monte Carlo modeling of light transport in multi-layered tissues*”, Comput. Meth. Prog. Bio*. **47**(2), 131–146 (1995).

[102] D. Yudovsky and L. Pilon, “Rapid and accurate estimation of blood saturation, melanin content, and epidermis thickness from spectral diffuse reflectance”, *Appl. Opt*. **49**(10), 1707–1719 (2010).

[103] F. Urbach, *Biological Responses to Ultraviolet A Radiation*, Valdenmar Pub, Overland Park (1992).

[104] N. Kollias and A. Baqer, “An experimental study of the changes in pigmentation in human skin in vivo with visible and near infrared light”, *Photochem. Photobiol*. **39**(5), 651–659 (1984).

[105] N. Kollias and A. H. Baqer, “Absorption mechanisms of human melanin in the visible, 400-720 nm”, *J. Invest. Dermatol*. **89**(4), 384–388 (1987).

[106] I. A. Vitkin, J. Woolsey, B. C. Wilson, and R. R. Anderson, “Optical and thermal characterization of natural (Sepia officinalis) melanin”, *Photochem. Photobiol*. **59**(4), 455–462 (1994).

[107] A. R. Young, “Chromophores in human skin”, *Phys. Med. Biol*. **42**(5), 789–802 (1997).

[108] G. Zonios, A. Dimou, I. Bassukas, D. Galaris, A. Tsolakidis, and E. Kaxiras, “Melanin absorption spectroscopy: new method for noninvasive skin investigation and melanoma detection”, *JBO* **13**(1), 014017 (2008).

[109] A. Garcia-Uribe, J. Zou, M. Duvic, J. H. Cho-Vega, V. G. Prieto, and L. V. Wang, “In vivo diagnosis of melanoma and nonmelanoma skin cancer using oblique incidence diffuse reflectance spectrometry”, *Cancer. Res*. **72**(11), 2738–2745 (2012).

[110] M. Canpolat, A. Akman-Karakaş, G. A. Gökhan-Ocak, I. C. Başsorgun, M. Akif Çiftçioğlu, and E. Alpsoy, “Diagnosis and demarcation of skin malignancy using elastic light single-scattering spectroscopy: a pilot study”, *Dermatol. Surg*. **38**(2), 215–223 (2012).

[111] M. Canpolat, A. Akman, M. A. Çiftçioğlu, and E. Alpsoy, “Detecting Skin Malignancy Using Elastic Light Scattering Spectroscopy”, in *Diagnostic Optical Spectroscopy in Biomedicine IV*, 6628_20 (2007).

[112] Y. Jiao, T. Upile, W. Jerjes, H. Rhadi, S. Mosse, S. G. Brown, and C. Hopper, “Interrogation of skin pathology using elastic scattering spectroscopy”, *Head Neck Oncol*. **1**(1), O19 (2009).

[113] T. Upile, W. Jerjes, H. Radhi, J. Mahil, A. Rao, and C. Hopper, “Elastic scattering spectroscopy in assessing skin lesions: an “in vivo” study”, *Photodiagnosis Photodyn. Ther*. **9**(2), 132–141 (2012).

[114] B. G. Frushour and J. L. Koenig, “Raman scattering of collagen, gelatin, and elastin”, *Biopolymers* **14**(2), 379–391 (1975).

[115] M. Gniadecka, H. C. Wulf, O. F. Nielsen, D. H. Christensen, and J. Hercogova, “Distinctive molecular abnormalities in benign and malignant skin lesions: studies by Raman spectroscopy”, *Photochem. Photobiol*. **66**(4), 418–423 (1997).

[116] M. Gniadecka, O. Faurskov Nielsen, D. H. Christensen, and H. C. Wulf, “Structure of water, proteins, and lipids in intact human skin, hair, and nail”, *J. Invest. Dermatol*. **110**(4), 393–398 (1998).

[117] P. J. Caspers, G. W. Lucassen, R. Wolthuis, H. A. Bruining, and G. J. Puppels, “In vitro and in vivo Raman spectroscopy of human skin”, *Biospectroscopy* **4**(5), S31-39 (1998).

[118] P. J. Caspers, G. W. Lucassen, E. A. Carter, H. A. Bruining, and G. J. Puppels, “In vivo confocal Raman microspectroscopy of the skin: noninvasive determination of molecular concentration profiles”, *J. Invest. Dermatol*. **116**(3), 434–442 (2001).

[119] K. U. Schallreuter, J. Moore, J. M. Wood, W. D. Beazley, D. C. Gaze, D. J. Tobin, H. S. Marshall, A. Panske, E. Panzig, and N. A. Hibberts, "In vivo and in vitro evidence for hydrogen peroxide (H2O2) accumulation in the epidermis of patients with vitiligo and its successful removal by a UVB-activated pseudocatalase", *J. Invest. Dermatol. Symp. P*. **4**(1), 91–96 (1999).

[120] T. R. Hata, T. A. Scholz, I. V. Ermakov, R. W. McClane, F. Khachik, W. Gellermann, and L. K. Pershing, "Non-Invasive Raman Spectroscopic Detection of Carotenoids in Human Skin", *J. Invest. Dermatol*. **115**(3), 441–448 (2000).

[121] J. Wohlrab, A. Vollmann, S. Wartewig, W. C. Marsch, and R. Neubert, "Noninvasive characterization of human stratum corneum of undiseased skin of patients with atopic dermatitis and psoriasis as studied by Fourier transform Raman spectroscopy", *Biopolymers* **62**(3), 141–146 (2001).

[122] J. Zhao, H. Lui, D. I. McLean, and H. Zeng, "Real-time raman spectroscopy for non-invasive skin cancer detection - preliminary results", in *2008 30th Annual International Conference of the IEEE Engineering in Medicine and Biology Society*, 3107–3109 (2008).

[123] H. Lui, J. Zhao, D. McLean, and H. Zeng, "Real-time Raman spectroscopy for in vivo skin cancer diagnosis", *Cancer Res*. **72**(10), 2491–2500 (2012).

[124] L. Silveira Jr., F. L. Silveira, B. Bodaneze, R. A. Zangaro, and M. T. T. Pacheco, "Discriminating model for diagnosis of basal cell carcinoma and melanoma in vitro based on the Raman spectra of selected biochemicals", *JBO* **17**(7), 077003 (2012).

[125] M. Larraona-Puy, A. Ghita, A. Zoladek, W. Perkins, S. Varma, I. H. Leach, A. A. Koloydenko, H. Williams, and I. Notingher, "Development of Raman microspectroscopy for automated detection and imaging of basal cell carcinoma", *JBO* **14**(5), 054031 (2009).

[126] A. F. de Oliveira, I. D. A. O. Santos, S. B. Cartaxo, R. A. Bitar, M. M. S. S. Enokihara, H. da Silva Martinho, A. A. Martin, and L. M. Ferreira, "Differential diagnosis in primary and metastatic cutaneous melanoma by FT-Raman spectroscopy", *Acta Cir. Bras*. **25**(5), 434–439 (2010).

[127] S. B. Cartaxo, I. D. A. O. Santos, R. Bitar, A. F. Oliveira, L. M. Ferreira, H. S. Martinho, and A. A. Martin, "FT-Raman spectroscopy for the differentiation between cutaneous melanoma and pigmented nevus", *Acta Cir. Bras*. **25**(4), 351–356 (2010).

[128] L. de O. Nunes, A. A. Martin, L. Silveira Jr., and M. Zampieri, "FT-Raman spectroscopy study for skin cancer diagnosis", *Spectroscopy* **17**(2–3), 597–602 (2003).

[129] M. Gniadecka, P. A. Philipsen, S. Sigurdsson, S. Wessel, O. F. Nielsen, D. H. Christensen, J. Hercogova, K. Rossen, H. K. Thomsen, R. Gniadecki, L. K. Hansen, and H. C. Wulf, "Melanoma diagnosis by Raman spectroscopy and neural networks: structure alterations in proteins and lipids in intact cancer tissue", *J. Invest. Dermatol*. **122**(2), 443–449 (2004).

[130] C. A. Lieber, S. K. Majumder, D. L. Ellis, D. D. Billheimer, and A. Mahadevan-Jansen, "In vivo nonmelanoma skin cancer diagnosis using Raman microspectroscopy", *Laser. Surg. Med*. **40**(7), 461–467 (2008).

[131] H. Zeng, H. Lui, and D. McLean, "Skin cancer detection using in vivo Raman spectroscopy", available at https://spie.org/news/3705-skin-cancer-detection-using-in-vivo-raman-spectroscopy (2011).

[132] P. Corcuff, C. Bertrand, and J. L. Leveque, "Morphometry of human epidermis in vivo by real-time confocal microscopy", *Arch. Dermatol. Res*. **285**(8), 475–481 (1993).

[133] M. Rajadhyaksha, M. Grossman, D. Esterowitz, R. H. Webb, and R. R. Anderson, “In vivo confocal scanning laser microscopy of human skin: melanin provides strong contrast”, *J. Invest. Dermatol*. **104**(6), 946–952 (1995).

[134] S. González, M. Rajadhyaksha, and R. R. Anderson, “Non-invasive (real-time) imaging of histologic margin of a proliferative skin lesion in vivo”, *J. Invest. Dermatol*. **111**(3), 538–539 (1998).

[135] L. J. Bussau, L. T. Vo, P. M. Delaney, G. D. Papworth, D. H. Barkla, and R. G. King, “Fibre optic confocal imaging (FOCI) of keratinocytes, blood vessels and nerves in hairless mouse skin in vivo”, *J. Anat*. **192**(2), 187–194 (1998).

[136] L. T. Vo, G. D. Papworth, P. M. Delaney, D. H. Barkla, and R. G. King, “A study of vascular response to thermal injury on hairless mice by fibre optic confocal imaging, laser doppler flowmetry and conventional histology”, *Burns* **24**(4), 319–324 (1998).

[137] A. Gerger, S. Koller, T. Kern, C. Massone, K. Steiger, E. Richtig, H. Kerl, and J. Smolle, “Diagnostic applicability of in vivo confocal laser scanning microscopy in melanocytic skin tumors”, *J. Invest. Dermatol*. **124**(3), 493–498 (2005).

[138] P. J. Rigby and R. G. Goldie, “Confocal microscopy in biomedical research”, *Croat. Med. J*. **40**(3), 346–352 (1999).

[139] R. Lima, T. Ishikawa, Y. Imai, M. Takeda, S. Wada, and T. Yamaguchi, “Measurement of individual red blood cell motions under high hematocrit conditions using a confocal micro-PTV system”, *Ann. Biomed. Eng*. **37**(8), 1546–1559 (2009).

[140] A. Gerger, S. Koller, W. Weger, E. Richtig, H. Kerl, H. Samonigg, P. Krippl, and J. Smolle, “Sensitivity and specificity of confocal laser-scanning microscopy for in vivo diagnosis of malignant skin tumors”, *Cancer* **107**(1), 193–200 (2006).

[141] S. González, “Confocal reflectance microscopy in dermatology: promise and reality of non-invasive diagnosis and monitoring”, *Actas Dermosifiliogr*. **100**(2), 59–69 (2009).

[142] M. Ulrich, A. Maltusch, F. Rius-Diaz, J. Röwert-Huber, S. González, W. Sterry, E. Stockfleth, and S. Astner, “Clinical applicability of in vivo reflectance confocal microscopy for the diagnosis of actinic keratoses”, *Dermatol. Surg*. **34**(5), 610–619 (2008).

[143] M. Ulrich, S. Lange-Asschenfeldt, and S. Gonzalez, “Clinical applicability of in vivo reflectance confocal microscopy in dermatology”, *G. Ital. Dermatol. Venereol*. **147**, (2), 171–178 (2012).

[144] M. Ulrich, S. Lange-Asschenfeldt, and S. Gonzalez, “The use of reflectance confocal microscopy for monitoring response to therapy of skin malignancies”, *Dermatol. Pract. Concept*. **2**(2), 202a10 (2012).

[145] C. Curiel-Lewandrowski, C. M. Williams, K. J. Swindells, S. R. Tahan, S. Astner, R. A. Frankenthaler, and S. González, “Use of in vivo confocal microscopy in malignant melanoma: an aid in diagnosis and assessment of surgical and nonsurgical therapeutic approaches”, *Arch. Dermatol*. **140**(9), 1127–1132 (2004).

[146] A. Scope, U. Mahmood, D. S. Gareau, M. Kenkre, J. A. Lieb, K. S. Nehal, and M. Rajadhyaksha, “In vivo reflectance confocal microscopy of shave biopsy wounds: feasibility of intraoperative mapping of cancer margins”, *Br. J. Dermatol*. **163**(6), 1218–1228 (2010).

[147] M. Ulrich, D. Krueger-Corcoran, J. Roewert-Huber, W. Sterry, E. Stockfleth, and S. Astner, “Reflectance confocal microscopy for noninvasive monitoring of therapy and detection of subclinical actinic keratoses”, *Dermatology* **220**(1), 15–24 (2010).

[148] S. P. Hicks, K. J. Swindells, M. A. Middelkamp-Hup, M. A. Sifakis, E. González, and S. González, "Confocal histopathology of irritant contact dermatitis in vivo and the impact of skin color (black vs white)", *J. Am. Acad. Dermatol*. **48**(5), 727–734 (2003).

[149] K. Swindells, N. Burnett, F. Rius-Diaz, E. González, M. C. Mihm, and S. González, "Reflectance confocal microscopy may differentiate acute allergic and irritant contact dermatitis in vivo", *J. Am. Acad. Dermatol*. **50**(2), 220–228 (2004).

[150] S. Astner, S. Dietterle, N. Otberg, H.-J. Röwert-Huber, E. Stockfleth, and J. M. Lademann, "Clinical applicability of in vivo fluorescence confocal microscopy for noninvasive diagnosis and therapeutic monitoring of nonmelanoma skin cancer", *JBO* **13**(1), 014003 (2008).

[151] M. Amjadi, B. Coventry, and J. Greenwood, "Reflectance Confocal Microscopy in the Diagnosis of Non- Melanoma Skin Cancer and Benign Lesions Versus Normal Skin: A Blinded Prospective Trial", *The Internet Journal of Plastic Surgery* **7**(2), 2010.

[152] A. Gerger, R. Hofmann-Wellenhof, U. Langsenlehner, E. Richtig, S. Koller, W. Weger, V. Ahlgrimm-Siess, M. Horn, H. Samonigg, and J. Smolle, "In vivo confocal laser scanning microscopy of melanocytic skin tumours: diagnostic applicability using unselected tumour images", *Br. J. Dermatol*. **158**(2), 329–333 (2008).

[153] R. G. B. Langley, E. Burton, N. Walsh, I. Propperova, and S. J. Murray, "In vivo confocal scanning laser microscopy of benign lentigines: comparison to conventional histology and in vivo characteristics of lentigo maligna", *J. Am. Acad. Dermatol*. **55**(1), 88–97 (2006).

[154] R. G. B. Langley, N. Walsh, A. E. Sutherland, I. Propperova, L. Delaney, S. F. Morris, and C. Gallant, "The diagnostic accuracy of in vivo confocal scanning laser microscopy compared to dermoscopy of benign and malignant melanocytic lesions: a prospective study", *Dermatology* **215**(4), 365–372 (2007).

[155] G. Pellacani, P. Guitera, C. Longo, M. Avramidis, S. Seidenari, and S. Menzies, "The impact of in vivo reflectance confocal microscopy for the diagnostic accuracy of melanoma and equivocal melanocytic lesions", *J. Invest. Dermatol*. **127**(12), 2759–2765 (2007).

[156] G. Pellacani, C. Longo, J. Malvehy, S. Puig, C. Carrera, S. Segura, S. Bassoli, and S. Seidenari, "In vivo confocal microscopic and histopathologic correlations of dermoscopic features in 202 melanocytic lesions", *Arch. Dermatol*. **144**(12), 1597–1608 (2008).

[157] V. Ahlgrimm-Siess, C. Massone, A. Scope, R. Fink-Puches, E. Richtig, I. H. Wolf, S. Koller, A. Gerger, J. Smolle, and R. Hofmann-Wellenhof, "Reflectance confocal microscopy of facial lentigo maligna and lentigo maligna melanoma: a preliminary study", *Br. J. Dermatol*. **161**(6), 1307–1316 (2009).

[158] P. Guitera, G. Pellacani, K. A. Crotty, R. A. Scolyer, L. L. Li, S. Bassoli, M. Vinceti, H. Rabinovitz, C. Longo, and S. W. Menzies, "The impact of in vivo reflectance confocal microscopy on the diagnostic accuracy of lentigo maligna and equivocal pigmented and nonpigmented macules of the face", *J. Invest. Dermatol*. **130**(8), 2080–2091 (2010).

[159] W. Zong, R. Wu, M. Li, Y. Hu, Y. Li, J. Li, H. Rong, H. Wu, Y. Xu, Y. Lu, H. Jia, M. Fan, Z. Zhou, Y. Zhang, A. Wang, L. Chen, and H. Cheng, "Fast high-resolution miniature two-photon microscopy for brain imaging in freely behaving mice", *Nat. Methods* **14**(7), 713-719 (2017).

[160] J. Paoli, M. Smedh, and M. B. Ericson, "Multiphoton laser scanning microscopy--a novel diagnostic method for superficial skin cancers", *Semin. Cutan. Med. Surg*. **28**(3), 190–195 (2009).

[161] S. W. Perry, R. M. Burke, and E. B. Brown, "Two-photon and second harmonic microscopy in clinical and translational cancer research", *Ann. Biomed. Eng*. **40**(2), 277–291 (2012).

[162] B. H. Oh, K. H. Kim, and K. Y. Chung, “Skin Imaging Using Ultrasound Imaging, Optical Coherence Tomography, Confocal Microscopy, and Two-Photon Microscopy in Cutaneous Oncology”, *Front. Med*. **6**, 274 (2019).

[163] M. B. Ericson, C. Simonsson, S. Guldbrand, C. Ljungblad, J. Paoli, and M. Smedh, “Two-photon laser-scanning fluorescence microscopy applied for studies of human skin”, *J. Biophotonics* **1**(4), 320–330 (2008).

[164] N. Y. Bentolila, R. L. Barnhill, C. Lugassy, and L. A. Bentolila, “Intravital Imaging of Human Melanoma Cells in the Mouse Ear Skin by Two-Photon Excitation Microscopy”, *Methods Mol. Biol*. **1755**, 223–232 (2018).

[165] P. A. Franken, A. E. Hill, C. W. Peters, and G. Weinreich, “Generation of Optical Harmonics”, *Phys. Rev. Lett*. **7**(4), 118–119 (1961).

[166] P. J. Campagnola, A. C. Millard, M. Terasaki, P. E. Hoppe, C. J. Malone, and W. A. Mohler, “Three-dimensional high-resolution second-harmonic generation imaging of endogenous structural proteins in biological tissues”, *Biophys. J*. **82**(1), 493–508 (2002).

[167] S. Plotnikov, V. Juneja, A. B. Isaacson, W. A. Mohler, and P. J. Campagnola, “Optical Clearing for Improved Contrast in Second Harmonic Generation Imaging of Skeletal Muscle”, *Biophys. J*. **90**(1), 328–339 (2006).

[168] M. Müller, J. Squier, K. R. Wilson, and G. J. Brakenhoff, “3D microscopy of transparent objects using third-harmonic generation”, *J. Microsc*. **191**(3), 266–274 (1998).

[169] A. Keikhosravi, J. S. Bredfeldt, A. K. Sagar, and K. W. Eliceiri, “Chapter 28 - Second-harmonic generation imaging of cancer”, in *Methods in Cell Biology* **123**, 531–546 (2014).

[170] S. Yue, M. N. Slipcheko, and J. X. Cheng, “Multimodal nonlinear optical microscopy”, *Laser Photonics Rev*. **5**, 496-512 (2011).

[171] C. Thrasivoulou, G. Virich, T. Krenacs, I. Korom, and D. L. Becker, “Optical delineation of human malignant melanoma using second harmonic imaging of collagen”, *Biomed. Opt. Express* **2**(5), 1282–1295 (2011).

[172] D. Huang, E. A. Swanson, C. P. Lin, J. S. Schuman, W. G. Stinson, W. Chang, M. R. Hee, T. Flotte, K. Gregory, C. A. Puliafito, and J. G. Fujimoto, “Optical Coherence Tomography”, *Science* **254**(5035), 1178-1181 (1991).

[173] J. G. Fujimoto and W. Drexler, “Introduction to OCT”, in *Optical Coherence Tomography: Technology and Applications*, W. Drexler and J. G. Fujimoto, Eds., 3–64, Springer, Cham (2015).

[174] F. Harms, A. Latrive, and A. C. Boccara, “Time Domain Full Field Optical Coherence Tomography Microscopy”, in *Optical Coherence Tomography: Technology and Applications*, W. Drexler and J. G. Fujimoto, Eds., 791–812, Springer, Cham (2015).

[175] J. F. de Boer, “Spectral/Fourier Domain Optical Coherence Tomography”, in *Optical Coherence Tomography: Technology and Applications*, W. Drexler and J. G. Fujimoto, Eds., 165-193, Springer, Cham (2015).

[176] J. Ogien, O. Levecq, H. Azimani, A. Dubois, and A. Dubois, “Dual-mode line-field confocal optical coherence tomography for ultrahigh-resolution vertical and horizontal section imaging of human skin in vivo”, *Biomed. Opt. Express* **11**(3), 1327–1335 (2020).

[177] J. K. Barton, K. W. Gossage, W. Xu, J. R. Ranger-Moore, K. Saboda, C. A. Brooks, L. D. Duckett, S. J. Salasche, J. A. Warneke, and D. S. Alberts, “Investigating sun-damaged skin and actinic keratosis

with optical coherence tomography: a pilot study", *Technol. Cancer. Res. Treat*. **2**(6), 525–535 (2003).

[178] V. R. Korde, G. T. Bonnema, W. Xu, C. Krishnamurthy, J. Ranger-Moore, K. Saboda, L. D. Slayton, S. J. Salasche, J. A. Warneke, D. S. Alberts, and J. K. Barton, "Using optical coherence tomography to evaluate skin sun damage and precancer", *Lasers Surg. Med*. **39**(9), 687–695 (2007).

[179] T. M. Jørgensen, A. Tycho, M. Mogensen, P. Bjerring, and G. B. E. Jemec, "Machine-learning classification of non-melanoma skin cancers from image features obtained by optical coherence tomography", *Skin Res. Technol*. **14**(3), 364–369 (2008).

[180] M. Mogensen, T. M. Joergensen, B. M. Nürnberg, H. A. Morsy, J. B. Thomsen, L. Thrane, and G. B. E. Jemec, "Assessment of optical coherence tomography imaging in the diagnosis of non-melanoma skin cancer and benign lesions versus normal skin: observer-blinded evaluation by dermatologists and pathologists", *Dermatol. Surg*. **35**(6), 965–972 (2009).

[181] J. M. Olmedo, K. E. Warschaw, J. M. Schmitt, and D. L. Swanson, "Optical coherence tomography for the characterization of basal cell carcinoma in vivo: a pilot study", *J. Am. Acad. Dermatol*. **55**(3), 408–412 (2006).

[182] J. M. Olmedo, K. E. Warschaw, J. M. Schmitt, and D. L. Swanson, "Correlation of Thickness of Basal Cell Carcinoma by Optical Coherence Tomography In Vivo and Routine Histologic Findings: A Pilot Study", *Dermatologic Surgery* **33**(4), 421–426 (2007).

[183] T. Hinz, L. Ehler, T. Hornung, H. Voth, I. Fortmeier, T. Maier, T. Höller, and M. Wendtner, "Preoperative characterization of basal cell carcinoma comparing tumour thickness measurement by optical coherence tomography, 20-MHz ultrasound and histopathology", *Acta Derm. Venereol*. **92**(2), 132–137 (2012).

[184] R. Alfano and L. Shi, *Neurophotonics and Biomedical Spectroscopy*, 1st ed., Elsevier, Amsterdam (2018).

[185] G. Lu and B. Fei, "Medical hyperspectral imaging: a review", *JBO* **19**(1), 010901 (2014).

[186] F. Melgani and L. Bruzzone, "Classification of hyperspectral remote sensing images with support vector machines", *IEEE T. Geosci. Remote* **42**(8), 1778–1790 (2004).

[187] Z. Liu, J. Yan, D. Zhang, and Q. L. Li, "Automated tongue segmentation in hyperspectral images for medicine", *Appl. Opt*. **46**(34), 8328–8334 (2007).

[188] L. Zhi, D. Zhang, J. Yan, Q.-L. Li, and Q. Tang, "Classification of hyperspectral medical tongue images for tongue diagnosis", *Comput. Med. Imag. Grap*. **31**(8), 672–678 (2007).

[189] S. G. Kong and L. J. Park, "Hyperspectral Image Analysis for Skin Tumor Detection", in *Augmented Vision Perception in Infrared: Algorithms and Applied Systems*, R. I. Hammoud, Ed., Springer, London (2009).

[190] D. Lu and Q. Weng, "A survey of image classification methods and techniques for improving classification performance", *Int. J. Remote Sens*. **28**(5), 823–870 (2007).

[191] Y. Guan, Q. Li, H. Liu, Z. Zhu, and Y. Wang, "Pathological leucocyte segmentation algorithm based on hyperspectral imaging technique", *OE* **51**(5), 053202 (2012).

[192] P. Constantinou, R. S. Dacosta, and B. C. Wilson, "Extending immunofluorescence detection limits in whole paraffin-embedded formalin fixed tissues using hyperspectral confocal fluorescence imaging", *J. Microsc*. **234**(2), 137–146 (2009).

[193] D. T. Dicker, J. Lerner, P. Van Belle, S. F. Barth, D. Guerry 4th, M. Herlyn, D. E. Elder, and W. S. El-Deiry, "Differentiation of normal skin and melanoma using high resolution hyperspectral imaging", *Cancer Biol. Ther*. **5**(8), 1033–1038 (2006).

[194] D. Hattery, M. Hassan, S. Demos, and A. Gandjbakhche, "Hyperspectral imaging of Kaposi's Sarcoma for disease assessment and treatment monitoring", in *Applied Imagery Pattern Recognition Workshop, 2002. Proceedings*, 124–130 (2002).

[195] L. A. Courtenay, D. González-Aguilera, S. Lagüela, S. Del Pozo, C. Ruiz-Mendez, I. Barbero-García, C. Román-Curto, J. Cañueto, C. Santos-Durán, M. E. Cardeñoso-Álvarez, M. Roncero-Riesco, D. Hernandez-Lopez, D. Guerrero-Sevilla, and P. Rodríguez-Gonzalvez, "Hyperspectral imaging and robust statistics in non-melanoma skin cancer analysis", *Biomed. Opt. Express* **12**(8), 5107–5127 (2021).

[196] L. Annala, N. Neittaanmaki, J. Paoli, O. Zaar, and I. Polonen, "Generating Hyperspectral Skin Cancer Imagery using Generative Adversarial Neural Network", *Annu. Int. Conf. IEEE Eng. Med. Biol. Soc*. **2020**, 1600–1603 (2020).

[197] R. Leon, B. Martinez-Vega, H. Fabelo, S. Ortega, V. Melian, I. Castaño, G. Carretero, P. Almeida, A. Garcia, E. Quevedo, J. A. Hernandez, B. Clavo, G. M. Callico, "Non-Invasive Skin Cancer Diagnosis Using Hyperspectral Imaging for In-Situ Clinical Support", *Journal of Clinical Medicine* **9**(6), 1662 (2020).

[198] G. B. Christensen, T. Nagaoka, Y. Kiyohara, I. Johansson, C. Ingvar, A. Nakamura, T. Sota, and K. Nielsen, "Clinical performance of a novel hyperspectral imaging device for cutaneous melanoma and pigmented skin lesions in Caucasian skin", *Skin Res. Technol*. **27**(5), 803–809 (2021).

[199] P. Troyanova, E. Borisova, and L. Avramov, "Fluorescence and reflectance properties of hemoglobin-pigmented skin disorders", in *International Conference on Lasers, Applications, and Technologies 2007: Laser Technologies for Medicine* **6734**, 142-149 (2007).

[200] B. Kim, H. Le, B. H. Oh, and K. H. Kim, "High-speed combined reflectance confocal and moxifloxacin based two-photon microscopy", *Biomed. Opt. Express* **11**(3), 1555–1567 (2020).

[201] E. Carstea, L. Ghervase, G. Pavelescu, D. Savastru, and A. M. Forsea, "Combined optical techniques for skin lesion diagnosis: Short communication", *Optoelectron. Adv. Mat*. **4**(12), 1960-1963 (2010).

[202] R. Cicchi, S. Sestini, V. De Giorgi, D. Massi, T. Lotti, and F. S. Pavone, "Nonlinear laser imaging of skin lesions", *J. Biophotonics* **1**(1), 62–73 (2008).

[203] S. Heuke, N. Vogler, T. Meyer, D. Akimov, F. Kluschke, H. J. Röwert-Huber, J. Lademann, B. Dietzek, and J. Popp, "Detection and Discrimination of Non-Melanoma Skin Cancer by Multimodal Imaging", *Healthcare* **1**(1), 64-83 (2013).

[204] V. V. Tuchin, *Optical Clearing of Tissues and Blood*, SPIE, Bellingham (2005).

[205] A. N. Bashkatov, E. A. Genina, V. I. Kochubey, and V. V. Tuchin, "Estimation of wavelength dependence of refractive index of collagen fibers of scleral tissue", in *Controlling Tissue Optical Properties: Applications in Clinical Study*, 265–268 (2000).

[206] L. M. Oliveira, M. I. Carvalho, E. M. Nogueira, and V. V. Tuchin, "Diffusion characteristics of ethylene glycol in skeletal muscle", *JBO* **20**(5), 051019 (2014).

[207] L. Oliveira, M. Carvalho, E. Nogueira, and V. Tuchin, "Optical clearing mechanisms characterization in muscle", *J. Innov. Opt. Heal. Sci*. **9**(5), 1650035 (2016).

[208] K. V. Larin, M. G. Ghosn, A. N. Bashkatov, E. A. Genina, N. A. Trunina, and V. V. Tuchin, "Optical Clearing for OCT Image Enhancement and In-Depth Monitoring of Molecular Diffusion", *IEEE J. Sel. Top. Quant*. **18**(3), 1244–1259 (2012).

[209] D. K. Tuchina, R. Shi, A. N. Bashkatov, E. A. Genina, D. Zhu, Q. Luo, V. V. Tuchin, "Ex vivo optical measurements of glucose diffusion kinetics in native and diabetic mouse skin", *J. Biophotonics* **8**(4), 332–346 (2015).

[210] A. K. Bui, R. A. McClure, J. Chang, C. Stoianovici, J. Hirshburg, A. T. Yeh, and B. Choi, "Revisiting optical clearing with dimethyl sulfoxide (DMSO)", *Lasers Surg. Med*. **41**(2), 142–148 (2009).

[211] X. Wen, Z. Mao, Z. Han, V. V. Tuchin, and D. Zhu, "In vivo skin optical clearing by glycerol solutions: mechanism", *J. Biophotonics* **3**(1–2), 44–52 (2010).

[212] V. V. Tuchin, "A Clear Vision for Laser Diagnostics (Review)", *IEEE J. Sel. Top. Quant.* **13**(6), 1621–1628 (2007).

[213] F. S. Pavone, *Laser Imaging and Manipulation in Cell Biology*, 1st ed., Wiley-VCH, Weinheim (2010).

[214] V. V. Tuchin, *Handbook of Optical Biomedical Diagnostics*, 2nd ed., SPIE, Bellingham (2016).

[215] I. L. Kon, V. V. Bakutkin, N. V. Bogomolova, S. V. Tuchin, D. A. Zimnyakov, and V. V. Tuchin, "Trazograph influence on osmotic pressure and tissue structures of human sclera", in *Ophthalmic Technologies VII*, 198-206 (1997).

[216] V. V. Tuchin, I. L. Maksimova, D. A. Zimnyakov, I. L. Kon, A. H. Mavlyutov, and A. A. Mishin, "Light propagation in tissues with controlled optical properties", *JBO* **2**(4), 401–417 (1997).

[217] H. Hama, H. Kurokawa, H. Kawano, R. Ando, T. Shimogori, H. Noda, K. Fukami, A. Sakaue-Sawano, and A. Miyawaki, "Scale: a chemical approach for fluorescence imaging and reconstruction of transparent mouse brain", *Nat. Neurosci*. **14**(11), 1481-8 (2011).

[218] H. Hama, H. Hioki, K. Namiki, T. Hoshida, H. Kurokawa, F. Ishidate, T. Kaneko, T. Akagi, T. Saito, T. Saido, and A. Miyawaki, "ScaleS: an optical clearing palette for biological imaging", *Nat. Neurosci*. **18**(10), 1518-29 (2015).

[219] V. V. Tuchin, X. Xu, and R. K. Wang, "Dynamic optical coherence tomography in studies of optical clearing, sedimentation, and aggregation of immersed blood", *Appl. Opt*. **41**(1), 258–271 (2002).

[220] E. A. Genina, A. N. Bashkatov, A. A. Korobko, E. A. Zubkova, V. V. Tuchin, I. Yaroslavsky, and G. B. Altshuler, "Optical clearing of human skin: comparative study of permeability and dehydration of intact and photothermally perforated skin", *JBO* **13**(2), 021102 (2008).

[221] D. Y. Churmakov, I. Meglinski, and D. A. Greenhalgh, "Amending of fluorescence sensor signal localisation in human skin by matching of the refractive index", *JBO* **9**(2), 339-346 (2004).

[222] I. Meglinski and D. Y. Churmakov, "Spatial Localisation of Biosensor Fluorescence Signals in Human Skin under the Effect of Equalisation of the Refractive Index of the Surrounding Medium", *Opt. Spectrosc*. **96**(6), 946-951 (2004).

[223] G. Vargas, E. K. Chan, J. K. Barton, H. G. Rylander III, and A. J. Welch, "Use of an agent to reduce scattering in skin", *Lasers Surg. Med*. **24**(2), 133–141 (1999).

[224] V. V. Tuchin, *Handbook of Optical Sensing of Glucose in Biological Fluids and Tissues*, 1st ed., Routledge & CRC Press, London (2009).

[225] A. T. Yeh, B. Choi, J. S. Nelson, and B. J. Tromberg, "Reversible dissociation of collagen in tissues", *J. Invest. Dermatol*. **121**(6), 1332–1335 (2003).

[226] I. Yanina, A. Popov, A. Bykov, I. Meglinski, and V. Tuchin, “Monitoring of temperature-mediated phase transitions of adipose tissue by combined OCT and Abbe refractometry”, *JBO* **23**(1), 016003 (2018).

[227] J. Hirshburg, B. Choi, J. S. Nelson, and A. T. Yeh, “Correlation between collagen solubility and skin optical clearing using sugars”, *Lasers Surg. Med*. **39**(2), 140–144 (2007).

[228] J. M. Hirshburg, K. M. Ravikumar, W. Hwang, and A. T. Yeh, “Molecular basis for optical clearing of collagenous tissues”, *JBO* **15**(5), 055002 (2010).

[229] E. A. Genina, A. N. Bashkatov, Y. P. Sinichkin, and V. V. Tuchin, “Optical clearing of the eye sclera in vivo caused by glucose”, *Quantum Electron*. **36**(12), 1119 (2006).

[230] A. Bashkatov, A. N. Korolevich, V. V. Tuchin, Yu. P. Sinichkin, E. A. Genina, M. Stolnitz, N. S. Dubina, S. I. Vecherinski, and M. Belsley, “In vivo investigation of human skin optical clearing and blood microcirculation under the action of glucose solution”, *Asian J. Phys*. **15**(1), 1-14 (2006).

[231] E. I. Galanzha, V. V. Tuchin, A. V. Solovieva, T. V. Stepanova, Q. Luo, and H. Cheng, “Skin backreflectance and microvascular system functioning at the action of osmotic agents”, *J. Phys. D: Appl. Phys*. **36**(14), 1739–1746 (2003).

[232] D. Zhu, J. Zhang, H. Cui, Z. Mao, P. Li, and Q. Luo, “Short-term and long-term effects of optical clearing agents on blood vessels in chick chorioallantoic membrane”, *JBO* **13**(2), 021106 (2008).

[233] M. G. Ghosn, V. V. Tuchin, and K. V. Larin, “Depth-resolved monitoring of glucose diffusion in tissues by using optical coherence tomography”, *Opt. Lett*. **31**(15), 2314–2316 (2006).

[234] A. Bashkatov, E. Genina, Yu. P. Sinichkin, V. Kochubey, N. Lakodina, and V. Tuchin, “Estimation of the glucose diffusion coefficient in human eye sclera”, *Biophysics* **48**, 292–296 (2003).

[235] J. Wang, N. Ma, R. Shi, Y. Zhang, T. Yu, and D. Zhu, “Sugar-Induced Skin Optical Clearing: From Molecular Dynamics Simulation to Experimental Demonstration”, *IEEE J. Sel. Top. Quant*. **20**(2), 256–262 (2014).

[236] A. Bykov, T. Hautala, M. Kinnunen, A. Popov, S. Karhula, S. Saarakkala, M. T. Nieminen, V. Tuchin, and I. Meglinski, “Imaging of subchondral bone by optical coherence tomography upon optical clearing of articular cartilage”, *J. Biophotonics* **9**(3), 270–275 (2016).

[237] E. A. Genina, A. N. Bashkatov, and V. V. Tuchin, “Optical clearing of human dura mater by glucose solutions”, *JBPE* **3**(1), 010309 (2017).

[238] A. N. Bashkatov, E. A. Genina, Y. P. Sinichkin, V. I. Kochubey, N. A. Lakodina, and V. V. Tuchin, “Glucose and Mannitol Diffusion in Human Dura Mater”, *Biophys. J*. **85**(5), 3310–3318 (2003).

[239] E. A. Genina, A. N. Bashkatov, and V. V. Tuchin, “Optical Clearing of Cranial Bone”, *Advances in Optical Technologies* **2008**, e267867 (2008).

[240] G. Vargas, J. K. Barton, and A. J. Welch, “Use of hyperosmotic chemical agent to improve the laser treatment of cutaneous vascular lesions”, *JBO* **13**(2), 021114 (2008).

[241] Z. Zhu, G. Wu, H. Wei, H. Yang, Y. He, S. Xie, Q. Zhao, and X. Guo, “Investigation of the permeability and optical clearing ability of different analytes in human normal and cancerous breast tissues by spectral domain OCT”, *J. Biophotonics* **5**(7), 536–543 (2012).

[242] B. Choi, L. Tsu, E. Chen, T. S. Ishak, S. M. Iskandar, S. Chess, and J. S. Nelson, “Determination of chemical agent optical clearing potential using in vitro human skin”, *Lasers Surg. Med*. **36**(2), 72–75 (2005).

[243] Z. Mao, D. Zhu, Y. Hu, X. Wen, and Z. Han, “Influence of alcohols on the optical clearing effect of skin in vitro”, *JBO* **13**(2), 021104 (2008).

[244] E. Genina, A. Bashkatov, Y. Sinichkin, and V. Tuchin, “Optical clearing of skin under action of glycerol: Ex vivo and in vivo investigations”, *Opt. Spectrosc*. **109**, 225–231 (2010).

[245] S. G. Proskurin and I. V. Meglinski, “Optical coherence tomography imaging depth enhancement by superficial skin optical clearing”, *Laser Phys. Lett*. **4**(11), 824 (2007).

[246] M. H. Khan, B. Choi, S. Chess, K. M Kelly, J. McCullough, and J. S. Nelson, “Optical clearing of in vivo human skin: implications for light-based diagnostic imaging and therapeutics”, *Lasers Surg. Med*. **34**(2), 83–85 (2004).

[247] J. Jiang and R. K. Wang, “Comparing the synergistic effects of oleic acid and dimethyl sulfoxide as vehicles for optical clearing of skin tissuein vitro”, *Phys. Med. Biol*. **49**(23), 5283–5294 (2004).

[248] R. Shi, M. Chen, V. V. Tuchin, and D. Zhu, “Accessing to arteriovenous blood flow dynamics response using combined laser speckle contrast imaging and skin optical clearing”, *Biomed. Opt. Express* **6**(6), 1977–1989 (2015).

[249] X. Xu and R. K. Wang, “Synergistic effect of hyperosmotic agents of dimethyl sulfoxide and glycerol on optical clearing of gastric tissue studied with near infrared spectroscopy”, *Phys. Med. Biol*. **49**(3), 457–468 (2004).

[250] J. Jiang, M. Boese, P. Turner, and R. K. Wang, “Penetration kinetics of dimethyl sulphoxide and glycerol in dynamic optical clearing of porcine skin tissue in vitro studied by Fourier transform infrared spectroscopic imaging”, *JBO* **13**(2), 021105 (2008).

[251] Z. Deng, L. Jing, N. Wu, P. Lv, X. Jiang, Q. Ren, and C. Li, “Viscous optical clearing agent for in vivo optical imaging”, *JBO* **19**(7), 76019 (2014).

[252] L. Guo, R. Shi, C. Zhang, D. Zhu, Z. Ding, and P. Li, “Optical coherence tomography angiography offers comprehensive evaluation of skin optical clearing in vivo by quantifying optical properties and blood flow imaging simultaneously”, *JBO* **21**(8), 081202 (2016).

[253] X. Jin, Z. Deng, J. Wang, Q. Ye, J. Mei, W. Zhou, C. Zhang, and J. Tian, “Study of the inhibition effect of thiazone on muscle optical clearing”, *JBO* **21**(10), 105004 (2016).

[254] Y. Ding, J. Wang, Z. Fan, D. Wei, R. Shi, Q. Luo, D. Zhu, and X. Wei, “Signal and depth enhancement for in vivo flow cytometer measurement of ear skin by optical clearing agents”, *Biomed. Opt. Express* **4**(11), 2518–2526 (2013).

[255] H. Zhong, Z. Guo, H. Wei, L. Guo, C. Wang, Y. He, H. Xiong, S. Liu, “Synergistic effect of ultrasound and thiazone-PEG 400 on human skin optical clearing in vivo”, *Photochem. Photobiol*. **86**(3), 732–737 (2010).

[256] R. Shi, L. Guo, C. Zhang, W. Feng, P. Li, Z. Ding, and D. Zhu, “A useful way to develop effective in vivo skin optical clearing agents”, *JBO* **10**(6–7), 887–895 (2017).

[257] R. Cicchi, F. S. Pavone, D. Massi, and D. D. Sampson, “Contrast and depth enhancement in two-photon microscopy of human skin ex vivo by use of optical clearing agents”, *Opt. Express* **13**(7), 2337–2344 (2005).

[258] X. Wen, S. L. Jacques, V. V. Tuchin, and D. Zhu, “Enhanced optical clearing of skin in vivo and optical coherence tomography in-depth imaging”, *JBO* **17**(6), 066022 (2012).

[259] A. Nicholson, J. Sandler, and T. Seidle, “An evaluation of the US High Production Volume (HPV) chemical-testing programme: A study in (Ir)relevance, redundancy and retro thinking”, *Altern. Lab. Anim*. **32**, 335–341 (2004).

[260] S. J. Jiang, S. M. Hwang, E. H. Choi, P. M. Elias, S. K. Ahn, and S. H. Lee, “Structural and functional effects of oleic acid and iontophoresis on hairless mouse stratum corneum”, *J. Invest. Dermatol*. **114**(1), 64–70 (2000).

[261] S. J. Jiang and X. J. Zhou, “Examination of the mechanism of oleic acid-induced percutaneous penetration enhancement: an ultrastructural study”, *Biol. Pharm. Bull*. **26**(1), 66–68 (2003).

[262] G. Vargas, A. Readinger, S. S. Dozier, and A. J. Welch, “Morphological Changes in Blood Vessels Produced by Hyperosmotic Agents and Measured by Optical Coherence Tomography”, *Photochem. Photobiol*. **77**(5), 541–549 (2003).

[263] P. Wan, J. Zhu, J. Xu, Y. Li, T. Yu, and D. Zhu, “Evaluation of seven optical clearing methods in mouse brain”, *Neurophotonics* **5**(3), 035007 (2018).

[264] A. V. Liopo, R. Su, D. A. Tsyboulski, and A. A. Oraevsky, “Optical clearing of skin enhanced with hyaluronic acid for increased contrast of optoacoustic imaging”, *JBO* **21**(8), 081208 (2016).

[265] P. A. Timoshina, E. M. Zinchenko, D. K. Tuchina, M. M. Sagatova, O. V. Semyachkina-Glushkovskaya, and V. V. Tuchin, “Laser speckle contrast imaging of cerebral blood flow of newborn mice at optical clearing”, in *Saratov Fall Meeting 2016: Optical Technologies in Biophysics and Medicine XVIII*, 1033610 (2017).

[266] X. Xu and Q. Zhu, “Evaluation of skin optical clearing enhancement with Azone as a penetration enhancer”, *Opt. Commun*. **279**, 223–228 (2007).

[267] T. Kurihara-Bergstrom, K. Knutson, L. J. DeNoble, and C. Y. Goates, “Percutaneous absorption enhancement of an ionic molecule by ethanol-water systems in human skin”, *Pharm. Res*. **7**(7), 762–766 (1990).

[268] E. Genina, A. Bashkatov, and V. Tuchin, “Effect of ethanol on the transport of methylene blue through stratum corneum”, *Medical Laser Application* **23**, 31–38 (2008).

[269] I. Vejnovic, L. Simmler, and G. Betz, “Investigation of different formulations for drug delivery through the nail plate”, *Int. J. Pharm*. **386**(1–2), 185–194 (2010).

[270] R. Notman, W. K. den Otter, M. G. Noro, W. J. Briels, and J. Anwar, “The Permeability Enhancing Mechanism of DMSO in Ceramide Bilayers Simulated by Molecular Dynamics”, *Biophys. J*. **93**(6), 2056–2068 (2007).

[271] P. J. Caspers, A. C. Williams, E. A. Carter, H. G. M. Edwards, B. W. Barry, H. A. Bruining, and G. J. Puppels, “Monitoring the penetration enhancer dimethyl sulfoxide in human stratum corneum in vivo by confocal Raman spectroscopy”, *Pharm. Res*. **19**(10), 1577–1580 (2002).

[272] C. H. Chang, E. M. Myers, M. J. Kennelly, and N. M. Fried, “Optical clearing of vaginal tissues, ex vivo, for minimally invasive laser treatment of female stress urinary incontinence”, *JBO* **22**(1), 018002 (2017).

[273] A. P. Funke, R. Schiller, H. W. Motzkus, C. Günther, R. H. Müller, and R. Lipp, “Transdermal delivery of highly lipophilic drugs: in vitro fluxes of antiestrogens, permeation enhancers, and solvents from liquid formulations”, *Pharm. Res*. **19**(5), 661–668 (2002).

[274] J. M. Andanson, K. L. A. Chan, and S. G. Kazarian, “High-throughput spectroscopic imaging applied to permeation through the skin”, *Appl. Spectrosc*. **63**(5), 512–517 (2009).

[275] A. C. Williams and B. W. Barry, “Penetration enhancers”, *Adv. Drug Deliver. Rev*. **64**, 128–137 (2012).

[276] M. B. Brown and S. A. Jones, “Hyaluronic acid: a unique topical vehicle for the localized delivery of drugs to the skin”, *Journal of the European Academy of Dermatology and Venereology* **19**(3), 308–318 (2005).

[277] H. S. Jung, K. S. Kim, S. H. Yun, and S. K. Hahn, “Enhancing the transdermal penetration of nanoconstructs: could hyaluronic acid be the key?”, *Nanomedicine* **9**(6), 743–745 (2014).

[278] M. Witting, A. Boreham, R. Brodwolf, K. Vávrová, U. Alexiev, W. Friess, and S. Hedtrich, “Interactions of hyaluronic Acid with the skin and implications for the dermal delivery of biomacromolecules”, *Mol. Pharm*. **12**(5), 1391–1401 (2015).

[279] H. J. Weigmann, J. Lademann, S. Schanzer, U. Lindemann, R. von Pelchrzim, H. Schaefer, W. Sterry, and V. Shah, “Correlation of the local distribution of topically applied substances inside the stratum corneum determined by tape-stripping to differences in bioavailability”, *Skin Pharmacol. Appl. Skin Physiol*. **14**, 98–102 (2001).

[280] R. J. McNichols, M. A. Fox, A. Gowda, S. Tuya, B. Bell, and M. Motamedi, “Temporary dermal scatter reduction: quantitative assessment and implications for improved laser tattoo removal”, *Lasers Surg. Med*. **36**(4), 289–296 (2005).

[281] O. Stumpp, B. Chen, and A. J. Welch, “Using sandpaper for noninvasive transepidermal optical skin clearing agent delivery”, *JBO* **11**(4), 041118 (2006).

[282] W. R. Lee, R. Y. Tsai, C. L. Fang, C. J. Liu, C. H. Hu, and J. Y. Fang, “Microdermabrasion as a novel tool to enhance drug delivery via the skin: an animal study”, *Dermatol. Surg*. **32**(8), 1013–1022 (2006).

[283] C. Tse, M. J. Zohdy, J. Y. Ye, and M. O’Donnell, “Penetration and Precision of Subsurface Photodisruption in Porcine Skin Tissue With Infrared Femtosecond Laser Pulses”, *IEEE T. Bio-Med. Eng*. **55**(3), 1211–1218 (2008).

[284] C. Liu, Z. Zhi, V. V. Tuchin, Q. Luo, and D. Zhu, “Enhancement of skin optical clearing efficacy using photo-irradiation”, *Lasers Surg. Med*. **42**(2), 132–140 (2010).

[285] V. V. Tuchin, G. B. Altshuler, A. A. Gavrilova, A. B. Pravdin, D. Tabatadze, J. Childs, and I. V. Yaroslavsky, “Optical clearing of skin using flash lamp-induced enhancement of epidermal permeability”, *Lasers Surg. Med*. **38**(9), 824–836 (2006).

[286] J. Yoon, T. Son, E. H. Choi, B. Choi, J. S. Nelson, and B. Jung, “Enhancement of optical skin clearing efficacy using a microneedle roller”, *JBO* **13**(2), 021103 (2008).

[287] O. F. Stumpp, A. J. Welch, T. E. Milner, and J. Neev, “Enhancement of transepidermal skin clearing agent delivery using a 980 nm diode laser”, *Lasers Surg. Med*. **37**(4), 278–285 (2005).

[288] N. S. Ksenofontova, E. A. Genina, A. N. Bashkatov, G. S. Terentyuk, and V. V. Tuchin, “OCT study of skin optical clearing with preliminary laser ablation of epidermis”, *JBPE* **3**(2), 020307 (2017).

[289] E. A. Genina, A. N. Bashkatov, G. S. Terentyuk, and V. V. Tuchin, “Integrated effects of fractional laser microablation and sonophoresis on skin immersion optical clearing in vivo”, *J. Biophotonics* **13**(7), e202000101 (2020).

[290] A. K. Nugroho, G. L. Li, M. Danhof, and J. A. Bouwstra, “Transdermal iontophoresis of rotigotine across human stratum corneum in vitro: influence of pH and NaCl concentration”, *Pharm. Res*. **21**(5), 844–850 (2004).

[291] E. A. Genina, Y. I. Surkov, I. A. Serebryakova, A. N. Bashkatov, V. V. Tuchin, and V. P. Zharov, “Rapid Ultrasound Optical Clearing of Human Light and Dark Skin”, *IEEE T. Med. Imaging* **39**(10), 3198–3206 (2020).

[292] X. Xu and Q. Zhu, “Sonophoretic Delivery for Contrast and Depth Improvement in Skin Optical Coherence Tomography”, *IEEE J. Sel. Top. Quant*. **14**(1), 56–61 (2008).

[293] A. Davidson, B. Al-Qallaf, D. Bhusan Das, “Transdermal drug delivery by coated microneedles: Geometry effects on effective skin thickness and drug permeability”, *Chem. Eng. Res. Des*. **86**(11), 1196-1206 (2008).

[294] T. Rattanapak, J. Birchall, K. Young, M. Ishii, I. Meglinski, T. Rades, and S. Hook, “Transcutaneous immunization using microneedles and cubosomes: Mechanistic investigation using Optical Coherence Tomography and Two-Photon Microscopy”, *J. Control. Release* **172**(3), 894 – 903 (2013).

[295] B. E. Polat, D. Hart, R. Langer, and D. Blankschtein, “Ultrasound-mediated transdermal drug delivery: Mechanisms, scope, and emerging trends”, *J. Control. Release* **152**(3), 330–348 (2011).

[296] X. Xu and C. Sun, “Ultrasound enhanced skin optical clearing: microstructural changes”, *J. Innov. Opt. Health Sci*. **3**(3), 189–194 (2010).

[297] A. Tezel and S. Mitragotri, “Interactions of Inertial Cavitation Bubbles with Stratum Corneum Lipid Bilayers during Low-Frequency Sonophoresis”, *Biophys. J*. **85**(6), 3502–3512 (2003).

[298] X. Xu, Q. Zhu, and C. Sun, “Assessment of the effects of ultrasound-mediated alcohols on skin optical clearing”, *JBO* **14**(3), 034042 (2009).

[299] X. Xu, Q. Zhu, and C. Sun, “Combined Effect of Ultrasound-SLS on Skin Optical Clearing”, *IEEE Photonic. Tech. L*. **20**(24), 2117–2119 (2008).

[300] S. M. Zaytsev, Yu. I. Svenskaya, E. V. Lengert, G. S. Terentyuk, A. N. Bashkatov, V. V. Tuchin, and E. A. Genina, “Optimized skin optical clearing for optical coherence tomography monitoring of encapsulated drug delivery through the hair follicles”, *J. Biophotonics* **13**(4), e201960020 (2020).

[301] M. A. Fox, D. G. Diven, K. Sra, A. Boretsky, T. Poonawalla, A. Readinger, M. Motamedi, and R. J. McNichols, “Dermal scatter reduction in human skin: a method using controlled application of glycerol”, *Lasers Surg. Med*. **41**(4), 251–255 (2009).

[302] J. Yoon, D. Park, T. Son, J. Seo, J. S. Nelson, and B. Jung, “A physical method to enhance transdermal delivery of a tissue optical clearing agent: Combination of microneedling and sonophoresis”, *Lasers Surg. Med*. **42**(5), 412–417 (2010).

[303] Y. A. Menyaev, D. A. Nedosekin, M. Sarimollaoglu, M. A. Juratli, E. I. Galanzha, V. V. Tuchin, and V. P. Zharov, “Optical clearing in photoacoustic flow cytometry”, *Biomed. Opt. Express* **4**(12), 3030–3041 (2013).

[304] A. Sdobnov, M. E. Darvin, J. Lademann, and V. Tuchin, “A comparative study of ex vivo skin optical clearing using two-photon microscopy”, *J. Biophotonics* **10**(9), 1115–1123 (2017).

[305] Y. M. Liew, R. A. McLaughlin, F. M. Wood, and D. D. Sampson, “Reduction of image artifacts in three-dimensional optical coherence tomography of skin in vivo”, *JBO* **16**(11), 116018 (2011).

[306] R. K. Wang and V. V. Tuchin, “Enhance light penetration in tissue for high resolution optical imaging techniques by the use of biocompatible chemical agents”, *J. Xray Sci. Technol*. **10**(3), 167–176 (2002).

[307] L. Pires, V. Demidov, I. A. Vitkin, V. S. Bagnato, C. Kurachi, and B. C. Wilson, “Optical clearing of melanoma in vivo: characterization by diffuse reflectance spectroscopy and optical coherence tomography”, *JBO* **21**(8), 081210 (2016).

[308] R. He, H. Wei, H. Gu, Z. Zhu, Y. Zhang, X. Guo, T. Cai, “Effects of optical clearing agents on noninvasive blood glucose monitoring with optical coherence tomography: a pilot study”, *JBO* **17**(10), 101513 (2012).

[309] Q. Zhao, C. Dai, S. Fan, J. Lv, and L. Nie, “Synergistic efficacy of salicylic acid with a penetration enhancer on human skin monitored by OCT and diffuse reflectance spectroscopy”, *Sci. Rep*. **6**(1), 34954 (2016).

[310] A. N. Bashkatov, E. A. Genina, I. V. Korovina, V. I. Kochubey, Y. P. Sinichkin, and V. V. Tuchin, “In-vivo and in-vitro study of control of rat skin optical properties by action of osmotical liquid”, in *Biomedical Photonics and Optoelectronic Imaging*, 300–311 (2000).

[311] Z. Mao, X. Wen, J. Wang, and D. Zhu, “The biocompatibility of the dermal injection of glycerol in vivo to achieve optical clearing”, in *Eighth International Conference on Photonics and Imaging in Biology and Medicine*, 75191N (2009).

[312] D. K. Tuchina, P. A. Timoshina, V. V. Tuchin, A. N. Bashkatov, and E. A. Genina, “Kinetics of Rat Skin Optical Clearing at Topical Application of 40%Glucose: Ex Vivo and In Vivo Studies”, *IEEE J. Sel. Top. Quant*. **25**(1), 1–8 (2019).

[313] E. D. Jansen, P. M. Pickett, M. A. Mackanos, and J. Virostko, “Effect of optical tissue clearing on spatial resolution and sensitivity of bioluminescence imaging”, *JBO* **11**(4), 041119 (2006).

[314] S. Karma, J. Homan, C. Stoianovici, and B. Choi, “Enhanced fluorescence imaging with dmso-mediated optical clearing”, *J. Innov. Opt. Health Sci*. **3**(3), 153–158 (2010).

[315] A. F. Pena, A. Doronin, V. V. Tuchin, and I. Meglinski, “Monitoring of interaction of low frequency electric field with biological tissues upon optical clearing with Optical Coherence Tomography”, *JBO* **19**(8), 086002 (2014).

[316] M. E. Darvin, J. Schleusener, F. Parenz, O. Seidel, C. Krafft, J. Popp, and J. Lademann, “Confocal Raman microscopy combined with optical clearing for identification of inks in multicolored tattooed skin in vivo”, *Analyst* **143**(20), 4990–4999 (2018).

[317] W. Feng, R. Shi, C. Zhang, T. Yu, and D. Zhu, “Lookup-table-based inverse model for mapping oxygen concentration of cutaneous microvessels using hyperspectral imaging”, *Opt. Express* **25**(4), 3481–3495 (2017).

[318] P. Rakotomanga, C. Soussen, G. Khairallah, M. Amouroux, S. Zaytsev, E. Genina, H. Chen, A. Delconte, C. Daul, V. Tuchin, and W. Blondel, “Source separation approach for the analysis of spatially resolved multiply excited autofluorescence spectra during optical clearing of ex vivo skin”, *Biomed. Opt. Express* **10**(7), 3410–3424 (2019).

[319] S. M. Zaytsev, W. Blondel, M. Amouroux, G. Khairallah, A. N. Bashkatov, V. V. Tuchin, and E. A. Genina, “Optical spectroscopy as an effective tool for skin cancer features analysis: applicability investigation”, in *Saratov Fall Meeting 2019: Optical and Nano-Technologies for Biology and Medicine* **11457**, 1145706 (2020).

[320] H. Takeuchi, Y. Mano, S. Terasaka, T. Sakurai, A. Furuya, H. Urano, and K. Sugibayashi, “Usefulness of Rat Skin as a Substitute for Human Skin in the in Vitro Skin Permeation Study”, *Experimental Animals* **60**(4), 373–384 (2011).

[321] A. N. Bashkatov, E. A. Genina, V. I. Kochubey, and V. V. Tuchin, “Optical properties of human skin, subcutaneous and mucous tissues in the wavelength range from 400 to 2000 nm”, *J. Phys. D: Appl. Phys*. **38**(15), 2543–2555 (2005).

[322] G. Vargas, K. F. Chan, S. L. Thomsen, and A. J. Welch, “Use of osmotically active agents to alter optical properties of tissue: Effects on the detected fluorescence signal measured through skin”, *Lasers Surg. Med*. **29**(3), 213–220 (2001).

[323] X. Wen, V. V. Tuchin, Q. Luo, and D. Zhu, “Controling the scattering of Intralipid by using optical clearing agents”, *Phys. Med. Biol*. **54**(22), 6917–6930 (2009).

[324] P. D. Ninni, F. Martelli, and G. Zaccanti, “The use of India ink in tissue-simulating phantoms”, *Opt. Express* **18**(26), 26854–26865 (2010).

[325] S. K. S. Lightbourne, H. B. Gobeze, N. K. Subbaiyan, and F. D’Souza, “Chlorin e6 sensitized photovoltaic cells: effect of co-adsorbents on cell performance, charge transfer resistance, and charge recombination dynamics”, *J. Photon. Energy* **5**(1), 053089 (2015).

[326] M. Amouroux, W. Blondel, and A. Delconte (2017). *Medical Device for Fibred Bimodal Optical Spectroscopy* (patent No. WO2017093316). Available: https://patentscope.wipo.int/search/en/detail.jsf?docId=WO2017093316

[327] W. Blondel, A. Delconte, G. Khairallah, F. Marchal, A. Gavoille, and M. Amouroux, “Spatially-Resolved Multiply-Excited Autofluorescence and Diffuse Reflectance Spectroscopy: SpectroLive Medical Device for Skin In Vivo Optical Biopsy”, *Electronics* **10**(3), 243 (2021).

[328] N. Kollias, G. Zonios, and G. N. Stamatas, “Fluorescence spectroscopy of skin”, *Vib. Spectrosc*. **28**(1), 17–23 (2002).

[329] E. A. Genina, A. N. Bashkatov, Y. P. Sinichkin, I. Y. Yanina, and V. V. Tuchin, “Optical clearing of biological tissues: prospects of application in medical diagnostics and phototherapy”, *JBPE* **1**(1), 22–58 (2015).

[330] A. A. Gurjarpadhye, W. C. Vogt, Y. Liu, and C. G. Rylander, “Effect of Localized Mechanical Indentation on Skin Water Content Evaluated Using OCT”, *Int. J. Biomed. Imaging* **2011**, 817250 (2011).

[331] V. Carrer, C. Alonso, M. Pont, M. Zanuy, M. Córdoba, S. Espinosa, C. Barba, M. A. Oliver, M. Martí, and L. Coderch, “Effect of propylene glycol on the skin penetration of drugs”, *Arch. Dermatol. Res*. **312**(5), 337–352 (2020).

[332] A. N. C. Anigbogu, A. C. Williams, B. W. Barry, and H. G. M. Edwards, “Fourier transform raman spectroscopy of interactions between the penetration enhancer dimethyl sulfoxide and human stratum corneum”, *Int. J. Pharm*. **125**(2), 265–282 (1995).

[333] C. R. Idelson, W. C. Vogt, B. King-Casas, S. M. LaConte, and C. G. Rylander, “Effect of mechanical optical clearing on near-infrared spectroscopy”, *Lasers Surg. Med*. **47**(6), 495–502 (2015).

[334] M. Y. Kirillin, P. D. Agrba, and V. A. Kamensky, “In vivo study of the effect of mechanical compression on formation of OCT images of human skin”, J. Biophotonics 3(12), 752–758 (2010).

[335] C. Li, J. Jiang, and K. Xu, “The variations of water in human tissue under certain compression: studied with diffuse reflectance spectroscopy”, *J. Innov. Opt. Health Sci*. **6**(1), 1350005 (2012).

[336] I. A. Nakhaeva, O. A. Zyuryukina, M. R. Mohammed, and Yu. P. Sinichkin, “The effect of external mechanical compression on in vivo water content in human skin”, *Opt. Spectrosc*. **118**(5), 834–840 (2015).

[337] A. Popov, A. Bykov, and I. Meglinski, “Influence of probe pressure on diffuse reflectance spectra of human skin measured in vivo”, *JBO* **22**(11), 110504 (2017).

[338] “U. S. Food and Drug Administration, Inactive Ingredients Database”, *FDA.gov*, Retrieved 12 February 2019, https://www.accessdata.fda.gov/scripts/cder/iig/index.cfm.

[339] C. Gorzelanny, C. Mess, S. W. Schneider, V. Huck, and J. M. Brandner, “Skin Barriers in Dermal Drug Delivery: Which Barriers Have to Be Overcome and How Can We Measure Them?”, *Pharmaceutics* **12**(7), 684 (2020).

[340] J. A. Bouwstra and M. Ponec, “The skin barrier in healthy and diseased state”, *Biochim. Biophys. Acta* **1758**(12), 2080–2095 (2006).

[341] E. A. Genina, A. N. Bashkatov, V. P. Zharov, and V. V. Tuchin, “In vivo skin optical clearing in humans”, in *Handbook of Tissue Optical Clearing: New Prospects in Optical Imaging*, V. V. Tuchin, D. Zhu, and E. A. Genina, Eds., 682, Routledge & CRC Press, Boca Raton (2022).

[342] V. V. Tuchin, A. N. Bashkatov, E. A. Genina, Yu. P. Sinichkin, and N. A. Lakodina, “In vivo investigation of the immersion-liquid-induced human skin clearing dynamics”, *Tech. Phys. Lett*. **27**(6), 489–490 (2001).

[343] N. Sudheendran, M. Mohamed, M. G. Ghosn, V. V. Tuchin, and K. V. Larin, “Assessment of tissue optical clearing as a function of glucose concentration using optical coherence tomography”, *J. Innov. Opt. Health Sci*. **3**(3), 169–176 (2010).

[344] I. Meglinski, A. N. Bashkatov, E. A. Genina, D. Y. Churmakov, and V. V. Tuchin, “Study of the possibility of increasing the probing depth by the method of reflection confocal microscopy upon immersion clearing of near-surface human skin layers”, *Quantum Electron*. **32**(10), 875-882 (2002).

[345] I. Meglinski, D. Y. Churmakov, A. N. Bashkatov, E. A. Genina, and V. V. Tuchin, “The Enhancement of Confocal Images of Tissues at Bulk Optical Immersion”, *Laser Phys*. **13**(1), 65 – 69 (2003).

[346] I. Meglinski and V. V. Tuchin, “The enhancement of confocal probing with optical clearing”, in *Advances in Biomedical Photonics and Imaging*, Q. Luo, L. V. Wang, and V. V. Tuchin, Eds., 33-38, World Scientific, Singapore (2008).